AN INVESTIGATION OF SATELLITES TO THE RESONANCE LINES IN SOME HYDROGEN-LIKE IONS

by

Nelson Wayne Jalufka

B.S., Lamar University, 1962

M.A., College of William and Mary, 1967

A thesis submitted to the Faculty of the Graduate School of the University of Colorado in partial fulfillment of the requirements for the degree of

Doctor of Philosophy

Department of Physics and Astrophysics

1972

This Thesis for the Doctor of Philosophy Degree by

Nelson Wayne Jalufka

has been approved for the

Department of

Physics and Astrophysics

by

_____

John Cooper

_____

Date_____

ABSTRACT

Jalufka, Nelson Wayne (Ph.D., Physics)

An Investigation of Satellites to the Resonance Lines in Some Hydrogen-Like Ions

Thesis directed by Professor John Cooper

This research has been an experimental and theoretical investigation of the origin of satellites to the resonance lines of the hydrogen-like ions of boron, carbon, and nitrogen.

A theta pinch was employed in conjunction with a grazing incidence spectrograph to measure the wavelengths of the satellites. The spectroscopic data also provided an estimate of the satellite to resonance line intensity ratio.

Wavelenghts of spectral lines due to transition from doubly excited states were calculated by a Hartree-Fock computer program. Wave-functions were also calculated by this program and were used to obtain the oscillator strengths of the transitions.

Calculations of the upper limit of the satellite to resonance line intensity ratio showed that the observed intensity of the satellites was much greater than could be explained by present theories, and further experimental work confirmed that the lines investigated were not satellites but were due to highly ionized argon which was present as an impurity in the filling gas of this and many previous experiments.

This abstract is approved as to form and content. I recommend its publication.

Signed_____
John Cooper

ACKNOWLEDGMENTS

I would like to express my appreciation to my advisor, Professor John Cooper, for the support, encouragement and the instruction that he has given me.

Thanks are due to Dr. Louis Shamey for his instruction and help with the computer programs.

I would also like to thank Mr. John Fryer for his very able assistance with the operation of the theta-pinch facility and Mr. M. D. Williams for his help in locating and correcting the problems associated with the operation of a large capacitor bank.

Special thanks are due to Bob Alvis and his staff at JILA for their courteousness and help.

Thanks are also due the Langley Research Center of NASA for the support given me during the course of this investigation.

This research was supported by the Physics and Astronomy Program at NASA Headquarters, Washington, D. C. and I am grateful to Dr. Goetz Oertel for this support.

Finally I would like to thank my wife, Jean, for her encouragement and understanding.

TABLE OF CONTENTS

LIST OF TABLES

LIST OF FIGURES

CHAPTER I

INTRODUCTION

A. History

Long-wavelength satellites to the resonance line of a hydrogen-like ion were first observed in the laboratory by Compton and Boyce (1928). They reported two weak satellites to the resonance line of singly ionized helium and suggested that these lines were due to the excitation of both electrons of neutral helium into the $n = 2$ level and the radiation accompanying the return of one electron to the ground state. This explanation was later confirmed by theoretical calculations (Kiang, Ma, and Wu, 1936).

Edlén and Tyrén (1939) published a vacuum spark spectrum of carbon covering the region from 60 Å to 15 Å. It was expected that the spectrum in this region would be very simple, consisting of the normal helium-like and hydrogen-like series. However, a considerable number of additional lines appeared in distinct groups to the long-wavelength side of the helium-like and hydrogen-like resonance lines. The proximity of these lines to the resonance lines indicated that they were due to transitions of essentially the same type as the resonance transition but at a slightly lower energy. These lines were explained by transitions of the type

$$1s^2\ n\ell - 1s\ 2p\ n\ell \qquad (1.1)$$

for the helium-like satellites and

$$1s\ n\ell - 2p\ n\ell \qquad (1.2)$$

for the hydrogen-like case. This explanation appeared reasonable as the presence of the additional outer electron would reduce the potential field in which the transition takes place and, consequently, cause a shift to longer wavelength. The prominent satellites were attributed to n = 2, as those with greater n would rapidly move nearer to, and merge with, the resonance line. As a consequence of this explanation, the existence of discrete energy levels, lying well above the ionization limit of the ion in which the transition takes place, had to be assumed.

More recently, the observation of such satellites has been reported from a number of laboratory plasmas, including sparks (Flemberg, 1942; Feldman and Cohen, 1969; Goldsmith, 1969; Lie and Elton, 1971), high-temperature pinches (Sawyer, 1962; Roth and Elton, 1968; Peacock, Speer, and Hobby, 1969; Gabriel and Paget, 1972;), and laser-produced plasmas (Gabriel, 1971). The observation of similar satellites in recent solar spectra (Fritz, et al., 1967; Rugge and Walker, 1968; Jones, Freeman, and Wilson, 1968; Walker and Rugge, 1970) has led to a renewed interest in the origin of these lines.

B. Applications to Astrophysics

In order to establish the importance of doubly excited states to problems of astrophysical interest, it is first necessary to investigate the physical processes by which these states may be populated and depopulated. This is necessary since most astrophysical plasmas cannot be described in the limited framework of thermodynamic equilibrium and a knowledge of the rate coefficients of the different competing processes is important in determining such properties as ionization balance as well as the distribution of electrons among the various energy levels of the atom or ion.

Doubly excited states may be populated, as well as depopulated, by electron collisions. Photoexcitation may also populate these states. The inverse processes is spontaneous and stimulated (if a radiation field is present) emission. Spontaneous emission is the process responsible for the emission of the satellite lines. A more interesting process, for the formation of the doubly excited state and the one that was the basis for this research, is inverse autoionization. In this process an electron combines in a radiationless transition with an ion of charge Z to form an ion of charge $Z - 1$ in a doubly excited state. The doubly excited state then decays by spontaneous emission and the two step process is called dielectronic recombination These two processes are not applicable to all doubly excited states, as certain selection rules must be obeyed. These selection rules which consist of conservation of energy, total angular momentum, and parity will be discussed in Chapter II.

Transitions between doubly excited states, which may undergo autoionization and normal (singly excited) states, have several astrophysical applications. The natural width of such lines are often much greater than widths due to random Doppler broadening or collisional broadening, since the lifetime to autoionization is often small. This large width makes these lines very efficient absorbers of radiation, as they will only become saturated at relatively large values of the equivalent width. There is a very large probability that each absorption of a photon in the line will be followed by ionization, so that the mechanism of line formation is pure absorption. This greatly simplifies the analysis.

The astrophysical importance of dielectronic recombination has been pointed out by Burgess (1965a). This process is, perhaps, the most important role played by doubly excited states in astrophysical situations. The problem which led Burgess to examine the process in sufficient detail to realize its importance was the discrepancy between the temperature of the Solar Corona as deduced from the observed widths of the "forbidden" emission lines of FeX, FeXIV, and CaXV and as deduced from ionization balance calculations. The widths of the emission lines were interpreted as Doppler widths and indicated a temperature of about 2×10^6 ^{o}K (Evans, 1963). The ionization balance calculations were carried out by balancing the rates of ionization due to electron collisions and the rates of recombination, which was assumed to be radiative. These calculations indicated a temperature of 10^6 ^{o}K. The factor of two discrepancy

does not, at first, appear to be serious. However, in order to bring the calculated temperature into agreement with the Doppler temperature the recombination rate had to be increased by a factor of 30. The same results could have been achieved by decreasing the ionization rate by the same factor. Careful examination of this process however, revealed that the ionization cross section used was essentially correct since the theoretical values were verified by experimental measurements. Burgess performed detailed calculation of the dielectronic recombination rates for many elements in various stages of ionization. These calculations showed that if the temperature was high enough so that a substantial fraction of free electrons could make radiationless transition to doubly excited levels with large principal quantum number, then the total rate coefficient summed over many levels close to the second and higher series limits might exceed the corresponding rate coefficient for radiative recombination by one or more orders of magnitude. These results were applied to the Solar Corona and were successful in removing the discrepancy in the temperature.

The processes of autoionization and dielectronic recombination have also been shown to be of importance in the interstellar medium (Goldberg, 1966). In particular, a discrepancy exists in the Ca/Na abundance ratio of the interstellar medium. Analysis of interstellar line intensities leads to a Ca/Na abundance ratio of about 0.03, whereas its value in the sun and other stars is about 0.70

which is a factor of 23 larger (Aller, 1963). The observed intensities are for the D lines of NaI and the K lines of CaII. Since NaII and CaIII are expected to be the most abundant ionization stages, determination of the abundance ratio requires a knowledge of the ionization balance. The interstellar ionization theory developed by Strömgren (1948) depends on an ionizational balance between photoionization and radiative recombination. The abundance discrepancy has been attributed to a lack of knowledge of the stellar ultraviolet radiation field which determines the photoionization rate. However, it now appears possible that the photoionization rates may be in error because they do not take into account transitions in NaI and CaII from their ground states to levels which undergo autoionization. It is not clear if the inclusion of these transitions will clear up the abundance ratio anomaly. In any case however, the effects of autoionization must be taken into account if the ionization equilibrium of the interstellar medium is to be properly discussed.

CHAPTER II

THEORY AND CALCULATIONS

A. Multi-Electron Atoms and the Central Field Approximation

An analysis of the radiation emitted by a plasma requires not only a knowledge of the various atomic processes which occur in the plasma but also attention to the details of atomic structure. Calculations of the energy levels of the various atoms or ions in the plasma must be carried out in the context of a well defined model of atomic structure. The details of the model which was employed in this investigation will now be developed (Slater, 1960).

The general Hamiltonian (in atomic units) for a multi-electron atom may be written (including only the spin-orbit relativistic term)

$$H = \sum_i \left[\frac{1}{2}\nabla_i^2 - \frac{z}{r_i}\right] + \sum_{i\neq j} \frac{1}{r_{ij}} + \sum_i \xi(\vec{r}_i)\vec{L}_i \cdot \vec{S}_i \quad (2.1)$$

alternatively

$$H = H_o + H_1 + H_2 \quad (2.2)$$

with two alternative ways of expressing the components. The general expression is given first followed by the central field approximation expression in brackets,

$$H_o = \sum_i \left(\frac{1}{2}\nabla_i^2 - \frac{z}{r_i}\right) = \left[\sum_i \left(\frac{1}{2}\nabla_i^2 + V(\vec{r}_i)\right)\right] \tag{2.3}$$

and

$$H_1 = \sum_{i\neq j} \frac{1}{r_{ij}} = \left[\sum_i \left(-\frac{z}{r_i} - V(\vec{r}_i)\right) + \sum_{i\neq j} \frac{1}{r_{ij}}\right] \tag{2.4}$$

and

$$H_2 = \sum_i H_2^i = \sum_i \xi(\vec{r}_i)\vec{L}_i \cdot \vec{S}_i \tag{2.5}$$

with

$$\xi(\vec{r}_i) = \frac{1}{2m^2c^2}\frac{1}{r_i}\frac{\partial V(\vec{r}_i)}{\partial r_i}$$

where $V(\vec{r}_i)$ is the approximate central field in which the electron moves (Shore and Menzel, 1968).

The term H_o is just a sum of terms which are the Hamiltonians of single, spinless electrons moving in a central force field. Schrödinger's equation for such an electron treated as a point charge is

$$H_o\,\psi = \left[\frac{1}{2}\nabla^2 + V_o(\vec{r})\right]\psi = E_o\psi \tag{2.6}$$

where $V_o(\vec{r})$ is the potential field and is a function of $|\vec{r}|$ only. Since the atomic nucleus and the electron possess a charge,

the potential function of particular interest in atomic structure theory is the Coulomb potential (in atomic units)

$$V_o(\vec{r}_i) = -\frac{z}{r_i} \tag{2.7}$$

with z equal to the nuclear charge. Equation (2.6) then becomes Schrödinger's equation for the one electron atom (hydrogenic) and has the great advantage of being both separable and exactly soluble, that is, exact analytic solutions for the eigenfunctions ψ can be found. The eigenfunctions of H_o are well known

$$\psi(n,\ell,m_\ell) = R_{n\ell}(r)Y_{\ell m}(\theta,\phi) \tag{2.8}$$

which is just the product of a radial function

$$R_{n\ell}(r) = \frac{P_{n\ell}(r)}{r} \tag{2.9}$$

and a spherical harmonic $Y_{\ell m}(\theta,\phi)$. The radial function is

$$R_{n\ell}(r) = \frac{P_{n\ell}(r)}{r} \tag{2.10}$$

with

$$P_{n\ell}(r) = \left(\frac{(n-\ell-1)!z}{n^2[(n+\ell)!]^3}\right)^{1/2} X^{\ell+1}\exp\left(-\frac{X}{2}\right) L_{n+\ell}^{2\ell+1}(X) \tag{2.11}$$

The quantity $L_{n+\ell}^{2\ell+1}(X)$ is the Laguerre polynomial with

$$X = \frac{2zr}{n} \tag{2.12}$$

The function $P_{n\ell}(r)$ is normalized in the sense that

$$\int_0^\infty |P_{n\ell}(r)|^2 dr = 1 \tag{2.13}$$

and the spherical harmonics $Y_{\ell m}(\theta,\phi)$ are normalized in the sense that

$$\int |Y_{\ell m}(\theta,\phi)|^2 d\Omega = 1 \tag{2.14}$$

The total wavefunction $\psi(n\ell m_\ell)$ is normalized and also orthogonal

$$\int \psi^*(n',\ell',m_\ell')\psi(n,\ell,m_\ell)dV = \delta_{n'n}\delta_{\ell'\ell}\delta_{m_\ell' m_\ell} \tag{2.15}$$

due to the orthonormal properties of the Laguerre polynomials and the spherical harmonics. The eigenfunctions of the one electron atom are designated by the principal quantum number n, the orbital angular momentum ℓ, and the projection of ℓ on the z-axis, m_ℓ. Thus the eigenfunctions are mutual eigenfunctions of the three commuting operators H_o, $\vec{L}^2$, and L_z with eigenvalues E_o, $\ell(\ell+1)$, and m_ℓ respectively.

When more than one electron is present the potential function in H_o is no longer the Coulomb potential due to the presence of the other electrons, however the separable form of equation (2.8) is still appropriate. The term H_1, which includes the interaction between the electron of interest and all the other electrons in the atom, is no longer zero so that Schrödinger's equation, including H_1, is neither separable nor solvable in closed analytical form. Therefore, approximation methods must be employed to obtain eigenfunctions of Schrödinger's equation. These approximation methods are based on the central-field model for the atom. The central-field model was developed concurrently with wave mechanics and quantum mechanics. The development started with Bohr's first proposal (1922) for the explanation of the periodic table and was supplemented by the discovery of the electron spin by Uhlenbeck and Goudsmit (1925, 1926) and by the exclusion principle of Pauli (1926). The method was completed with Hartree's proposal (1928) of the method of the self consistent field and with the so-called Hartree-Fock method (V. Fock, 1930a, 1930b, Slater 1930).

Three postulates are required for the central-field model. The first of these follows from wave mechanics and is merely an approximation method of solving Schrödinger's equation for the many body problems of N electrons moving about a nucleus of charge z units. The other two postulates are extensions of the wave mechanical principles and are the postulates of the electron

spin and of the exclusion principle. The latter two postulates are required since the electrons are Fermions (spin of 1/2) and are therefore represented by anti-symmetric wavefunctions which require that no two electrons occupy the same state.

The simple central-field model in fact,consists of replacing the instantaneous action of all the electrons of an atom on one of their number by the much simpler problem in which each electron is assumed to be acted on by the average charge distribution of each of the other electrons. This average charge density is obtained by taking the quantity $\psi^*\psi$ for the corresponding wavefunction, summing over all the electrons in the atom and taking a spherical average. The potential, arising from this spherically averaged charge distribution and the nucleus, is itself spherically symmetric or, in other words, a central field. Eigenfunctions of H_o may then be found since $V(\vec{r})$ is now a central field. These eigenfunctions which represent single electrons moving in the central field are very nearly those obtained for the one electron atom [i.e., $\psi = R_{n\ell}(r)Y_{\ell m}(\theta,\phi)$] since the angular dependence will be the same. The radial part of the wavefunction, however, may be different. The eigenfunctions of H_o therefore represent the individual electrons and designates each with a particular n, ℓ, and m_ℓ. By specifying n and ℓ for each electron, a configuration is denoted in this approximation. The simplest wavefunction which is an eigenfunction of H_o is a product function of the one electron wavefunctions. This product

function will have a well defined parity with the property

$$(\vec{P} \cdot \vec{P})\Psi = \Psi \tag{2.16}$$

where the parity operator $\vec{P}$ commutes with H_o. Equation (2.16) shows that the only eigenvalues of $\vec{P}$ are ± 1 with the eigenfunction -1 called odd parity and + 1 even parity. For the simple product function the parity is given by

$$\vec{P} = (-1)^{\sum_i \vec{\ell}_i} \tag{2.17}$$

and is determined by the orbital angular momentum of the electron obtained from the central field approximation. The one electron wavefunctions must also contain a function of spin since the electron spin is postulated in the central-field approximation. The spin function is taken as an eigenfunction of the operators $\vec{S}^2$ and S_z with eigenvalues 3/4 [= s(s + 1)] and m_s, respectively. The product of the one electron wavefunction and the spin function are designated spin-orbitals and are represented by

$$u(n\ell m_\ell s m_s) = \psi(n\ \ell\ m_\ell)\ \overset{\pm}{X}(s) \tag{2.18}$$

where $\overset{\pm}{X}(s)$ are the spin functions corresponding to $m_s = \pm \frac{1}{2}$. The operators $\vec{S}^2$ and S_z commute with H_o, $\vec{L}^2$, L_z and $\vec{P}$ since

they operate in a different space so that the spin orbitals are eigenfunctions of these operators.

The coupling of the various orbital and spin angular momenta may be carried out in the Russel-Saunders or LS coupling scheme. In this scheme the individual orbital angular momenta of the electrons is added vectorally to give a total orbital angular momentum

$$\vec{L} = \sum_i \vec{\ell}_i \quad . \tag{2.19}$$

The individual spins add in the same manner to give a resultant spin

$$\vec{S} = \sum_i \vec{s}_i \tag{2.20}$$

The specification of $\vec{L}$ and $\vec{S}$ denotes a term in a given configuration.

The terms H_1 and H_2 in the Hamiltonian are treated as perturbations with the assumption that they make small corrections to the total energy of the atomic state. This is not always the case but for many atoms (especially the ligher ones) it is a very good approximation. The operator H_1 commutes with $\vec{L}^2$ and $\vec{S}^2$ and with $\vec{J}^2$ where

$$\vec{J} = \vec{L} + \vec{S} \tag{2.21}$$

is the total angular momentum and the operator $\vec{J}^2$ has the eigenvalues $j(j + 1)$. The operator H_1 also commutes with the parity operator and therefore matrix elements of H_1 between functions of the same $\vec{J}$ and parity will be non-zero. Thus the interelectron Coulomb repulsion will mix the single particle product functions (i.e. spin orbitals) and the concept of a configuration loses its identity. The existence of these non-zero matrix elements of H_1 between levels in different configurations is referred to as configuration mixing. While the effect of the operator H_1 can often be ignored, in many practical cases it can lead to rather interesting phenomena. The most interesting case and one which is of interest in this investigation is when one of the configurations contains continuum states. The mixing of bound and continuum states leads to the phenomena of autoionization as well as its inverse. These processes involve doubly excited states and will be discussed in detail along with the other atomic processes in Chapter III.

The spin angular momentum of the electron may interact with the orbital angular momentum so that the operator H_2 is non-zero even for hydrogenic atoms. The one electron spin-orbitals $u(n\ell m_\ell s m_s)$ are not eigenfunctions of H_2 since H_2 does not commute with L_z or S_z. The operator H_2 does commute with $\vec{J}^2$ and J_z but not with $\vec{L}^2$ and $\vec{S}^2$. The eigenfunctions of H_2 should therefore also be eigenfunctions of the operators H_o, $\vec{J}^2$ and J_z.

Such eigenfunctions may be constructed from the one electron spin orbitals by using the Clebsh-Fordon coefficients to couple $\vec{L}$ and $\vec{S}$ (Shore and Menzel, 1968)

$$u(n\ell sjm_j) = \sum_{m_\ell m_s} C(\ell sj;\ m_\ell m_s m_j)u(n\ell m_\ell s m_s) \qquad (2.22)$$

where $C(\ell sj;\ m_\ell m_s m_j)$ is the Clebsh-Gordon or vector coupling coefficient.

Matrix elements of the spin orbit interaction operator H_2 are tabulated by Condon and Shortley (1938) for various configurations. Since H_2 does not commute with $\vec{L}$ or $\vec{S}$ they are no longer "good" quantum numbers. However, the total angular momentum $\vec{J}$ is a "good" quantum number as the matrix elements of H_2 are diagonal in $\vec{J}$ (i.e.,H_2 and $\vec{J}$ commute). For the levels considered in this investigation the effects of configuration interaction and spin-orbit interaction were found to contribute very small corrections so that the levels are labeled in the LS notation.

It has been pointed out that the one electron eigenfunctions in the central-field model differ from the hydrogenic functions only in that the radial dependence is different. These radial functions must be determined if the eigenfunction is to be a reasonable approximation to the true eigenfunction. A most useful procedure which has been employed with a large degree of success is the variational principle of wave mechanics.

B. The Variational Method

The variational method assumes that a function W exists which is variable at will subject only to the condition that it is always normalized. The average value of the Hamiltonian operation H for this function is

$$H_{avg} = \int W^* H W \, dv \tag{2.23}$$

where the asterisk denotes the complex conjugate. The function W is then allowed to vary to $W + \delta W$ where both W and δW are functions of the same variables and δW is small relative to W. An arbitrary change in W will in general destroy its normalization so that equation (2.23) is not correct for an unnormalized function. In the general case where W is an unnormalized function the corresponding normalized function is

$$\frac{W}{\left(\int W^* W \, dv\right)^{1/2}} \tag{2.24}$$

Equation (2-23) should then be more properly written

$$H_{avg} = \frac{\int W^* H W \, dv}{\int W^* W \, dv} \tag{2.25}$$

The function W is then replaced by $W + \delta W$ with the corresponding value of H_{avg} being $H_{avg} + \delta H_{avg}$. If terms of second and higher order are discarded, and expression for δH_{avg} may be

obtained

$$\delta H_{avg} = \frac{\int (W^* + \delta W^*) H (W + \delta W) dv}{\int (W^* + \delta W^*)(W + \delta W) dv} - H_{avg}$$

$$= \int \delta W^* H W \, dv + \int W^* H \delta W \, dv - H_{avg}\left(\int \delta W^* W \, dv + \int W^* \delta W \, dv\right)$$

$$+ \text{higher order terms} \qquad (2.26)$$

It has been assumed that the unvaried function W was normalized. The variational principle requires that H_{avg} be stationary (i.e., $\delta H_{avg} = 0$) so that H_{avg} is a minimum for the function W. To accomplish this, use is made of the fact that H is Hermitian, (Slater 1960) which implies that

$$\int W^* H \delta W \, dv = \int \delta W H^* W^* \, dv = \left(\int \delta W^* H W \, dv\right)^* \qquad (2.27)$$

Equation (2.26) may then be written

$$\int \delta W^* [H - H_{avg}] W \, dv + \text{Complex conjugate} = 0 \qquad (2.28)$$

which can be satisfied if

$$\int \delta W^* [H - H_{avg}] W \, dv = 0 \qquad (2.29)$$

since this makes the complex conjugate also equal to zero. Now δW^* is the variation of an arbitrary function so that equation (2.29) is satisfied for all values of the coordinates only if

$$[H - H_{avg}]W = 0 \quad \text{everywhere} \tag{2.30}$$

However, this means that

$$HW = H_{avg}W \tag{2.31}$$

which is just Schrödinger's equation since the eigenvalue E of Schrödinger's equation is just H_{avg}. Imposition of the variational principle leads therefore to functions W which are solutions of Schrödinger's equation.

A more convenient way of applying the variational principle is the method of undetermined multipliers whereby the variation of an integral may be made equal to zero subject to the auxiliary condition that another integral (or integrals) remain constant. Thus it is required to vary the function W so as to make H_{avg} stationary, subject to the condition that the normalization integral remains constant and equal to unity. The method of undetermined multipliers is to set up a linear combination of all the integrals concerned with undetermined multipliers and set the variation of this linear combination equal to zero. For the general case of k auxiliary conditions, and denoting the integrals by I_o, I_1, . . . I_k, the variation of the linear combination is

$$\delta(I_o + \lambda_1 I_1 + \lambda_2 I_2 + \ldots + \lambda_k I_k) = 0 \qquad (2.32)$$

where the λ's are constants to be determined. In the present case the variation is

$$\delta[H_{avg} + \lambda \int W^* W \, dv] = 0 \qquad (2.33)$$

It has already been shown that δH_{avg} may be written as the sum of a quantity and its complex conjugate and the same procedure may be applied to

$$\delta \int W^* W \, dv$$

Then equation (2.33) may be rewritten as

$$\int \delta W^* [H + \lambda] W \, dv + \text{Complex conjugate} = 0 \qquad (2.34)$$

The variational principle then demands that

$$HW = -\lambda W \qquad (2.35)$$

which is just Schrödinger's equation with the undetermined multiplier equal to $-H_{avg}$. It is now desired to consider the application of the variational principle to the problem of finding approximate solutions of Schrödinger's equation.

C. The Self-Consistent Field Method and Hartree's Equations

The self-consistent field method (Hartree, 1928) is an extension of the central-field approximation. The method assumes a total wavefunction for the N electron atom which is just a product of the one electron wavefunctions

$$\Psi(r_1\theta_1\phi_1 \ldots r_N\theta_N\phi_N) = \Psi(n_1\ell_1 m_{\ell_1} r_1\theta_1\phi_1) \ldots \Psi(n_N\ell_N m_{\ell_N} r_N\theta_N\phi_N) \tag{2.36}$$

which were discussed in the central-field approximation. This wavefunction, which is of the form of that given by equation (2·8) but with the radial function initially arbitrary, is used to determine charge densities and potentials. These potentials are then employed to find new solutions to Schrödinger's equation which give new wavefunctions, which are usually not the ones initially assumed. In fact, Hartree (1928) found that he could use these new wavefunctions as starting functions and repeat the above procedure. This iterative process was continued until self-consistency is achieved, that is, the final wavefunctions agree (within specified limits) with the initial functions. Fortunately the process converged after a few cycles producing wavefunctions which were self consistent to a very good approximation.

Hartree's equations however may be obtained by applying the variational principle to the wavefunction [equation (2.36)] and

taking the undetermined radial functions as the quantities which may vary. The first step in applying the variational principle to Hartree's wavefunction is to compute the average value of the Hamiltonian for the function. If the spin-orbit operator H_2 is neglected (consistent with the LS coupling approximation) the Hamiltonian is

$$H = H_o + H_1 \tag{2.37}$$

and

$$H_{avg} = \sum_i \int \psi_i^* H_o^i \psi_i dv_i + \sum_{j \neq i} \int \int \psi_i^* \psi_j^* H_1^{ij} \psi_i \psi_j dv_i dv_j \tag{2.38}$$

The quantity H_{avg} is now varied subject to the condition that the normalization integral remain equal to unity. Since only the radial part of the function is to be varied and since the spherical harmonics are orthonormal, equation (2.38) is just

$$H_{avg} = \sum_i \int_0^\infty P_{n_i \ell_i}(r_i) H_o^i P_{n_i \ell_i}(r_i) dr_i$$

$$+ \sum_{j \neq i} \int_0^\infty \int_0^\infty P_{n_i \ell_i}(r_i) P_{n_j \ell_j}(r_j) \langle H_1^{ij} \rangle P_{n_i \ell_i}(r_i) P_{n_j \ell_j}(r_j) dr_i dr_j \tag{2.39}$$

and where $\langle H_1^{ij} \rangle = 1/r_>$ where $r_>$ is the larger of r_i and r_j.

Employing the undetermined multipliers the variational principle requires

$$\delta H_{avg} + \lambda_{n_i \ell_i} \delta \int_0^\infty P^2_{n_i \ell_i}(r_i) dr_i = 0 \tag{2.40}$$

The variation of H_{avg} is then computed. The variation is carried out with respect to a single radial function since if H is to be a minimum it must be a minimum with respect to each function. The variation of the first term of H^i_{avg} is

$$\delta \int_0^\infty P_{n_i \ell_i} H^i_o P_{n_i \ell_i} dr_i = \int_0^\infty \delta P_{n_i \ell_i} H^i_o P_{n_i \ell_i} dr_i + \int_0^\infty P_{n_i \ell_i} H^i_o \delta P_{n_i \ell_i} dr_i \tag{2.41}$$

$$= 2 \int_0^\infty \delta P_{n_i \ell_i} H^i_o P_{n_i \ell_i} dr_i \tag{2.42}$$

since the variation may be written as a sum of a quantity plus its complex conjugate and the radial functions (being a function of r only) are real so that the function is equal to its complex conjugate. The variation of the second term is

$$\delta \int_0^\infty \int_0^\infty P_{n_i \ell_i} P_{n_j \ell_j} \langle H^{ij}_1 \rangle P_{n_i \ell_i} P_{n_j \ell_j} dr_i dr_j$$

$$= 2 \int_0^\infty \int_0^\infty \delta P_{n_i \ell_i}(r_i) P_{n_i \ell_i}(r_i) P^2_{n_j \ell_j} \langle H^{ij}_1 \rangle dr_i dr_j \tag{2.43}$$

and the variation

$$\delta \int_0^\infty P^2_{n_i \ell_i} dr_i = 2 \int_0^\infty \delta P_{n_i \ell_i} P_{n_i \ell_i} dr_i \tag{2.44}$$

is also required. These values may now be substituted into equation (2.40) and setting

$$\lambda_{n_i \ell_i} = -\varepsilon_{n_i \ell_i} \tag{2.45}$$

the result

$$2 \int_0^\infty \delta P_{n_i \ell_i}(r_i) \left[H_o^i + \sum_{j \neq 1} \int^\infty \langle H_1^{ij} \rangle P^2_{n_j \ell_j}(r_j) dr_j - \varepsilon_{n_i \ell_i} \right] P_{n_i \ell_i}(r_i)$$

$$dr_i = 0 \tag{2.46}$$

is obtained. Since the variation $\delta P_{n_i \ell_i}(r_i)$ is arbitrary equation (2.46) is only true for all values of r if

$$\left[H_o^i + \sum_{j \neq 1} \int_0^\infty \langle H_1^{ij} \rangle P^2_{n_j \ell_j}(r_j) dr_j \right] P_{n_i \ell_i}(r_i) = \varepsilon_{n_i \ell_i} P_{n_i \ell_i}(r_i) \tag{2.47}$$

which is just the fundamental equation of the Hartree method. Since the $P_{n_i \ell_i}(r_i)$ are one of the factors of the spin orbitals [equation (2.18)] and since the variation does not involve either the spin or the spherical harmonics both of which are orthonormal, equation (2.47) is also true for these spin orbitals, thus:

$$\left[H_o^i + \sum \int \langle H_1^{1,2} \rangle u_j^*(2) u_j(2) dr_j - \int u_i^*(2) H_1^{1,2} u_i(2) dr_i \right] u_i(1) = \varepsilon_i u_i(1) \tag{2.48}$$

where the summation has been extended over all the j's, the term j = i has been subtracted out, and the numbers 1 and 2 are used to denote the electron positions. Equation (2.48) is the wave equation for an electron moving in a spherical potential produced by the nuclear charge of z units and by the spherically averaged charge distribution of all the other electrons. This is just the set of equations which would be derived from Hartree's (1928) original postulate of the self-consistent field.

D. Hartree-Fock Equations

The application of the variational principle to derive Hartree's equations is informative in showing that the equations are not simply the results of Hartree's intuition. However, the wavefunction employed in the Hartree procedure does not meet the necessary requirements of wavefunctions which represent Fermions, since the simple product of one-electron functions does not satisfy the anti-symmetric principle of Dirac (1926). This principle, which is closely connected with Pauli's exclusion principle, relates to the symmetry properties of many electron wavefunctions when the coordinates of two of the electrons are interchanged. The simplest function which will satisfy this anti-symmetry principle is a determinantal function with more complicated examples being linear combinations of determinantal functions. The simplest case

to deal with is a wavefunction consisting of a single determinant which has been shown to apply rigorously to filled shells such as are found in the inert gases (Slater, 1960), and often will be a suitable approximation in other cases. For unfilled shells the potential is not truly spherically symmetric so that a spherical averaging process must be carried out. The single determinant representing a spherically symmetric potential is therefore only an approximation for unfilled shells. The anti-symmetric wavefunction written in the form of a single determinant (for simplicity) is

$$(N!)^{-1/2} \begin{vmatrix} u_1(1) & u_1(2) \ldots u_1(N) \\ u_2(1) & u_2(2) \ldots u_2(N) \\ \ldots\ldots\ldots\ldots \\ \ldots\ldots\ldots\ldots \\ \ldots\ldots\ldots\ldots \\ u_N(1) & u_N(2) \ldots u_N(N) \end{vmatrix} \tag{2.49}$$

The factor $(N!)^{-1/2}$ is just a normalization factor and the required anti-symmetry property follows from the theorem that if two rows or two columns of a determinant are interchanged the determinant changes sign and the interchange of the coordinates and spin of two electrons involves the interchange of the corresponding columns in the determinant. Each of the functions u_i is assumed to be a product of a function of coordinates and a function X^+

or X^- of spin and are called spin-orbitals. Each spin-orbital corresponds to a definite value of m_s. The function X^+ corresponds to $m_s = \frac{1}{2}$ (spin-up) and X^- to $m_s = \frac{1}{2}$ (spin down). All of the spatial functions corresponding to $m_s = \frac{1}{2}$ are assumed to be orthogonal to each other and all those corresponding to $m_s = -\frac{1}{2}$ are assumed orthogonal to each other. It is not necessary to assume that those spatial functions corresponding to $m_s = \frac{1}{2}$ are orthogonal to those corresponding to $m_s = -\frac{1}{2}$ since the spin functions guarantee the orthogonality of spin orbitals with different values of m_s. Furthermore, all spatial functions are assumed to be normalized. These assumptions are sufficient to insure that the determinantal wavefunction(with the same results applicable to sums of determinants)is normalized and that the diagonal matrix components of the Hamiltonian will be given by the sum of the expressions representing the diagonal components of one-electron and two-electron operators (Slater 1960).

The Hartree-Fock method, which will be outlined below, consists of applying the variational principle to the diagonal matrix elements of the Hamiltonian with the subsidiary conditions that the spin-orbitals remain normalized and that any two spin-orbitals associated with the same m_s are orthogonal. The spin-orbitals are varied in order to minimize the average energy (as in the previous section) and since the proper expression for the energy is minimized it is expected that this method would be more accurate than the Hartree method which employs an improper wavefunction and hence minimizes an incorrect average energy expression.

The Hamiltonian for the N electron atom is given by equation (2.1). It is not required that $z = N$ so that ions as well as atoms may be treated. The terminology defined by equations (2.3), (2.4), and (2.5) is employed with the H_1^{ij}s operating on the coordinates of only one electron and the $H_1^{i,j}$'s each operates on the coordinates of two electrons. With this notation the diagonal matrix component of the Hamiltonian is written in the form (neglecting H_2)

$$(H)_{avg} = \sum_i \int u_i^*(1) H_o^1 u_i(1) dv_1 + \sum_{\substack{i,j \\ \text{in pairs}}} \int\int u_i^*(1) u_j^*(2) H_1^{1,2} \, X$$

$$[u_i(1)u_j(2) - \delta m_{s_i} m_{s_j} u_i(2)u_j(1)]dv_1 dv_2 \qquad (2.50)$$

The integration over dv_1 and dv_2 is over spatial coordinates only and the delta function arises because the exchange integral is zero if $m_{s_i} \neq m_{s_j}$ (due to summation over the spins). The numbers 1 and 2 are dummy indices of integration. The Hartree-Fock equations may now be derived by varying the u_i [actually in practice, even for unclosed shells, this is just a variation of $R_{n,\ell}(r)$] in equation (2.50) to minimize the average energy with the conditions that the u_i's are all normalized and any two u_i's associated with the same m_s are orthogonal, that is, the variational principle is used to find the u_i's. These subsidiary conditions are handled by the method of undetermined multipliers.

In the variation of equation (2.50) it is required that

$$\delta \left\{ (H)_{avg} + \sum_i \lambda_{ii} \int u_i^*(1) u_i(1) dv_1 + \sum_{\substack{i,j \\ \text{pair}}} \delta m_{s_i} m_{s_j} \left[\lambda_{ij} \int u_i^*(1) \times \right. \right.$$

$$\left. \left. u_j(1) dv_1 + \lambda_{ji} \int u_j^*(1) u_i(1) dv_1 \right] \right\} = 0 \qquad (2.51)$$

where the sum over i, j is carried and for each pair of electrons and where it has been assumed that

$$\lambda_{ji} = \lambda_{ij}^* \qquad (2.52)$$

so that the last two terms are complex conjugates of each other. This procedure gives the correct number of independent multipliers, that is, one for each subsidiary condition. Then for any variation, which preserves normalization

$$\delta \int u_i^*(1) u_i(1) dv_1 = 0 \qquad (2.53)$$

for each i and if the variation preserves orthogonality

$$\delta \int u_i^*(1) u_j(1) dv_1 = 0 \qquad (2.54)$$

for each pair i and j. This procedure will give

$$\delta (H)_{avg} = 0 \qquad (2.55)$$

which is just what is required. The λ_{ii}'s and λ_{ij}'s, where $j \neq i$ are the undetermined multipliers, with i and j running from 1 to N or over all spin-orbitals of the atom. For a closed-shell atom each spatial orbital will appear twice, once associated with the spin function X^+ and once with X^-. These will correspond to different values of the index i or j. A particular u_i in equation (2.50) may now be varied and if $(H)_{avg}$ is really a minimum it will be a minimum as far as the variation of each u_i is concerned. The quantity $\delta(H)_{avg}$ is given by

$$\delta(H)_{avg} = \int \delta u_i^*(1) H_o^1 u_i(1) dv_1 + \int u_i^*(1) H_o^1 \delta u_i(1) dv_1$$

$$+ \sum_j \iint \delta u_i^*(1) u_j^*(2) H_1^{1,2} [u_i(1)u_j(2) - \delta m_{s_i} m_{s_j} u_i(2)u_j(1)] dv_1 dv_2$$

$$+ \sum_j \iint u_i^*(1) u_j^*(2) H_1^{1,2} [\delta u_2(1)u_j(2) - \delta m_{s_i} m_{s_j} \delta u_i(2)u_j(1)] dv_1 dv_2 \qquad (2.56)$$

which is just (Slater 1960)

$$\delta(H)_{avg} = \int \delta u_i^*(1) \{H_o^1 u_i(1) + \sum_j \int u_j^*(2) H_1^{1,2} [u_i(1)u_j(2)$$

$$- \delta m_{s_i} m_{s_j} u_i(2)u_j(1)] dv_2 \} dv_1 + \text{Complex conjugate} \qquad (2.57)$$

Using equation (2.57) in place of $\delta(H)_{avg}$ in equation (2.51) the variational principle becomes

$$\int \delta u_i^*(1)\{H_o^1 u_i(1) + \sum_j \int u_j^*(2) H_1^{1,2}[u_i(1)u_j(2) - u_i(2)u_j(1)]dv_2$$

$$+ \lambda_{ii}u_i(1) + \sum_{j\neq i} \delta m_{s_i} m_{s_j} \lambda_{ij} u_j(1)\}dv_1 + \text{Complex conjugate} = 0 \qquad (2.58)$$

The left-hand side of equation (2.58) will be zero if the first term is zero. Since the second term is the complex conjugate of the first it will also be zero. The variation $\delta u_i(1)$ is arbitrary and therefore if the first term is to be equal to zero the expression in braces must vanish

$$H_o^1 u_i(1) + \sum_j \int u_j^*(2) H_1^{1,2}[u_i(1)u_j(2) - u_i(2)u_j(1)]dv_2$$

$$+ \lambda_{ii}u_i(1) + \sum_{j\neq i} \delta m_{s_i} m_{s_j} \lambda_{ij} u_j(1) = 0 \qquad (2.59)$$

Combining the last two terms and transposing the resultant term to the right-hand side gives the Hartree-Fock equations

$$H_o^1 u_i(1) + \sum_j \int u_j^*(2) H_1^{1,2}[u_i(1)u_j(2) - u_i(2)u_j(1)]dv_2$$

$$= -\sum_j \lambda_{ij} u_j(1) \qquad (2.60)$$

These Hartree-Fock equations are very similar to those obtained by the simple Hartree procedure (disregarding the spherical averaging procedure) [equation (2.48)] and in fact there are

only two types of differences in the equations. The first difference is in the right-hand side of equation (2.60). The simple Hartree procedure results in only one term $i = j$ and with λ_{ii} replaced by ε_i. This discrepancy can be eliminated(for the case of filled shells only)by making a unitary transformation of the u_i's (Slater, 1960). Such a transformation leaves the determinantal function unchanged since it follows from the theory of determinants that a determinant whose rows or columns are found from those of another determinant by a unitary transformation is identical to the original determinant except for a constant multiplicative factor whose absolute value is unity. The parameter λ_{ii} (or ε_i) has been shown (Koopmans, 1933) to represent the energy required to remove the i^{th}electron from the atom, assuming that the orbitals for the ion are the same as for the atom (i.e., frozen core approximation). The second difference is in the second term of the summation over j on the left-hand side of equation (2.60). Of these terms

$$-\sum_j \left[\int u_j^*(2) H_1^{1,2} u_i(2) dv_2\right] u_j(1) \qquad (2.61)$$

only the $j = i$ term is present in equation (2.48). These terms [equation (2.61)] are the exchange terms and are the only real difference between the Hartree-Fock and the Hartree equations. It is therefore necessary to inquire into the physical meaning of these exchange terms. Equation (2.60) may be rewritten as

$$H_o^1 u_i(1) + \left[\sum_j \int u_j^*(2) H_1^{1,2} u_j(2) dv_2\right] u_i(1) - \left[\sum_j \delta m_{s_i} m_{s_j} \int u_j^*(2) \times H_1^{1,2} u_i(2) dv_2\right] u_j(1) = -\sum_j \delta m_{s_i} m_{s_j} \lambda_{ij} u_j(1) \quad (2.62)$$

If equation (2.62) is multiplied and divided by $u_i^*(1)u_i(1)$ it takes the form

$$H_o^1 u_i(1) + \left[\sum_j \int u_j^*(2) H_1^{1,2} u_j(2) dv_2\right] u_i(1) - \left[\sum_j \delta m_{s_i} m_{s_j} \frac{\int u_i^*(1) u_j^*(2) H_1^{1,2} u_j(1) u_i(2) dv_2}{u_i^*(1) u_i(1)}\right] u_i(1) = -\sum_j \delta m_{s_i} m_{s_j} \lambda_{ij} u_j(1) \quad (2.63)$$

Equation (2.63) shows that u_i is a solution of Schrödinger's equation with a Hamiltonian operator which is just the sum of the kinetic energy, the potential energy in the field of the nucleus (H_o^1 term), the potential energy in the field of N electrons distributed in the orbitals occupied in the determinantal wave-function (first term involving $H_1^{1,2}$) minus a correction term (second term involving $H_1^{1,2}$). The correction term involves the exchange integrals and it is this term which requires interpretation. Slater (1960) points out that the correction term may be regarded as representing the potential energy, at position

1 of the electron in question, of a charge distribution at point 2 of magnitude

$$\sum_j \delta_{m_{s_i} m_{s_j}} \frac{u_i^*(1)u_j^*(2)u_j(1)u_i(2)}{u_i^*(1)u_i(1)} \tag{2.64}$$

This charge density is called the exchange charge density due to its connection with the exchange terms in equation (2.63). Slater (1960) proves three properties of the exchange charge density. First, its total amount is one electronic charge (unity in atomic units) if u_i is one of the occupied spin-orbitals but is zero if u_i is an unoccupied spin-orbital. The proof is straightforward requiring the integration of equation (2.64) over dv_2. Since the u_i's and u_j's are orthogonal all terms in the summation are zero except $i = j$ which is unity if u_i is an occupied spin-orbital. If u_i is an unoccupied spin-orbital there is no $i = j$ term and the summation is zero.

The second property of the exchange charge density is that it consists of electronic charge having the same spin as the spin-orbital u_i whose wavefunction is being determined. This follows immediately from the delta function $\delta_{m_{s_i} m_{s_j}}$. The third property is that if point 2 is identical with point 1, then the exchange charge density reduces to

$$\sum_j \delta_{m_{s_i} m_{s_j}} u_j^*(1)u_j(1) \tag{2.65}$$

or the total density of all electrons of the same spin as the i^{th}, at position 1. These three properties allow the general nature of the exchange charge density and its physical significance to be determined.

Thus, the Hartree-Fock equations, as written in equation (2.63), show that the potential energy of the field in which the electron moves is the potential due to the nuclei plus the potential from all electrons of spin opposite to that of the electron under consideration, plus the potential from a charge distribution of electrons of the same spin as the electron under consideration and equal to the total charge of these electrons,minus the exchange charge density. The charge distribution of electrons of the same spin as the one considered adds up to one less than the total number of electrons of this spin for an occupied orbital and it includes all the electrons of that spin for an unoccupied orbital. For the occupied orbitals, the net charge density of electrons having the same spin as the electron under consideration, when corrected for the exchange charge, goes to zero at point 1 where the electron under consideration is located since when point 2 coincides with point 1 the exchange charge density cancels the total density of all electrons of this same spin. In other words the electron tends to keep other electrons, having the same spin as it, away. Thus the effect of the exchange terms is to remove electronic charge from the immediate vicinity of the electron whose wave function is being considered. This removal is more

effective with the Hartree-Fock method than with Hartree's original method. This has the effect of lowering the potential energy in the Hartree-Fock method so that it is expected that the one-electron energy parameter $\varepsilon_i = \lambda_{ii}$ would be lower in the Hartree-Fock method than the Hartree method. This lowering of the potential energy may also have an appreciable effect on the wavefunction. Such an effect is observed in that the Hartree-Fock equations, as compared to the Hartree equations, concentrate the charge density more at small values of r (Slater, 1960).

Equation (2.60) has N solutions representing the N spin-orbitals occupied in the determinantal wavefunction which represents the state of the N electron atom. An infinite number of solutions to equation (2.60) can be found which represent the unoccupied spin-orbitals. It has also been shown (Slater, 1960) that all solutions of the Hartree-Fock equations are orthogonal and when normalized they form a complete set of orthogonal spin-orbitals in terms of which an arbitrary function of coordinates and spin may be expanded. The above results (except for the unitary transformation for the λ_{ij}'s) do not depend on the fact that a central field problem (or a closed shells) is being considered but only on the fact that a determinantal wavefunction is being used. Energies are found in this approximation by solving equation (2.60) numerically and calculating H_{avg}.

It was first pointed out by Dëlbruck (1930) and later proven more explicitly by Roothaan (1951) using group theory, that for an atom which has all of its electrons in closed (completely

filled) shells the Hartree-Fock one-electron orbitals u_i must have the form of solutions of a central-field problem so a single determinant is appropriate. For this case Hartree's assumption of a spherical average is not necessary as the spherical behavior necessary for using the solution u_i comes about automatically. For nonclosed shells this is not the case and a spherically averaging process must be carried out in order to get one electron orbitals of the central field type. This procedure has been carried out (Brown, 1933; Hartree and Hartree, 1935; see Slater, 1960, for a discussion of this point) and is shown to be the result of just the variation of the radial part of the one electron orbitals (exactly as outlined in the above discussion). The two-electron integrals are however much more complicated for unfilled shells (and when a spherical average is not performed as in the simple Hartree case) (see Slater 1960 p. 310). Thus the best solutions of the spherically symmetric problem are obtained even when it is not actually spherically symmetric (i.e., the u_i's are not really appropriate). This is however, a good approximation since in most cases the potential is <u>almost</u> spherically symmetric. The Hartree-Fock procedure requires a considerable amount of computational time as each term ($\vec{L}$ and $\vec{S}$ specified) of a given configuration requires a separate calculation and it has only been through the use of electronic computer that other than simple problems can be handled.

E. Calculations

The calculations of the Hartree-Fock wavefunctions for this investigation were carried out with the Hartree-Fock computer program developed by C. Froese (Fischer) (1965) on the C.D.C. 6600 computer at NASA's Langley Research Center, Hampton, Virginia. This program calculates the spin-orbital functions, the total energy of the term, as well as the radial spin-orbit interaction parameter

$$\zeta_{n\ell} = \int P_{n\ell}(r)\xi(\vec{r})P_{n\ell}(r)dr \qquad (2.66)$$

where $\xi(\vec{r})$ is defined in section A.

The program also employs the configuration interaction representation which is an extension of the Hartree-Fock method. In this representation the total wavefunction is expanded in terms of the determinantal wavefunctions associated with more than one configuration although for the calculations performed this representation was not needed.

Initial estimates of the term energy, wavefunction and the initial slope of the wavefunction were obtained from the Hartree-Fock-Slater program of Herman and Skillman (1963) which employs a modified Hartree-Fock procedure with the exchange potentials for different occupied orbitals replaced by a universal exchange potential formed by using an exchange charge density taken from

the case of a free-electron gas. The exchange correction is then written as a constant multiplied by the cube root of the change density and therefore eliminates the necessity of computing an integral from the exchange charge density (Slater, 1951). The program also employs a single determinantal wavefunction built up of the one-electron spin orbitals. Furthermore, multiplet structure is ignored so that the energy obtained from the wavefunction is just an average energy of the configuration. These results, however, do make very good initial estimates for the more complicated Hartree-Fock program.

The wavefunctions obtained from the Hartree-Fock program were punched onto data cards and were employed to calculate the transition probabilities of the doubly excited states of interest. The transition probability between an upper level with total angular momentum $\vec{J}$ and a lower level with total angular momentum $\vec{J}'$ is given by (Garstang, 1969)

$$A(J \to J') = \frac{2.677 \times 10^9 \, (E_{JJ'})^3 S}{2J + 1} \text{ sec}^{-1} \qquad (2.67)$$

where $E_{J,J'}$ is the energy difference of the levels in Rydbergs, S is the absolute line strength for electric dipole radiation in atomic units

$$S^{1/2}(SLJ - S'L'J') = [(2J + 1)(2J' + 1)]^{1/2} W(LJL'J':S^1)(L||r^{(1)}||L')\delta_{SS'} \qquad (2.68)$$

for a transition from the level SLJ to the level S'L'J'. W is a Racah coefficient and the matrix element of the first order tensor $r^{(1)}$ is in reduced form. The reduced matrix element of the first order tensor $r^{(1)}$ may be evaluated in terms of the one-electron wavefunctions (Shore and Menzel, 1965).

$$(\ell_1\ell_2 L||r^{(1)}||\ell_1'\ell_2'L') = (-1)^{\ell_2+1-\ell_1'-L}(2L+1)^{1/2}(2L'+1)^{1/2}\delta\ell_2\ell_2'$$

$$(n)^{1/2}(\ell^n\{|\ell^{n-1}) \times W(\ell_1 L\ell_1'L';\ell_2 1)(\ell_1||r^{(1)}||\ell_1') \qquad (2.69)$$

where n is the number of equivalent electrons (n = 1 for no equivalent electrons) and $(\ell^n\{|\ell^{n-1})$ is the coefficient of fractional parentage. For two equivalent electrons the coefficient of fractional parentage is unity. This is the only possibility for the case being considered (two electron ions). The reduced one-electron matrix element has only two nonzero values (Garstang, 1969)

$$(\ell||r^{(1)}||\ell+1) = -[(\ell+1)(2\ell+1)(2\ell+3)]^{1/2}\sigma \qquad (2.70)$$

and

$$(\ell||r^{(1)}||\ell-1) = +[\ell(2\ell-1)(2\ell+1)]^{1/2}\sigma \qquad (2.71)$$

with

$$\sigma = \frac{1}{(4\ell_>^2 - 1)^{1/2}} \int_0^\infty r P_{n\ell}(r) P_{n'\ell'}(r') dr \qquad (2.72)$$

where ℓ is the greater of the two ℓ's involved in the integral. The Hartree-Fock wavefunctions were employed to numerically evaluate the integral in equation (2.72) using a computer program developed by Shamey (1970). The absorption oscillator strength $f(J' \rightarrow J)$ is given in terms of the absolute line strength by (Aller, 1963)

$$f(J',J) = \frac{303.7}{g\lambda} S(SLJ - S'L'J') \qquad (2.73)$$

where λ is the wavelength in Angstron unit. The quantity g $(g = 2J' + 1)$ is the statistical weight of the lower state and $g\, f(J',J)$ is often the quantity tabulated.

The numerical calculations indicate that the three ions of interest are in good LS coupling since the spin-orbit splitting of the terms was very small compared to the separation of the terms.

The wavefunctions and total energies of the ground state, singly excited and doubly excited states of the two-electron ions, boron IV, carbon V, and nitrogen VI were calculated with the Hartree-Fock program and the energy difference between terms for which electron dipole transitions were allowed was converted to wavelengths. Terms rather than levels were used since all levels

in a given term were assigned the same energy. In order to determine an order of magnitude error involved in the calculated wavelengths the energies of the singly excited states and ground state were used to calculate wavelengths of observed transitions in the two-electron ions of interest. These calculated values are compared with the observed values in table II.1. The observed values are taken from the listing of Kelly (1968). The calculated wavelengths are generally in very good agreement (< 0.5 percent error) with the observed values with the exception of transitions having 1snd ^1D as an upper term where the error is much larger (up to about 3 percent). The calculated wavelengths were in sufficiently good agreement with the observed values that including the effects of configuration interaction would not improve the agreement sufficiently to justify the rather large amount of labor involved. Wavelengths of electric dipole transition between the doubly excited and singly excited terms were then calculated in the above manner. The transition, wavelength, calculated absolute f value, and relative f value in the multiplet, are listed in table II.2. The wavelength, absolute f value, and relative f value for the hydrogen-like and helium-like resonance lines of each ion are also listed. While the calculated energy difference of the various terms of the singly excited states agrees rather well with the observed values, this is not the case for the oscillator strengths and resulting transition probabilities. The transition

probabilities for the helium-like resonance line is larger by a factor of 1.6 for boron IV,up to a factor of 7 for nitrogen VI when compared with the transition probabilities of Dalgarno and Parkinson (1967). These authors obtained oscillator strengths for the resonance transition of helium-like ion by expanding the electric dipole matrix elements connecting the $1s^2\ ^1S$ and $1s2p\ ^1P$ states in inverse powers of the ionic charge Z. By comparing their method with the Hartree-Fock approximation they find that the matrix element which they obtain differs from the Hartree-Fock approximation by one term which they regard as a virtual dipole excitation of the passive 1s electron plus a distortion due to the dynamic polarization of the 1s orbital at the 1s - 2p transition frequency. They further show the necessary correction to the Hartree-Fock approximation consists of mixing the $(1s^2)^1S$ and $(\alpha pnp)^1S$ configurations with αp representing the polarized 1s orbital. Consequently, it is expected that the calculated transition probabilities for the doubly excited states are too large and are only accurate to an order of magnitude.

Table II.1

Transition	λ, Calculated Å	λ, Observed Å	Δλ Å
$1s^2\ {}^1S_0 - 1s2p\ {}^1P^o_1$	40.523	40.270	+0.253
$1s^2\ {}^1S_0 - 1s3p\ {}^1P^o_1$	35.060	34.973	+0.087
$1s^2\ {}^1S_0 - 1s4p\ {}^1P^o_1$	33.483	33.426	+0.057
$1s2s\ {}^3S_1 - 1s3p\ {}^3P^o_{2,1,0}$	227.423	227.220	+0.203
$1s2s\ {}^3S_1 - 1s4p\ {}^3P^o_{2,1,0}$	173.468	173.270	+0.198
$1s2p\ {}^3P^o_1 - 1s4d\ {}^3D_2$	187.056	186.720	+0.354
$1s2p\ {}^1P^o_1 - 1s3d\ {}^1D_2$	258.954	267.260	-8.306
$1s2p\ {}^1P^o_1 - 1s4d\ {}^1D_2$	192.475	197.020	-4.845

TABLE II.2

	Boron			Carbon			Nitrogen		
Transition	λ, Å	f_{abs}	f_{rel}	λ, Å	f_{abs}	f_{rel}	λ, Å	f_{abs}	f_{rel}
$1s^2S_{1/2} - 2p^2P^o_{3/2}$	48.587	0.278	0.65	33.736	0.278	0.65	24.781	0.278	0.65
$1s^2\ ^1S_0 - 1s2p\ ^1P^o_1$	60.313	0.609	7.1	40.270	0.647	4.56	28.787	0.674	59.5
$1s3p\ ^1P^o - 2p3p\ ^1D$	48.743	0.0235	10.3	33.849	0.117	15.0	24.879	0.178	20.6
$1s3p\ ^3P^o - 2p3p\ ^3P*$	48.872	0.0077	3.38	33.939	0.0322	4.12	24.944	0.0486	5.6
$1s3s\ ^3S - 2p3s\ ^3P^o$	49.002	0.0076	3.34	34.029	0.0393	4.85	25.001	0.060	7.0
$1s3s\ ^1S - 2p3s\ ^1P^o$	49.006	0.0142	6.2	34.032	0.070	9.0	25.014	0.106	12.25
$1s3p\ ^3P^o - 2p3p\ ^3S$	49.084	0.00465	2.06	34.086	0.0232	2.97	25.053	0.035	4.05
$1s2p\ ^1P^o - 2p^2\ ^1S$	49.140	0.496	1.38	34.125	2.10	5.28	25.082	0.252	7.8
$1s3p\ ^3P^o - 2p3p\ ^3D$	49.180	0.00213	0.92	34.153	0.0106	1.38	25.102	0.016	1.85
$1s3p\ ^1P^o - 2p3p\ ^1P*$	49.316	0.00117	0.514	34.247	0.0595	0.77	25.172	0.0906	10.5
$1s2s\ ^1S - 2s2p\ ^1P^o$	49.575	0.1415	6.12	34.427	0.253	0.887	25.304	0.011	108
$1s2p\ ^1P^o - 2p^2\ ^1D$	49.884	0.0824	2.30	34.586	1.150	3.2	25.421	1.180	36.4
$1s2s\ ^3S - 2s2p\ ^3P^o$	49.946	0.0745	7.54	34.685	1.08	110.0	25.493	0.128	466
$1s2p\ ^3P^o - 2p^2\ ^3P*$	50.118	1.140	8.6	34.804	1.650	124.0	25.581	0.240	640

CHAPTER III

Atomic Processes and Plasma Models

A. Ionization Processes and Rate Equations

For many astrophysical as well as laboratory plasmas, thermodynamic equilibrium is never achieved and, consequently, an analysis of the emitted radiation requires a knowledge of the rates at which the various atomic processes take place. The rates of ionization and recombination as well as the population and depopulation of the various atomic states are of importance.

Let $X^{Z-1}(p)$ and $X^{Z}(i)$ denote two successive stages of ionization of an atom X with number density $n^{Z-1}(p)$ and $n^{Z}(i)$ per cm^{-3}. The superscript $Z - 1, Z$ represents the ionic charge of the atom and the ionization potential of the pth state of X^{Z-1} is denoted by I_p ($I_p = \frac{Z^2}{p^2} E_H$ for hydrogenic ions). The letters p or i represent an arbitrary level of the atom with statistical weight $g(p)$, $g(i)$. Free electrons e, having number density $n_e cm^{-3}$ are also present in the plasma and a radiation field of intensity $I(\nu)$ at the frequency ν may also be present. The reversible process

$$X^{Z-1}(p) \underset{\leftarrow}{\overset{\rightarrow}{}} X^{Z}(i) + e \qquad (3.1)$$

with the left to right process ionization and the right to left processes recombination may now be considered. Ionization by electron collisions

$$X^{Z-1}(p) + e \underset{\leftarrow}{\rightarrow} X^{Z}(i) + e + e \qquad (3.2)$$

has as its inverse three body recombinations. If $K(p,c)$ is the rate coefficient for collisional ionization then the rate at which ionization takes place is

$$n_e n^{Z-1}(p) K(p,c) \text{cm}^{-3}\text{sec}^{-1} \qquad (3.3)$$

and the rate at which three body recombination takes place is

$$n_e^2 n^{Z}(i) K(c,p) \text{cm}^{-3}\text{sec}^{-1} \qquad (3.4)$$

The rate coefficient $K(p,c)$ has been evaluated by Jefferies (1968) using an expression due to Fowler (1955), a Maxwellian velocity distribution for the free electrons and a dipole approximation cross section for the process derived by Seaton (1962). Those approximations, although quite crude, will be sufficient for the investigation considered here. He obtains the relation (in cgs units)

$$K(p,c) = 1.55 \times 10^{13} \frac{\bar{g}_i A(p) (kT_e)^{1/2}}{I_p} \exp(-I_p/kT_e) \text{cm}^{3}\text{sec}^{-1} \qquad (3.5)$$

where $A(p)$ is the photoionization absorption cross section at threshold of the level p, $\bar{g}_i$ is a scaling factor whose value depends on the charge of the atom ($\bar{g}_i = 0.3$ for $Z - 1 > 2$) and T_e is the electron temperature in ^{o}K.

The rate coefficient for three body recombination $K(c,p)$ is related to the rate coefficient for collisional ionization $K(p,c)$ by the relationship (Jefferies, 1968)

$$K(c,p) = 2.06 \times 10^{-16} \frac{g(p)K(p,c)}{U^Z(T_e)T_e^{3/2}} \exp(-I_p/kT_e)\,cm^6 sec^{-1} \qquad (3.6)$$

where $U^Z(T_e)$ is the partition function of the atom X^Z and the free electrons have a Maxwellian velocity distribution. Because of the dependence of I_p on p^2 and the statistical weight $g(p)$, $K(c,p)$ may become very large near the series limit. The inverse temperature dependence will cause $K(c,p)$ to decrease with increasing temperature, so that, for recombination into the first few excited levels of an atom at very high temperature the rate coefficient should be small.

Photoionization may also occur with its inverse, radiative recombination

$$X^{Z-1}(p) + h\nu \rightleftarrows X^Z(i) + e \qquad (3.7)$$

where $h\nu$ represents a photon of frequency ν. The rate of photoionization is

$$n^{Z-1}(p)R(p,c)\,cm^{-3}sec^{-1} \qquad (3.8)$$

where the rate coefficient $R(p,c)$ is (Jefferies 1968)

$$R(p,c) = 4\pi \int_{\nu_o}^{\infty} \frac{I(\nu)\alpha(\nu)d\nu}{h\nu} \text{ sec}^{-1} \qquad (3.9)$$

The absorption coefficient $\alpha(\nu)$ at the frequency ν is related to the optical depth $\tau(\nu)$ (Cooper, 1966)

$$d\tau(\nu) = -\alpha(\nu)dx \qquad (3.10)$$

where dx is an element of length along the line of sight. Plasmas for which $\tau(\nu) << 1$ are called optically thin at the frequency ν while those for which $\tau(\nu) \geq 1$ are referred to as optically thick at the frequency ν. Photoionization is therefore unimportant in optically thin plasmas as a photon will not be absorbed.

The rate at which the inverse process, radiative recombination, into the level p occurs is

$$n_e n^Z(i)R(c,p)\text{cm}^{-3}\text{sec}^{-1} \qquad (3.11)$$

The rate coefficient into a hydrogenic level p having a photoionization cross section $A(p)$ and a threshold ionization energy I_p is (Seaton 1959)

$$R(c,p) = \frac{1}{c^2}\sqrt{\frac{2}{\pi}} \frac{2p^2}{(mkT_e)^{3/2}} \exp(I_p/kT_e) \int_{I_p}^{\infty} (h\nu)^2 A(p) \exp(-\frac{h\nu}{kT_e}) d(h\nu) \text{ cm}^3\text{sec}^{-1} \qquad (3.12)$$

Radiative recombination depends on the electron temperature but its inverse does not.

In multi-electron atoms or ions doubly excited states having energies above the first ionization potential of the atom or ion are possible. These doubly excited states, subject to certain selection rules, may undergo a radiationless transition

$$X^{Z-1}(d) \underset{\leftarrow}{\overset{\rightarrow}{}} X^{Z}(i) + e \tag{3.13}$$

where d represents the doubly excited state. This process is known as autoionization and the selection rules are just those previously discussed for matrix elements of the operator H_1 to be non-zero, that is, the two states [right and left side of equation (3.1)] must have the same total angular momentum $\vec{J}$ (in LS coupling the same $\vec{L}$ and $\vec{S}$), the same parity and the same energy E. The rate at which autoionization occurs is

$$n^{Z-1}(d)A^{a}(d,c)\,cm^{-3}sec^{-1} \tag{3.14}$$

where $A^{a}(d,c)$ in the autoionization transition probability. The transition probability may often be quite high ($\sim 10^{13} - 10^{14}$ sec^{-1}) (Cooper 1966). The inverse process (right to left in equation (3.1)) is called inverse autoionization and occurs at a rate

$$n_e n^{Z}(i)A^{a}(c,d)\,cm^{-3}sec^{-1} \tag{3.15}$$

The movement of the electron from the continuum to the discrete doubly excited state leads to a transient recombination since autoionization maintains a quasi-equilibrium in which the number density of doubly excited states $n^{Z-1}(d)$ is small. If true recombination is to occur the doubly excited states must become immune to autoionization. Therefore it is necessary to discuss the process by which excited states (either singly or doubly excited) are formed and de-excited.

B. Bound-Bound Transitions and Rate Equations

An atom of charge Z having energy levels p,q with statistical weights g(p), g(q), an energy separation E(p,q), absorption oscillator strength f(p,q), and with the level p lying below q is considered. The index q may be either a doubly-excited or a singly excited level and p then represents either a singly excited or unexcited level (or a lower doubly excited level) respectively.

Electrons may be excited into a higher state by electron collisions

$$n^Z(p) + e \underset{\leftarrow}{\rightarrow} n^Z(q) + e \tag{3.16}$$

at a rate

$$n_e n^Z(p) K(p,q) \text{cm}^{-3}\text{sec}^{-1} \tag{3.17}$$

In high-temperature plasmas the excitation of ions rather than neutral atoms is important. An expression for the excitation of ions has been derived by Seaton (1962) in the Born approximation

$$K(p,q) = \frac{6.5 \times 10^{-4}}{E(p,q)T_e^{1/2}} f(p,q)\exp(- E(p,q)/kT_e)cm^3sec^{-1} \quad (3.18)$$

The inverse process is collisional de-excitation and is just the right to left process of equation (3.16). The rate at which collisional de-excitation from the level q to the level p occurs is

$$n_e n^Z(q)K(q,p)cm^{-3}sec^{-1} \quad (3.19)$$

where the collisional de-excitation coefficient $K(q,p)$ is related to the excitation coefficient by (McWhirter, 1965)

$$K(q,p) = \frac{g(p)}{g(q)} K(p,q)\exp(E(p,q)/kT_e)cm^3sec^{-1} \quad (3.20)$$

If a radiation field is present in the plasma, photoexcitation will occur if the plasma is not optically thin

$$X^Z(p) + h\nu \rightarrow X^Z(q) \quad (3.21)$$

The rate at which this photoexcitation takes place is (Jefferies, 1968)

$$n^Z(p)I(\nu)B(p,q)cm^{-3}sec^{-1} \tag{3.22}$$

where $I(\nu)$ is the intensity of the radiation field at the frequency ν and $B(p,q)$ is the Einstein transition probability for absorption. The inverse process of photoexcitation is radiative de-excitation

$$X^Z(q) \rightarrow X^Z(p) + h\nu \tag{3.23}$$

and is actually two processes, spontaneous emission with a rate

$$n^Z(q)A(q,p)cm^{-3}sec^{-1} \tag{3.24}$$

and stimulated emission with a rate

$$n^Z(q)B(q,p)I(\nu)cm^{-3}sec^{-1} \tag{3.25}$$

In practice, stimulated emission is treated as negative absorption so that the two processes which depend on the intensity of the radiation field are lumped together as a single process with a single rate coefficient.

C. Doubly Excited States and Dielectronic Recombination

The two step process consisting of inverse autoionization to form the doubly excited state followed by radiative decay of the

doubly excited state to a singly excited state is called dielectronic recombination and is the process of interest in this investigation since the radiative decay of the doubly excited state in a two electron atom will produce a photon that is of a slightly lower energy than the corresponding transition in the one electron atom and should therefore produce satellites to the hydrogen-like lines. If the probability of a radiative transition from the doubly excited state to a lower stable state is $A^s(d,p)$ then the rate at which the doubly excited state is depopulated by this process is

$$n^{Z-1}(d)A^s(d,p)\,cm^{-3}sec^{-1} \tag{3.26}$$

The rate coefficient for dielectronic recombination is denoted by $K_d(c,p)$ and the rate at which dielectronic recombination occurs is (Bates and Dalgarno, 1962)

$$n_e n^Z(i)K_d(c,p) \tag{3.27}$$

Figure 1 is a schematic of the various processes involved in dielectronic recombination and is useful in determining an expression for $K_d(c,p)$. The processes are:

#1. Spontaneous decay - rate given by equation (3.24)

#2. Autoionization - rate given by equation (3.14)

#3. Inverse Autoionization - rate given by equation (3.15)

Equating the rate into the doubly excited state with the rate out of the state

$$n^{Z-1}(d)[A^s(d,p) + A^a(d,c)] = n_e n^Z A^a(c,d) \quad . \tag{3.28}$$

The coefficient for inverse autoionization may be related to the equilibrium value of $n^{Z-1}(d)$ by detail balance and using full thermodynamic equilibrium.

Thus

$$n_E^{Z-1}(d)A^a(d,c) = n_e n^Z A^a(c,d) \quad . \tag{3.29}$$

Substituting for $n_e n^Z A^a(c,d)$ in equation (3.28)

$$n^{Z-1}(d) = n_E^{Z-1}(d) \frac{A^a(d,c)}{A^a(d,c) + A^s(d,p)} \text{ cm}^{-3} \quad . \tag{3.30}$$

The rate of stabilization of the doubly excited state is given by equation (3.26) and $n_E(d)$ is the number density in SAHA equilibrium (which will be discussed in the next section). Equating equation (3.27) with equation (3.26) (i.e. setting the rate of dielectronic recombination equal to the rate of stabilization of the doubly excited states)an expression for the rate coefficient is obtained

$$K_d(c,p) = \frac{n^{Z-1}(d)A^s(d,p)}{n^Z(i)n_e} \text{ cm}^3\text{sec}^{-1} \tag{3.31}$$

$$= \frac{n_E^{Z-1}(d)}{n^Z_{(i)}n_e} \frac{A^a(d,c)A^s(d,p)}{A^a(d,c) + A^s(d,p)} \text{ cm}^3\text{sec}^{-1}$$

where equation (3.30) has been substituted for $n^{Z-1}(d)$. Using the expression for Saha equilibrium (see the next section) the expression becomes (Bates and Dalgarno, 1962)

$$K_d(c,p) = \frac{A^a(d,c)A^s(d,p)}{A^a(d,c) + A^s(d,p)} \cdot \frac{g(d)}{2U^Z(T_e)} \frac{h^3}{(2\pi mkT_e)^{3/2}} \exp\left\{ - \frac{\varepsilon_s}{kT_e} \right\} \quad (3.32)$$

where ε_s is the amount of energy by which the doubly excited state exceeds that of the state (i). The state (i) is normally taken to be the ground state.

The doubly excited state may also be collisionally de-excited [equation (3.19)] and the conditions under which this is important must be examined since if collisional de-excitation competes with radiative the above arguments are no longer valid. The collisional de-excitation rate coefficient for a state may be expressed in terms of the lifetime of the state to radiative decay $\tau_r(d,p)$ (Bates and Dalgarno, 1962)

$$K_c(d,p) = b[10^{-29} \lambda^4/\tau_r(d,p)]cm^3sec^{-1} \quad (3.33)$$

where the parameter b is a characteristic of the process and is of order unity and λ is the wavelength of the emitted photon in Angstroms. The lifetime of the doubly excited state toward collisional de-excitation is (Bates and Dalgarno, 1962)

$$\tau_c(d,p) = 1/K_c(d,p)n_e \quad sec. \quad (3.34)$$

Substituting in equation (3·33) the ratio of collisional to radiative lifetime is obtained

$$\frac{\tau_c(d,p)}{\tau_r(d,p)} = 10^{29}/b\ \lambda^4 n_e \qquad (3.35)$$

The ratio becomes unity for $\lambda = 30$ Å and $b = 1$ if $n_e = 10^{23}$ cm^{-3}. Thus at high electron densities collisional stabilization of the doubly excited states may become important. At the electron densities encountered in this investigation ($n_e = 2.2 \times 10^{17}$ cm^{-3}) stabilization by radiative decay should dominate. It should not be concluded however, that collisional processes between the doubly excited states are unimportant.

Processes involving atom-atom, atom-ion, and ion-ion collisions have rates which are much smaller than those involving electron collisions if the degree of ionization of the plasma exceeds a few percent. These various processes have therefore been ignored as their contribution would be extremely small.

D. Equilibrium Relationships and Detail Balance

If multielectron atoms are present in the plasma, more than one stage of ionization is possible and the various processes must be considered in and between the various stages. The general procedure to obtain the population density of the various quantum states consists of setting up the rate equations for the various processes

which have been discussed and solving them simultaneously. In general, this is a laborious and time-consuming job and, in many cases, a complete solution is impossible to obtain due to the number of states involved. In complete thermodynamic equilibrium, each of the processes discussed is just balanced by its inverse. In other words, the pairs of processes occur in detailed balance. In this situation, the distribution between two stages of ionization n^Z and n^{Z-1} is given by Saha's equation

$$\frac{n_e n^Z}{n^{Z-1}} = 2 \left[\frac{2\pi m k T_e}{h^2}\right]^{3/2} \frac{U^Z(T_e)}{U^{Z-1}(T_e)} \exp\left(-\varepsilon^{Z-1}/kT_e\right) \qquad (3.36)$$

where the $U(T_e)$'s are the partition functions of the two atoms or ions and ε^{Z-1} is the ionization potential of the atoms n^{Z-1}. The population density of the state q of the ion n^Z is related to the total number density of n^Z by the Maxwell-Boltzmann equation (Cooper, 1966).

$$\frac{n^Z(q)}{n^Z} = \frac{g(q)}{U^Z(T_e)} \exp\left(-E(q,p)/kT_e\right) \qquad (3.37)$$

Furthermore, the free electrons have a Maxwellian velocity distribution and all distributions are characterized by a single temperature T.

In astrophysical and laboratory plasmas, complete thermodynamic equilibrium is almost never obtained. There are, however, two

regimes where useful approximations can be made. If the plasma density is sufficiently high, then collisional effects will completely dominate radiative effects and detail balance will be obtained between the collisional rates. The distribution of electrons among the various energy levels is the same as it would be if the system were in complete thermodynamic equilibrium. Although the plasma temperature and density may vary in space and time, the distribution of electrons (both bound and free) depends entirely on local values of temperature, density, and chemical composition of the plasma, and hence this regime is called local thermodynamic equilibrium (LTE). In plasmas, this equilibrium is characterized by the electron temperature T_e, since it is the electrons which dominate the collisional processes. In order for radiative decay rates to cause less than a 10 percent departure from LTE, the collisional rates must be at least about 10 times the radiative rates (McWhirter, 1965). This problem has been considered in detail by Wilson (1962), Griem (1963), and McWhirter (1965). Each of these authors arrived at essentially the same expression for the electron density required for the collisional de-excitation rates to exceed the radiative decay rate of a particular level with excitation energy $E(p,q)$ by a factor of 10, namely

$$n_e \geq C\, T_e^{\frac{1}{2}}\, E^3(p,q)\ \text{cm}^{-3} \qquad (3.38)$$

The three authors arrive at different values for the constant C although all three values agree to within a factor of 2. The values of C are 9.2×10^{11} (Griem), 1.3×10^{12} (Wilson), and 1.6×10^{12} (McWhirter). The inequality expressed in equation (3.38) is a necessary but not a sufficient condition for a plasma to be in LTE. The necessary and sufficient condition for the plasma to be in LTE requires in addition that the lifetime of the plasma exceed the relaxation time of the slowest collisional processes of importance (Griem 1964). This condition is often not fulfilled in laboratory plasmas.

If the plasma density is sufficiently low, radiative rates become important and may dominate some of the collisional processes. If the plasma is also optically thin, collisional ionization and excitation may be balanced by radiative and dielectronic (although this term was not originally included) recombination and spontaneous decay. This is the model which has been proposed to explain some features of the solar corona (Wooley and Stibbs, 1953; Elwert, 1952) and is often referred to as the coronal approximation. The state of ionization in a plasma in coronal equilibrium is determined by balance between collisional ionization from the ground state and radiative and dielectronic recombination. Radiative recombination into all levels is included, since recombination into an excited level is immediately followed by spontaneous emission to a lower level. Since the total transition probability

$$A(q) = \sum_{p<q} A(q,p) \qquad (3.39)$$

from the excited level q is large (at least if q is not too large as there will always be some q for which this is not true), the lifetime of the state toward radiative decay is small ($\tau = A^{-1}(q)$). If the time between collision is longer than the lifetime of the level (e.g., low density plasma) collisional excitation from the ground state only needs to be considered, since the population of the excited levels will be small. At equilibrium

$$n_e n^{Z-1}(1)K(1,c) = n_e n^{Z}(1) \sum_{p} [R(c,p) + K_d(c,p)] \qquad (3.40)$$

so that

$$\frac{n^{Z}(1)}{n^{Z-1}(1)} = \frac{K(1,c)}{\sum_{p} [R(c,p) + K_d(c,p)]} \qquad (3.41)$$

which is independent of the electron density and is a function of electron temperature only. The ratio n^Z/n^{Z-1} depends critically on the cross sections for the processes so that the accuracy of the calculated values of the ratio will be determined by the accuracy of the cross section used.

Post (1961) has calculated relative abundances of some common impurity ions in laboratory plasmas using approximate cross sections for hydrogenic (one electron) and lithium-like (three electron) ions. His results indicate that Saha's equation does not accurately predict the ratio n^Z/n^{Z-1} in the coronal regime and that at extremely high temperatures heavy ions may exist without being

completely ionized. A comparison of the population density of carbon ions calculated by the two methods for a density of $n_e = 10^{17}$ cm^{-3} is shown in figure 2.

It has been pointed out by Burgess (1965a) that under certain conditions, dielectronic recombination may compete with and may even exceed the rate of radiative recombination (which was included in equations (3.40) and (3.41)). Post's calculations did not include dielectronic recombination.

Since collisional excitation and collisional ionization from the ground state only is consistent with the coronal model, the population density of the excited states of a species is obtained by the balance between collisional excitation and radiative decay (Cooper, 1966).

$$n^{Z-1}(q)A(q) = n^{Z-1}(1)n_e K(1,q) \tag{3.42}$$

Then,

$$\frac{n(q)}{n(1)} = \frac{n_e K(1,q)}{A(q)} \tag{3.43}$$

The rate coefficients $K(1,q)$ [equation (3.18)] are, in general, strongly dependent on the electron temperature. Since $n(q) << n(1)$ is required with the coronal model, these values must be investigated by the substitution of known or estimated values.

E. Application to Laboratory Plasmas

The coronal model has been discussed in the context of a steady-state plasma in which it was assumed that changes in the population densities of the energy levels caused by variations in the electron temperature or density take place at a rate that is slow relative to the rate of relaxation of the atomic processes. The application of such a steady-state model to the analysis of pulsed high-temperature laboratory plasmas leads to the result that the plasma lifetime in the device is shorter or about the same as the relaxation times for the various dominant atomic processes (McWhirter, 1960). It is therefore important to consider a time-dependent model to describe such laboratory plasmas.

In a time-dependent coronal model, the spectrum is no longer a unique function of the local conditions in the plasma but will depend on the past history of the density, temperature, and state of ionization of the plasma. Mathematically, this means that a set of differential equations must be solved to predict the spectrum. If the plasma temperature and density vary with time as they certainly do in pulsed laboratory plasmas, the rate coefficient in the differential equation will also vary with time. Some assumptions must be made in order to apply such a model, including the assumption that the free electrons interchange energy at a sufficiently rapid rate by both elastic and inelastic collisions so that despite the changing conditions in the plasma, the velocity distribution is always closely Maxwellian. The same processes which

dominate in the steady-state corona model are also assumed to dominate in the time-dependent model (i.e., excitation and ionization by electron collisions and de-excitation and recombination by radiative decay and radiative and dielectronic recombination, respectively). These processes are not instantaneous, and therefore the bound electrons have a finite relaxation time into the new population distribution. This relaxation time is controlled by the slowest processes that influence the population distribution. These processes are the slowest ionization or recombination rates which are determined by the coefficients for the last ion to be produced in the plasma (Goldman and Kilb 1964, McWhirter 1965). For an ionizing plasma, this is the ion of greatest charge, and for a recombining plasma the ion of least charge.

The validity of such a time-dependent model is determined by how well it predicts the time history of line radiation from the various stages of ionization in a plasma with rapidly changing density and temperature. The power radiated per unit volume per unit solid angle per unit frequency interval is

$$\varepsilon(\nu) = \frac{h\nu}{4\pi} \phi(\nu) A(q,p) n(q) \tag{3.44}$$

where $\phi(\nu)$ is the line profile and is normalized such that

$$\int_{\text{line}} \phi(\nu) d\nu = 1 \tag{3.45}$$

The total power radiated in the line per unit solid angle is

$$\varepsilon_T = \frac{h\nu}{4\pi} A(q,p)n(q) \qquad (3.46)$$

For a plasma in coronal equilibrium, the intensity of a line is (McWhirter, 1965)

$$I(q,p) = \frac{h\nu}{4\pi} \int n_e n(1) \frac{K(1,q)}{A(q)} A(q,1)ds \qquad (3.47)$$

where equation (3.43) has been inserted for $n(q)$ and the integration is over the depth of plasma viewed by the detector and it has been assumed that the excited states are instantaneously in equilibrium with the ground state. For a pulsed laboratory plasma, n_e, $n(1)$ and $K(1,q)$ may all vary with time, and it has also been pointed out (Burton and Wilson, 1961) that the total number of particles is not conserved due to escape of the plasma as well as injection of atoms from the walls of the confining vessel. However, McWhirter (1965) shows that if temperature and density vary comparatively slowly, the excited level population establishes itself in a time which is just equal to the reciprocal of $A(q)$(i.e., the lifetime of the excited level against radiative decay), and that under these conditions the line intensity is given by equation (3.47), because the excited state population is in equilibrium with the ground state.

Investigations of the time dependency of line radiation have been conducted on several pulsed laboratory devices, including the

toroidal pinch (Burton and Wilson, 1961; Hobbs, et al., 1965) and the linear theta pinch (Goldman and Kilb, 1964; Kolb and McWhirter, 1964). These investigations verified that the time-dependent approximation could be successfully applied to laboratory plasmas of short lifetimes. Furthermore, the work of Goldman and Kilb (1964) and Kolb and McWhirter (1964) showed the applicability of this type of model to the high-temperature plasmas produced in theta pinches of the type employed in this investigation.

This investigation is concerned with the detectability of radiation emitted in transition from doubly excited states [equation (3.26)] and particularly if the satellite lines observed in theta pinch plasmas could be due to those transitions with the doubly excited state being formed by dielectronic recombination. The number of doubly excited states which could in principle exist in multielectron atoms or ions becomes exceedingly large as the number of electrons increases. For this reason, the simplest case was chosen for which doubly excited states could be formed [i.e., a two-electron (helium-like) ion]. If the doubly excited state is formed by inverse autoionization, then the rate at which they are formed [equation (3.15)] will depend on the number density of one-electron (hydrogen-like) ions available. The intensity of the satellite line must also be compared to a known, easily detectable line in order to determine the feasibility of detecting the line. For this purpose, the resonance line of the hydrogen-like ion

$$1s^2S_{1/2} - 2p^2P^o_{3/2} \tag{3.48}$$

was chosen. The satellite line would then correspond to a transition of the type

$$1s\ n\ell - 2p\ n\ell \tag{3.49}$$

with the prominent satellites due to $n = 2$. The upper state will consist of two equivalent electrons for $n = 2$ and $\ell = p$. This does not lead to any major problems but the equivalence of electrons must be taken into account in the calculation. The presence of the additional electron reduces the field in which the transition takes place, consequently reducing the energy of the transition causing the spectral line to be slightly shifted to the long wavelength side of the hydrogen-like resonance line. Satellites due to $n = 3$ move closer to and become merged with the resonance line so that they become undetectable. The elements which were investigated were chosen on the basis that the temperature and density in the theta pinch plasma be compatible with the existence of the desired stages of ionization as well as requiring that the elements be easily introduced into the deuterium plasma. Furthermore, it was required that the hydrogen-like resonance lines lie in an accessible region of the spectrum. Three elements were found to be compatible with the above requirements: boron, carbon, and nitrogen.

Since the coronal model (excluding doubly excited states) was developed for plasmas of very low electron density, the applicability of the model to the particular levels involved must be investigated. This is necessary since the maximum electron density compatible with this model is that density at which electron collisions start to interfere with the assumption that the only mechanism by which the excited level decays is spontaneous emission. The criterion of applicability for the coronal model to the resonance transition is then (McWhirter, 1965).

$$A(q) \geq n_e K(q,1) \tag{3.50}$$

For the hydrogen-like resonance lines, q = 2 and A(q) = A(2,1). The Einstein transition probability A(2,1) was calculated for the three elements of interest using equation (2.67).[Equation (3.50) would have to be modified slightly if doubly excited states are included.] The collisional de-excitation rate was calculated from equation (3.20) using an electron density of 2.2×10^{17} cm^{-3} and an electron temperature of 180 eV. The values of electron density and temperature were experimentally determined and are discussed in detail in Chapter IV. The results of these calculations are presented in table III.1 and verify that, for the lines of interest, the coronal model meets by a large margin the criteria of applicability with respect to the electron density.

Table III.1

Ion	λ, Å	gf	A, sec^{-1}	$n_e K(2,1)$ sec^{-1}
				$n_e = 2.2 \times 10^{17}$ cm^{-3}
				$T_e = 180$ eV
Boron V	48.587	0.5549	6.25×10^{12}	5.346×10^{7}
Carbon VI	33.736	0.5549	1.30×10^{13}	3.718×10^{7}
Nitrogen VII	24.781	0.5549	2.32×10^{13}	2.728×10^{7}

The intensities of the hydrogen-like resonance lines as well as the intensities of the satellite lines play an important part in this investigation, as the intensity ratio of the satellite to the resonance line established the criteria to determine if the satellites were, in fact, due to transitions from doubly excited states. The intensity of a spectral line emitted by a plasma in coronal equilibrium is given by equation (3.47) in the optically thin approximation. Since this investigation is concerned with the intensities of hydrogen-like resonance lines (Lyman-α) which are large contributors to optical depth, the assumption of optically thinness at the center of the resonance line which is needed for the coronal approximation must be considered further.

The equation of radiative transfer may be written (Chandrasekhar, 1950) for a homogeneous plasma

$$\frac{dI(\nu)}{d\tau(\nu)} = - I(\nu) + \frac{\varepsilon(\nu)}{\alpha(\nu)} \qquad (3.51)$$

where $\varepsilon(\nu)$ is the emission coefficient and $\alpha(\nu)$ is the absorption coefficient. In a uniform plasma $\varepsilon(\nu)/\alpha(\nu)$ is independent of the optical depth so that equation (3.51) has a simple solution (Hearn, 1964)

$$I(\nu) = \frac{\varepsilon(\nu)}{\alpha(\nu)} [1 - \exp (- \tau(\nu)] \qquad (3.52)$$

For a line broadened by the Doppler effect

$$\tau(\nu) = \tau(\nu_o) \exp\left[- (\nu - \nu_o)^2/(\Delta\nu_o)^2\right] \qquad (3.53)$$

where $\tau(\nu_o)$ is the optical depth at the central frequency of the line ν_o and $\Delta\nu_o$ is the exp(-1) frequency of the Gaussian profile. In a plasma close to LTE (i.e., collision dominated), $\varepsilon(\nu)/\alpha(\nu)$ is independent of frequency so that equation (3.52) may be expanded and equation (3.53) substituted in the expansion. Integrating the expression over frequency gives the total intensity of the line (Burton and Wilson, 1961),

$$I_T = \int_o^\infty I(\nu)d\nu = \Delta\nu_o \sqrt{\pi}\, \frac{\varepsilon(\nu)}{\alpha(\nu)} \left(\tau_o - \frac{\tau_o^2}{2!\ 2} + \frac{\tau_o^3}{3!\ 3} \ldots \right) \qquad (3.54)$$

Equation (3.54) shows that, for τ_o very small, the total intensity is linearly proportional to the optical depth or, that is, to the total number of atoms. However, if τ_o is 0.3, the total intensity of the line is off by 10 percent from the linear relation. Therefore, the optical depth must be restricted to less than 0.3 in collision-dominated plasma if the optically thin approximation is to be correct to 10 percent.

In the coronal model, radiative decay is much greater than collisional de-excitation so that the population of excited levels is determined by both collisional and radiative processes and the criteria for optical depth must be re-examined. This case, applied to the hydrogen-like resonance lines (Lyman-α), has been investigated

by Hearn (1964) using a model of the diffusion of resonance photons in frequency space. The criteria for the validity of the optical thin assumption are developed for Doppler-broadened resonance lines on the basis of a two-level atom. The two-level atom gives a good approximation to the Lyman-α line since the first excited level can only decay radiatively to the ground level with the emission of a resonance photon or it may be collisionally de-excited. The probability b that the atom in an excited state will emit a resonance photon is

$$b = \frac{A(2,1)}{n_e K(2,1) + A(2,1)} \quad . \tag{3.55}$$

Of these photons, a fraction k will escape and $(1 - k)$ will be absorbed, producing excited atoms. Of these excited atoms, a fraction b will emit resonance photons and a fraction k of these will escape. The total fraction W of photons emitted as the result of an original excitation is

$$W = k + b(1 - k)k + b^2(1 - k)^2k + \ldots$$

$$= \frac{k}{1 - b(1 - k)} \tag{3.56}$$

The limiting optical depth for the approximation may be calculated for the value of k which is necessary to reduce W by, at

most, 10 percent. If W is set equal to 0.90 in equation (3.56) the optically thin criteria becomes

$$k \geq k_{min} = \frac{0.90(1 - b)}{1 - 0.90\ b} \tag{3.57}$$

Calculated values of b and k_{min} are given in table III.2 for the resonance lines of interest and for the approximate plasma condition under which they were observed. The value of k for the plasma was estimated from the relation (Hearn, 1964).

$$k = 1 - \text{erf}(\ell n \tau_o)^{1/2} \tag{3.58}$$

where erf is the error function. Equation (3.58) is applicable if $\tau_o > 1$. The calculated values of k are listed in table III.2 with the values of b and k_{min}. From table III.2 it is seen that b is very close to unity and k_{min} is quite small so that the optically thin approximation for the total line intensity (not the profile shape) based on the Hearn's (1964) model should be valid for the lines investigated even though the optical depth calculated from equation (3.10) with

$$\alpha(\nu) = \frac{\pi e^2}{mc} n(p) f_{(p,q)} \frac{\Gamma}{4\pi^2(\nu - \nu_o)^2 + (\frac{\Gamma}{2})^2} \text{ cm}^{-1} \tag{3.59}$$

(Aller, 1963), for $\nu = \nu_o$ and $\Gamma = A(2,1)^{-1}$ gives values of τ_o for a length of 137 cm) of about 10^3 for concentrations of 5 percent impurity (boron, carbon,

Table III.2

Ion	λ	b	$k_{min.}$	$k_{calc.}$
Boron V	48.587	0.9999914	7.7399×10^{-5}	2.0×10^{-4}
Carbon VI	33.736	0.9999971	2.6099×10^{-5}	1.6×10^{-4}
Nitrogen VII	24.781	0.9999988	1.0800×10^{-5}	1.0×10^{-4}

or nitrogen) in the plasma. [If the effect of Doppler broadening (equation (3.53) is included τ_o will be reduced and k increased] This seemingly contradictory result is understandable since the resonance lines are being considered. Since most of the atoms are in the ground state absorption of the resonance photon will excite an electron into the upper state of the resonance transition from which it will decay radiatively (since collisional de-excitation is much smaller than radiative decay) emitting a resonance photon. This process may be repeated several times but in each case the photon does not change appreciably in frequency, although it may change direction, and will eventually (since k is large) escape from the plasma. The optical depth of the satellite lines will be considerably less than that for the resonance line. The optical depth of the satellite may be estimated from the relation

$$\frac{\tau_o^s}{\tau_o^{L\alpha}} \approx \frac{n(d)}{n(1)} \tag{3.60}$$

if it is assumed that both lines have the same shape. Equation (3.60) follows from equation (3.59) with $f(p,d) = f(1,2)$. The calculated ratio in equation (3.60) is of the order of 10^{-4} so that

$$\tau_o^s \approx \tau_o^{L\alpha} \cdot 10^{-4} \tag{3.61}$$

so that for $\tau_o^{L\alpha} \approx 10^3$ the optically thin approximation will hold for τ_o^s since

$$\tau_o^s < 1 \, . \tag{3.62}$$

The intensities of the Lyman-α lines of boron, carbon, and nitrogen emitted by the plasma produced in the theta-pinch are then given by equation (3·47) with p = 2. It is also assumed that the plasma is uniform so that the integral in equation (3·47) is straightforward. For a uniform thickness s of plasma, the intensity of the Lyman-α line is

$$I(L_\alpha) = \frac{h\nu}{4\pi} n_e n(1) K(1,2) s, \text{ ergs cm}^{-2}\text{sec}^{-1} \qquad (3\cdot63)$$

The effects of cascading from higher levels has been ignored in equation (3·63) as has the contribution to the intensity from unresolved satellites. This latter effect has been shown to be small and, to the of accuracy of the measurements made here, may be ignored (Gabriel and Paget, 1972). If the doubly excited states are formed by inverse autoionization then the intensity of the satellite line must be treated with a different approach than the resonance lines where the upper state is populated by collisions from the ground state. The intensity of the satellite may be obtained from equation (3·46) by integrating along the line of sight of the detector

$$I(d,p) = \int \frac{h\nu}{4\pi} A^s(d,p) n(d) ds, \text{ ergs cm}^{-2}\text{sec}^{-1} \qquad (3\cdot64)$$

With the assumption of a uniform plasma, the intensity becomes

$$I(d,p) = \frac{h\nu}{4\pi} A^s(d,p)n(d)s \text{ , ergs cm}^{-2}\text{sec}^{-1} \qquad (3.65)$$

where d denotes the doubly excited state, p is the singly excited state (after the transition), and n(d) is the number density of doubly excited states. The number density of doubly excited states n(d) was determined by use of equation (3.36) which gives the equilibrium value. This is a reasonable approximation since from equation (3.30) the number density of doubly excited states is just the equilibrium value if $A^s(d,p) << A^a(d,c)$. Estimates of $A^a(d,c)$ were obtained from the calculations of Perrott and Stewart (1968) and Drake and Dalgarno (1970) and indicate a value of about 10^{14} sec^{-1} while the present calculation indicate $A^s(d,c)$ is of the order of 10^{10} sec^{-1} so that the assumption $A^s(d,p) << A^a(d,c)$ is reasonable. With this result equation (3.30) becomes

$$n(d) \leq n_E(d) \qquad (3.66)$$

and the number density of doubly excited states is independent of the rate coefficient in this approximation. However, it should be clear that electrons are lost from the doubly excited system at a rate $A^s(d,p)^{-1}$ and must be supplied to the system at a rate $A^s(d,p)^{-1}$ which will only be true if, approximately

$$\tau_{ee}^{-1} > A^s(d,p) \qquad (3.67)$$

For the plasma under consideration $\tau_{ee} \approx 10^{-10}$ sec (Spitzer, 1967) and calculations of $A^s(d,p)$, which were discussed in the last chapter, indicate a value of 10^{10} sec so that the inequality of equation (3.67) does not hold completely. Equation (3.36) does, however, determine an upper limit to the number density of doubly excited states and, even though the actual density in the experiment may be well below this value, it is still useful in estimating the maximum intensity the satellite line would be expected to have. Since the intensity of the resonance line was determined in coronal equilibrium rather than LTE, its intensity should be a minimum [n(q) is coronal equilibrium is less than n(q) in LTE at the same temperature (i.e. radiation rate > collisional rate)]. Therefore the ratio of satellite to resonance line intensity should be a maximum. Under the above conditions the intensity of the satellite line is

$$I^s = \frac{h^4\nu}{8\pi} \frac{n_e n^H(1) g(d) A^s(d,p) s}{(2\pi\, mkT_e)^{3/2}\, g(1)} \exp\left(-\frac{\varepsilon_s}{kT_e}\right), \text{ ergs cm}^{-2}\text{sec}^{-1} \qquad (3.68)$$

The ratio of equation (3.68) to equation (3.63) is

$$R = \frac{I^s}{I(L_\alpha)} = \frac{h^3}{(2\pi\, mkT_e)^{3/2}} \cdot \frac{g(d)}{2g(1)} \cdot \frac{A^s(d,p)}{K(1,2)} \exp\left(\frac{-\varepsilon_s}{kT_e}\right) \qquad (3.69)$$

where it has been assumed that the frequency of the satellite line is equal to the frequency of the resonance line to the accuracy required. Using equation (3.18) for K(1,2) equation (3.69) becomes

$$R = \frac{h^3}{(2\pi mk)^{3/2}} \cdot \frac{g(d)}{2g(1)} \cdot \frac{A^s(d,p)\ E(2,1)}{6.5 \times 10^{-4}\ f(1,2)T_e} \cdot \exp\left(\frac{E(2,1)-\varepsilon_s}{kT_e}\right) \tag{3.70}$$

Setting $E(2,1) = (\frac{3}{4} Z^2 E_H)$ and writing $A^s(d,p)$ in terms of its oscillator strength [equation (2.67)] the ratio becomes

$$R = 3.5 \times 10^9 \frac{h^3}{(2\pi mk)^{3/2}} \cdot \frac{Z^6}{T_e} \cdot \frac{f(d,p)}{f(1,2)} \exp\left(\frac{E(2,1)-\varepsilon_s}{kT_e}\right) \tag{3.71}$$

The oscillator strengths were set equal [i.e., f(d,p) = f(1,2)] since in both cases the same "inner" electron is "jumping" and this should be a good approximation. Equation (3.67) was evaluated for each of the three elements of interest and for temperatures of 50,100, 150,200, and 250 electron volts. These results are given in table III.3 and show that R ranges from 10^{-2} to 10^{-4}. Values of R using the expression derived by Gabriel and Paget (1972) (who used a different excitation cross section including a gaunt factor of 0.2) are also given in parenthesis. Their ratios are typically a factor of 2 to 3 higher than those calculated here (for nitrogen). In the temperature range of interest ($\tilde{}$ 200 ev) the satellites would be extremely difficult to detect and consequently if observed intensity ratios exceed the calculated values by large amounts the lines could not be due to transitions from the doubly excited states.

Table III.3

Element	kT_e = 50 ev	100 ev	150 ev	200 ev	250 ev
Boron	$1.3 \cdot 10^{-3}$	$3.82 \cdot 10^{-4}$	$2.13 \cdot 10^{-4}$	$1.45 \cdot 10^{-4}$	$1.11 \cdot 10^{-4}$
	$(3.1 \cdot 10^{-3})$	$(9.0 \cdot 10^{-3})$	$(5.15 \cdot 10^{-4})$	$(3.5 \cdot 10^{-4})$	$(2.67 \cdot 10^{-4})$
Carbon	$7.16 \cdot 10^{-3}$	$1.55 \cdot 10^{-3}$	$7.75 \cdot 10^{-4}$	$5.06 \cdot 10^{-4}$	$3.72 \cdot 10^{-4}$
	$(1.74 \cdot 10^{-2})$	$(3.72 \cdot 10^{-3})$	$(1.86 \cdot 10^{-3})$	$(1.23 \cdot 10^{-3})$	$(8.95 \cdot 10^{-4})$
Nitrogen	$3.84 \cdot 10^{-2}$	$5.7 \cdot 10^{-3}$	$2.53 \cdot 10^{-3}$	$1.55 \cdot 10^{-3}$	$1.09 \cdot 10^{-3}$
	$(7.6 \cdot 10^{-2})$	$(9.0 \cdot 10^{-3})$	$(5.0 \cdot 10^{-3})$	$(3.0 \cdot 10^{-3})$	$(2.0 \cdot 10^{-3})$

CHAPTER IV

EXPERIMENTAL METHOD

A. Theta-Pinch Device

The theta-pinch is one of several devices which were developed for the production and confinement of high-temperature plasmas relevant to the study of controlled thermonuclear reactions. The production of such high-temperature laboratory plasmas at moderate-to-high particle densities presented the opportunity for the study of radiation emitted by highly ionized atoms and spectroscopy has indeed served as a major means of diagnostics on these devices. Extensive studies in various countries and over a wide range of discharge conditions have established the basic characteristics of this experimental configuration (Little, et al., 1962; Kolb, et al., 1962; Goldman, et al., 1962; Beerwald, et al., 1962; and Bodin, et al., 1962). The theta-pinch utilizes a fast magnetic compression of an ionized gas to produce the high-temperature plasma. The rapidly rising magnetic field, which makes the compression possible, is produced by a large current passing through a single-turn coil which surrounds the vacuum vessel containing the ionized gas. The coil and field geometry are shown in Figure 3. The magnetic field due to the current in the coil may be obtained from the integral form of Amperes' law (Jackson, 1962)

$$\oint \vec{B} \cdot d\vec{\ell} = \frac{4\pi}{c} I \tag{4.1}$$

where I is the total current in the coil in statamps and $\vec{B}$ is in Gauss. For the physical arrangement shown in Figure 3 and with the length ℓ of the coil much greater than its diameter equation (4.1) gives

$$B_z(t) = \frac{2\pi}{c\ell} I_\theta(t) \tag{4.2}$$

The time variation in $B_z(t)$ induces an azimuthal electric field in the ionized gas. This induced current field is given by Faraday's law

$$\nabla \times \bar{E} = - \frac{1}{c} \frac{\partial \bar{B}}{\partial t} \tag{4.3}$$

For the particular case of a B_z field only, equation (4.3) becomes

$$\frac{1}{r} \left[\frac{\partial}{\partial r} (rE_\theta) - \frac{\partial E_r}{\partial \theta} \right] = - \frac{1}{c} \frac{\partial B_z}{\partial t} \tag{4.4}$$

The applied field has a frequency ω and will be attenuated to 1/e of its original value in a distance (Spitzer, 1967; Jackson, 1962)

$$d = \frac{c}{\omega_p \left(1 - \frac{\omega^2}{\omega_p^2}\right)^{1/2}} \text{ cm.} \tag{4.5}$$

where ω_p is the plasma frequency

$$\omega_p = \left[\frac{4\pi n_e e^2}{m_e}\right]^{\frac{1}{2}} \text{sec}^{-1} \qquad (4.6)$$

For a typical experiment, the electron density, n_e, is about 10^{16} cm^{-3}, which gives

$$\omega_p = 5.6 \times 10^{12} \text{ sec}^{-1} .$$

Typically, the driving field frequency ω is of the order of 10^5 sec^{-1}, so that

$$\frac{\omega}{\omega_p} << 1$$

The depth of penetration is then

$$d = \frac{c}{\omega_p} = 0.536 \times 10^{-2} \text{ cm}$$

and the fields are restricted to the surface of the plasma cylinder. The radial electric field, E_r, should be independent of θ due to symmetry of the coil so that $\frac{\partial E_r}{\partial \theta}$ may be ignored. Equation (4.4) becomes

$$E_\theta = - \frac{r}{2c} \frac{\partial B_z}{\partial t} \qquad (4.7)$$

with B_z equal to its value at the surface of the plasma and r equal to the radius of the plasma column.

The induced current then follows from Ohm's law

$$\vec{J} = \sigma\vec{E}$$

where σ is the conductivity of the plasma. The induced current density is then

$$J_{i\theta} = \sigma E_\theta = -\frac{\sigma r}{2c}\frac{\partial B_z}{\partial t} \tag{4.8}$$

The Lorentz force acting on the plasma surface inward is given by

$$F_r = \frac{1}{c} J_{i\theta} \times B_z \tag{4.9}$$

The current sheet initially moves inward at a high velocity and heats the plasma. Further compression of the plasma occurs adiabatically when the thermal energy of the plasma particle exceeds the velocity of the current sheet. If end losses and radiation cooling are ignored, the plasma will be compressed until the magnetic pressure is equal to the internal pressure

$$\frac{B_z^2}{8\pi} = n_e kT_e + \sum_i n_i kT_i \tag{4.10}$$

The sum must extend over all of the various ions at their individual temperatures. In general, the electrons and the ions will be at different temperatures, since the electrons are compressed adiabatically during compression of the plasma while the ions are shock heated (Rose and Clark, 1961). In fact, the average radial speed of the current sheet is of the order of 10^7 cm/sec. For the electrons this velocity corresponds to a mean thermal energy of about 0.04 eV which is considerably less than their actual energy which will be of the order of a few eV, thus adiabatic compression results. For ions the situation is quite different. The velocity of 10^7 cm/sec corresponds to a mean thermal energy of 150 eV for deuterons and the initial velocity of the deuterons will be much less than this. Since the mean thermal velocity of the ions is less than the velocity of the current sheet a shock wave will develop and the ions will be heated by the passage of the shock wave (Rose and Clark, 1961). However, since collisional rates for electrons exceed those for ions it is the electron temperature that is generally of interest in the discussion of the various atomic processes.

A common feature of the magnetically compressed plasma experiments is the existence of a trapped internal magnetic field which, depending on the plasma conductivity and breakdown conditions, can reach large values antiparallel to the external field during compression. A number of authors (Kolb, 1959; Fay, Hintz, and Jordan, 1959; Kolb, Dobbie, and Griem, 1959) have observed that the strength, sign, and spatial distribution of the initially trapped magnetic field are

the most critical parameters in these experiments. These values can be varied to some extent by the addition of a static magnetic bias field of variable sign and amplitude. Experiments on this technique (Quinn, Little, and Ribe, 1960; Goldman, et al., 1959) have shown the fundamental importance of the trapped field and also have shown characteristic difference in the plasma behavior during compression for the cases of bias fields parallel and antiparallel to the internal fields. With an externally applied antiparallel bias field, high mean ion energies have been observed in the first compression half-cycle (Little, Quinn, and Ribe, 1961).

The large current which is required in the single-turn coil is produced by the discharge of a large capacitor bank. The requirements on the capacitance, C, and inductance, L, of the system is governed by the differential equation describing the current in an L-R-C circuit

$$\frac{d^2I(t)}{dt^2} + \frac{R}{L}\frac{dI(t)}{dt} - \frac{I(t)}{LC} = 0 \qquad (4.11)$$

R is the resistance of the system. Equation (4.11) is not strictly true for the situation being considered as the presence of the plasma which is being compressed causes L, R, and C to vary with time. However, equation (4.11) is a good approximation to the circuit and since the time dependence of L, R, and C cannot be easily calculated the equation is used as is. If the inductance, resistance, and capacitance satisfy the relation

$$\frac{1}{LC} >> \frac{R^2}{4L^2}$$

the solution of equation (4.11) is the damped oscillatory current

$$I(t) = V_o \left(\frac{C}{L}\right)^{1/2} \exp(-\gamma t) \sin \omega t \qquad (4.12)$$

where $\omega = (1/LC)^{1/2}$, $\gamma = R/2L$, and V_o is the initial voltage on the capacitor. The maximum current is obtained when $\sin \omega t = 1$.

$$I_{max} = V_o \left(\frac{C}{L}\right)^{1/2} \exp(-\gamma t) \qquad (4.13)$$

The rise time (i.e., dI/dt) is

$$\left.\frac{dI}{dt}\right|_{t=0} = \frac{V_o}{L} \qquad (4.14)$$

Equations (4.13) and (4.14) show that a large maximum current with a fast rise time may be obtained in the circuit with a large initial voltage, a large capacitance, and a small inductance. The desired ratio of a large capacitance to a small inductance is accomplished by connecting a large number of capacitors in parallel to a collector plate assembly which terminates in a single-turn coil.

The theta-pinch device employed in this experiment consisted of three separate capacitor banks, each of which was connected to the collector plate assembly with coaxial cables. The various parameters

of these banks are listed in table IV.1. The bias field bank established the slowly varying reverse magnetic field, while the preheater bank heated and ionized the cold gas in the shock tube. The large current required to produce the high magnetic field which compresses the ionized gas was obtained by the discharge of the main capacitor bank. This bank consisted of 410 capacitors connected in parallel with one triggered spark gap for each pair of capacitors. The bank could be switched in less than 25 nanoseconds (Oertel and Williams, 1965). The single-turn coil had an inside diameter of 10 centimeters and was constructed of nine segments , each of which was 15 centimeters long. The segments were assembled with a 0.25 cm gap between segments so that observations could be made perpendicular to the longitudinal axis of the coil. This arrangement gave a total coil length of 137 cm. The shock tube was constructed of quartz (SiO_2) and had an outside diameter of 9.6 cm., a wall thickness of 0.5 cm., and a total length of 183 cm. The general physical arrangement of the experiment is shown in Figure 4 and a schematic of the electrical circuit is shown in Figure 5.

A schematic of the vacuum system is shown in Figure 6 and consists of a mechanical pump which may be used to evacuate the entire system to about 10^{-2} torr and a turbomolecular pump which evacuates the system to pressures of about 10^{-9} torr. The turbomolecular pump is basically a turbine type and its principle of operation is a gas molecule-wall collision process. The molecules enter the pump at the inlet port, collide with all of the interior surfaces of the inlet

Table IV.1

Capacitance	Main Bank	- 5 mF
	Bias Field Bank	- 220 μF
	Preheater Bank	- 5 μF
Voltage	Main Bank	- 20 kV
	Bias Field Bank	- 10 kV
	Preheater Bank	- 20 kV
Frequency	Main Bank	- 22 kHz
	Bias Field Bank	- 10 kHz
	Preheater Bank	- 200 kHz
Coil	Radius	- 5 cm
	Length	- 137 cm
Load Inductance		10 Nanohenries
Switching Time	Main Bank	< 25 Nanoseconds
Rise Time - Magnetic Field		≈ 10 μsec
Peak Current		12.7 meg Amperes

portion and some of them are accelerated axially toward the ends of the pump when they are struck by the blades on the first rotating disk (rotating at 16,000 RPM). The molecules are guided in the proper direction by impinging upon the first set of fixed blades which are oriented in such a fashion as to increase the probability of the molecules being struck by the second set of rotating blades. This process is repeated through several stages (nineteen on each side for the particular pump used) resulting in a compression of the gas. This compression depends on the relative motion of the blades and molecules with the compression increasing as the blades move faster relative to the molecules. The compressed gases are removed by the mechanical pump and exhausted to the atmosphere. The leak rate of the vacuum system was investigated by evacuating the system to its lowest pressure and then closing the valve between the vacuum pump and the shock tube. The pressure in the system was measured by means of a nude ion gage and it was found that the system pressure had reached 1×10^{-6} torr at the time the fill gas was admitted into the shock tube. While this leak rate was rather high it was thought at the time that the background particle density at 10^{-6} torr ($\approx 3.5 \times 10^{10}$ cm^{-3}) would not interfere critically with the investigation since most experiments of this type employ oil diffusion pumps to evacuate their systems and normally work with a base pressure of this magnitude. Furthermore, the leakage was thought to be past the viton "O" rings which sealed the quartz tube to the vacuum system and to repair the leak would have required considerable time and effort. The leak

was located in the latter part of the experiment and was actually due to leakage past a valve stem which was repaired by simply replacing the valve. The operating conditions for the experiment are listed in table IV.2.

The various elements whose spectra were to be investigated were introduced into the deuterium fill gas prior to its introduction into the shock tube. To insure that the gases were well mixed, a stainless steel tank equipped with a slowly rotating paddle was connected directly to the vacuum system and served as a mixing and storage tank. This tank was filled with deuterium to a predetermined pressure, and the amount of the specific element required was added in a gaseous form to obtain the desired percentage of the element in the mixture. Carbon spectra were obtained by the introduction of methane (CH_4) or acetylene (C_2H_2), boron spectra by the introduction of diborane (B_2H_6), and nitrogen spectra by the introduction of molecular nitrogen (N_2). Normally, a volume sufficient for several hundred shock tube fillings was mixed at one time, insuring that the gas mixture did not change during the course of the investigation. The amount of the impurity element which could be added was restricted to 5 percent of the total volume. At higher concentrations, the plasma did not reach a sufficiently high temperature due to radiation losses, or the plasma column became subject to violent instabilities.

The gas was introduced into the shock tube through a leak valve. The pressure in the shock tube was continuously monitored during filling by means of a calibrated thermocouple gage. A filling pressure of 50 millitorr, corresponding to a particle density of

Table IV.2

Main Bank Energy		660 kJ
Peak Compression Field		90 kG
Bias Field at Main Bank Discharge		-2.2 kG
Preheater Bank Energy		1 kJ
Initial Filling Pressure		50 m Torr
Impurity Concentration		Up to 5% of the initial filling gas.
Discharge Sequence	Bias Field	t = 0
	Preheater	t = 0
	Main Bank	t = 25 μsec
Peak Voltage at Coil	Bias Field	200 V
	Preheater	1.35 kV
	Main Bank	10 kV

1.8×10^{15} cm^{-3}, was used in this experiment, as it was experimentally determined that a higher filling pressure produced a plasma of insufficient temperature while a lower filling pressure did not produce spectral lines of sufficient intensity to allow photographic recording with a single discharge. After filling the shock tube, the three capacitor banks were charged and then dicharged in a predetermined sequence. The bias field bank and the preheater bank were discharged at the same time, producing a voltage at the coil which consisted of the slowly varying voltage from the bias field bank with the higher frequency voltage from the preheater bank superimposed. The time at which the main bank was discharged was determined by the requirement that the preheater plasma be relatively stable and have a high degree of ionization at the start of the magnetic compression phase. An investigation of the preheater plasma indicated that a stable plasma having an electron density of about 10^{15} cm^{-3} and an electron temperature of from 1 to 2 electron volts existed at 25 microseconds after the preheater bank had been triggered (Oertel and Jalufka, 1966). This time delay for the discharge of the main bank was used throughout this investigation.

An image converter camera, operated in the streak mode, was employed to investigate the compression of the ionized gas. The camera viewed a 0.25 cm portion of the plasma column through the slit between two of the coil sections and near the center of the coil assembly. The image of the plasma portion was streaked across a film by the camera and the resulting photograph showed the time history of the plasma column diameter during the compression of the

plasma. Figure 7 is a tracing of a typical photograph taken with the image converter camera. The total sweep time was 20 microseconds. The preheated and ionized gas fills the shock tube to its full diameter (8.6 cm) prior to the application of the main compression field. With the application of the compression field, the plasma column collapses radially, reaching its minimum diameter in about 2.5 microseconds. This rapid collapse is followed by a relatively stable period of about 10 microseconds with the luminous plasma column situated at the coil axis. If losses out of the ends of the tube are neglected and it is assumed that all of the ionized gas is swept up ahead of the current sheet, then the particle density in the plasma column minimum diameter is given by

$$n_i = n_e = n_o \left(\frac{r_o}{r_c}\right)^2 \qquad (4.15)$$

The filling gas is predominantly deuterium so that the ion density n_i is approximately equal to the electron density n_e. The radius of the plasma column before compression is r_o and r_c is the radius of the collapsed column. From Figure 7, $r_o/r_c \approx 11$ and knowing the initial density n_o, the density in the collapsed column is

$$n_i = n_e = 2.2 \times 10^{17} \text{ cm}^{-3}$$

This value is in very good agreement with the value of n_e obtained by a measurement of the absolute continuum intensity (Conrads and Oertel, 1968).

The electron temperature of the plasma was determined by the line intensity ratio method assuming corona equilibrium which was justified in Chapter III. The intensity of a spectral line is given by equation (3.47) and the ratio R of the intensities of two spectral lines corresponding to transitions between states p, q in an ion of charge Z + 1 and states i, j in an ion of charge Z is

$$R = \frac{I(p,q,Z+1)}{I(i,j,Z)} = \frac{N^{Z+1}(q)A(p,q)\lambda(i,j)}{N^{Z}(j)A(i,j)\lambda(p,q)} \tag{4.16}$$

The density ratio of the upper states of the lines may be obtained by assuming that the states are populated by electron collisions from the ground state only as in the coronal approximation and ignoring effects due to cascading. Using the expression due to Seaton (1962) for the threshold excitation of ions, the ratio of the upper states is

$$\frac{N^{Z+1}(q)}{N^{Z}(j)} = \frac{N^{Z+1}(1)f(r,q)E(s,j)}{N(1)f(s,j)E(r,q)} \exp\left(\frac{E(1,j) - E(1,q)}{kT_e}\right) \tag{4.17}$$

where $N^{Z+1}(1)$ and $N^{Z}(1)$ are the ground state population, the f's are the absorption oscillator strengths, and the E's are the excitation energy of the excited states above the ground states. The ground state density ratio is obtained from the corona equilibrium ionization equation. Using the expression given by McWhirter (1965), which ignores dielectronics recombination

$$\frac{N^{Z+1}(1)}{N^{Z}(1)} = 1.27 \times 10^{8} \frac{1}{(\varepsilon^{Z})^{2}} \left(\frac{kT_e}{\varepsilon^{Z}}\right)^{3/4} \exp\left(-\frac{\varepsilon^{Z}}{kT_e}\right) \quad (4.18)$$

ε^{Z} is the ionization potential of the species of charge Z. Time dependency has been ignored in equation (4.18) since the data was obtained in a time integrated mode so that only average values were obtained. This dependency would have to be considered if time resolved intensities were recorded as there is some indication that lines of a given stage of ionization appear at a higher temperature in transient plasmas with rapidly rising temperature than in the steady state coronal approximation. This is due to the finite relaxation times of the ionization processes (Kunze, Gabriel,and Griem, 1968). Equation (4.18) may therefore indicate a lower temperature than that actually obtained. The effect of ignoring dielectronic recombination may be estimated from the ionization balance calculations for oxygen including radiative and dielectronic recombination (Burgess and Summers, 1969). A comparison of their values with those calculated from equation (4.18) indicates that at electron densities of 10^{16} cm^{-3}, the effect of including dielectronic recombination is to shift the curves to a higher temperatures (by about 20%). At the higher densities obtained in this experiment (i.e., 2.2×10^{17} cm^{-3}) the effect should be less due to the inverse dependence of the dielectronic rate coefficient on the electron density. At lower electron densities the effect would increase up to a discrepency of a factor of 2 in the solar corona ($n_e \simeq 10^{8}$ cm^{-3}).

McWhirter indicates that equation (4.18) should be accurate to $\pm$ 50% for the ratio of hydrogen-like ions to bare nuclei (no dielectronic recombination possible for this case) but also points out that the strong influence of the exponential should allow temperature to be estimated to an accuracy of 10%. For the ratio of helium-like to hydrogen-ions the results should be considerably poorer and the above discussion would indicate that a factor of up to two in temperature may be obtained. Substituting equations (4.17) and (4.18) in equation (4.16), the intensity ratio becomes

$$R = \frac{A(p,q)\lambda(i,j)f(1,q)E(1,j)1.27 \times 10^{8}}{A(i,j)\lambda(p,q)f(1,j)E(1,q)(\varepsilon^{Z})^{2}}\left(\frac{kT_e}{\varepsilon^{Z}}\right)^{3/4}\exp\left(\frac{E(1,j)-E(1,q)-\varepsilon^{Z}}{kT_e}\right) \tag{4.19}$$

If the resonance lines of the two successive stages of ionization are used, then $p = 1$ and $i = 1$. Equation (4.19) was evaluted for the resonance lines of the hydrogen-like and helium-like ions of oxygen over the range of temperatures expected. The results are plotted in Figure 8 and the graph was then used to determine the plasma electron temperature. Including the effects of dielectronic recombination would shift the curve to about a 20% higher temperature. Oxygen was chosen as the most convenient element since it is injected into the plasma from the shock tube walls during the preheating phase and also because the two resonance lines were separated by only 2.63 $\mathring{A}$, (i.e., 21.602 $\mathring{A}$ for helium-like and 18.969 $\mathring{A}$ for hydrogen-like) so the problem of film response as a function of

wavelength was virtually eliminated. The intensities of the two lines were measured from the microdensitometer trace of the spectra which had been recorded on film. The spectra were recorded in the time-integrated mode and the resultant intensities represented an average over several cycles of plasma compression and expansion so that the temperature obtained was at best an estimate. Furthermore, the approximation that the upper states of the lines were populated from the ground state only is somewhat suspect since both ions have meta-stable states lying below the upper state of the resonance line. These meta-stable states can be populated by radiative transitions from higher states and, since they cannot decay to a lower state, are depopulated by electron collisions. Thus the upper states of the resonance lines may also be populated by electron collisions from the meta-stable states. (Gabriel and Jordan, 1969) However, the electron temperature obtained in this manner varied from 160 eV to 220 eV, which is in good agreement with the measured temperature reported in other similar devices (Roth and Elton, 1968; Sawyer, et al., 1962). More accurate measurements of the electron temperature carried out on a similar experiment and based on Thompson scattering of laser light indicate higher temperatures, up to about 240 eV. (Kunze, Gabriel and Griem, 1968). This latter result appears to be more in agreement with the inclusion of dielectronic recombination. However, the higher temperature would decrease the intensity ratio of satellite to resonance line due to the T^{-1} dependence. At the lower temperatures (i.e., $T_e \leq 200$ eV) the calculations of Landini and Fossi (1971) indicate that dielectronic recombination should be

important but not dominant. Using a simple result of Goldberg (1966) the temperature at which dielectronic recombination is expected to be a maximum is just equal to the wavenumber of the recombining ion so that the lower temperature should be appropriate for boron V while the higher temperatures would be more compatable with carbon VI.

The relevant plasma parameters are listed in table IV.3.

B. Grazing Incidence Spectrograph

The hydrogen-like resonance lines of the elements investigated all lie below 50 Å, which is beyond the range of normal incidence vacuum spectrographs. The spectra were therefore obtained at grazing incidence with a 1-meter radius of curvature, platinum-coated grating rules with 3,600 lines/millimeter (Leybold-Heraeus GMBH and Co.).

The theory of the concaved grating and its use in the grazing incidence mounting has been discussed in detail (Samson, 1967; Beutler, 1945; Namioka, 1959, 1961; Mack, Stehn, and Edlen, 1932) and no useful purpose would be served by repeating these discussions here. Therefore, only those parameters of the grating and the grazing incidence mounting which are pertinent to the analysis of laboratory spectra will be discussed.

The optical arrangement for the grazing incidence mounting is shown in Figure 9. The concave grating of radius of curvature R is mounted tangent to the Rowland circle of radius $R/2$. If the entrance slit lies on this circle at an angle of incidence α, then the image will lie on the circle at an angle of diffraction β. These two angles are related by the grating equation

Table IV.3

Electron Density	$n_e \approx 2.2 \times 10^{17}$ cm^{-3}
Electron Temperature	$kT_e \approx 180$ to 200 eV
Electron-Electron Collision Time	$\tau_{ee} \approx 10^{-4}$ μsec
Proton-Proton Collision Time	$\tau_{pp} \approx 10^{-2}$ μsec

$$m\lambda = \sigma(\sin \alpha + \sin \beta) \qquad (4.20)$$

The grating factor σ is the reciprocal of the number of lines per Angstrom ruled on the grating, m is the order of the spectrum, and λ is the wavelength of the spectral line in Angstroms. The dispersion of the grating expresses how the various wavelengths are distributed along the Rowland circle. The angular dispersion $d\beta/d\lambda$ is obtained by differentiating equation (4.20). For a fixed angle of incidence (α = constant)

$$\frac{d\beta}{d\lambda} = \frac{m}{\sigma \cos \beta} \quad . \qquad (4.21)$$

For an analysis of the spectrum, the actual number of angstroms per millimeter dispersed along the Rowland circle is of more interest. This quantity is called the plate factor and is the reciprocal of the linear dispersion. The plate factor may be obtained from equation (4.21). Referring to Figure 9

$$\frac{d\lambda}{d\ell} = \frac{d\lambda}{d\beta} \frac{d\beta}{d\ell} \qquad (4.22)$$

and

$$d\ell = - R d\beta \qquad (4.23)$$

With these substitutions, equation (4.21) becomes

$$\frac{d\lambda}{d\ell} = \frac{\sigma \cos \beta}{mR} \tag{4.24}$$

In the grazing incidence mounting, the dispersion changes rapidly with increasing wavelength so that the linear relationship used for normal incidence mountings is not applicable and the dispersion curve must be determined if accurate wavelength measurements are to be made. Figure 10 is the theoretical dispersion curve which was calculated for an 85° angle of incidence and a 1-meter radius of curvature grating ruled with 3,600 lines per millimeter corresponding to the instrument used in the experiment.

Closely related to the dispersion is a quantity known as the resolving power. While the dispersion determines the separation of two wavelengths (spectral lines), the resolving power determines whether this separation can be distinguished. Each monochromatic beam from the grating forms a diffraction pattern, the principal maxima of which are represented by the order number m. Between these principal maxima, secondary maxima are formed whose intensities decrease as the number of ruled lines N exposed to the incident radiation increase. In a normal laboratory instrument, these secondary maxima are very much weaker than the principal maxima. The angular half-width of a principle maximum $d\beta$ is the angular distance between the principal maximum and its first minimum and, for a plane grating, is given by the expression

$$d\beta = \frac{\lambda}{N\sigma \cos \beta} \tag{4.25}$$

This width provides a theoretical limit to the resolving power of the grating. If Rayleigh's criterion is used, two lines of equal intensity will just be resolved when the maximum of one falls on the minimum of the other. The resolving power P is defined as $\lambda/d\lambda$, where $d\lambda$ is the minimum wavelength separation which can be resolved. This minimum wavelength separation may be expressed in terms of $d\beta$

$$d\lambda = d\beta \frac{d\lambda}{d\beta} \tag{4.26}$$

Substituting in equation (4.25) the resolving power is obtained

$$P = \frac{\lambda}{d\lambda} = mN \tag{4.27}$$

Equation (4.27) represents the theoretical limit of the resolving power and whether this limit is achieved will depend on the quality of the grating. The finite width of the entrance slit is also a major factor in determining the resolution of a given instrument. For the concave grating mountings the entrance slit to grating distance is equal to the image to grating distance so that the image width can be no less than the slit width. This width, and hence a measure of the limit of resolution imposed by the slit, may be obtained by multiplying the slit width in millimeter by the equation

(4.24) in $\mathring{A}$/mm. This value of $d\lambda$ (and λ at which it is calculated) may then be used to obtain the resolution limit [equation (4.27)]due to the slit width. It is clear from equation (4.27) that the resolving power increases with the order number, m. The major aberration of the concave diffraction grating is astigmatism, which results in a point on the vertical entrance slit being imaged into a vertical line; that is, focusing is achieved only in the horizontal plane. (i.e., perpendicular to the slit height) The theory of the astigmatism of a concave grating was first developed by Runge and Munnkopf (1927). More recently the problem has been dealt with in detail by Beutler (1945) and Namioka (1959, 1961). The length of the astigmatic image is given by (Beutler, 1945)

$$z = \left[\ell \frac{\cos \beta}{\cos \alpha}\right] + L[\sin^2\beta + \sin \alpha \tan \alpha \cos \beta] \qquad (4.28)$$

where the first term gives the contribution due to the entrance slit of finite vertical length ℓ and the second term is the astigmatism produced by a point on the entrance slit. L represents the length of the ruled lines illuminated. Equation (4.28) indicates that the image becomes less astigmatic near normal incidence and that astigmatism is most severe at grazing incidence. While this astigmatism does not cause the spectral line to be less sharp in the grazing incidence mount it does greatly reduce the energy per unit length received at the focal plane. For the grating used in this experiment and with $\alpha = 85^\circ$ and $\beta = 80^\circ$ (corresponding to $\lambda = 30$ $\mathring{A}$) the

first term of equation (4.28) contributes approximately 2ℓ to the height while the second term contributes about $3L$ to height. While some control may be exercised over the first term it is normally small relative to the second term which for a given instrument is controlled by the height L of commercially available grating. It is possible, of course, to mask the grating and reduce L but the improvement in the image height is gained at the expense of reduced intensity per unit area at the focal plane, since both intensity and astigmatism are proportional to L.

Equation (4.27) is strictly true for a plane grating but is also applicable to a concaved grating if the width of the grating is less than its optimum value which is given below. Namioka (1959, 1961) and Mack, Stehn, and Edlen (1932) have shown that for a concave grating the angular half-width of the principal maximum deviates from that given by equation (4.25) and that the diffracted minima do not reach zero. Therefore, a modified Rayleigh criterion was introduced which states that two lines of equal intensity will be just resolved when the wavelength difference between them is such that the minimum total intensity between the lines is $8/\pi^2$ (= 0.8106) times as great as the total intensity at the central maximum of either of the lines. With this new criterion, they have shown that the resolving power of a concave grating is equal to mN when the width W of the grating illuminated is less than or equal to $W_{opt}/1.18$. The optimum width is obtained from physical optics (Samson, 1967),

$$W_{opt} = 2.51 \left[R^3 \lambda \frac{\cos \alpha \cos \beta}{\sin^2 \alpha \cos \beta + \sin^2 \beta \cos \alpha} \right]^{1/4} \qquad (4.29)$$

For the 1-meter radius of curvature grating used in this experiment at an angle of incidence of 85°, the optimum width for a detected wavelength of 50 Å is 3.34 millimeters, which is much smaller than the actual width of the 20-millimeter-wide grating used.

The greater width of the grating is beneficial in increasing the intensity of a line in the focal plane, since intensity is proportional to the area of the grating illuminated. Since the investigation required the recording of spectra from a pulsed discharge of very short duration and since it was desired to record spectra with a single discharge some resolution had to be sacrificed in order to obtain sufficient intensities at the focal plane (i.e., a larger grating was used in order to get more intensity which is dependent on the ruled area of the grating). Thus the grating employed was a compromise which gave adequate resolution with sufficient intensity.

For gratings having widths greater than the optimum width the resolution is given by (Samson, 1967)

$$P = 0.75 \left(\frac{W_{opt}}{\sigma} \right) m \qquad (4.30)$$

Thus, if $W > W_{opt}$ the resolution is independent of the width.

Solving equation (4.30) for the grating used in the experiment, the theoretical resolving power of the grating is

$$\frac{\lambda}{d\lambda} \simeq 10^4 \qquad (4.31)$$

The actual resolution of the instrument does not depend on the grating alone but depends on the slit width also. The slit must be narrow enough to provide adequate resolution but still of sufficient width to allow an adequate amount of light to pass.(i.e., the wider the slit the more light is passed through.) Mack, Stehn, and Edlen (1932) treat the slit and grating together, which is necessary if the resolving power of each of the two elements is nearly equal. If the resolving power of one element is greatly different from the resolving power of the other element, then the resolving power of the combination is determined by the smaller value. In practice this is generally the case, with the resolving power being determined by the slit width. The resolution is also degraded by thermal broadening of spectral lines in the light source and also by the film. For these reasons, it is more convenient to establish the instrument resolution experimentally. This was accomplished by recording, on film, the spectrum of a high-temperature aluminum plasma, produced by firing a large pulsed ruby laser at a solid aluminum sample. A microdensitometer trace of the film showed the aluminum VIII lines at 66.704 Å and 66.731 Å to be clearly resolved. Therefore, the resolving power at 66 Å is

$$\frac{\lambda}{d\lambda} > 2000 \qquad (4.32)$$

This procedure was also used to establish the optimum slit width. A series of exposures taken of the plasma with various slit widths showed that a slit width less than 17 microns only decreased the intensity of the spectral line of the film without improving the resolution. The calculated value of P corresponding to this width and at a wavelength 66.7 Å is P~ 6,000. This slit width was used for all spectra recorded in this experiment.

The physical arrangement of the components is shown in Figure 11. The adjustable entrance slit, grating, and film holder are mounted on a base plate with the grating holder and film holder attached to arms pivoting around the center of the Rowland circle. The base plate is mounted so that it may pivot around a vertical axis through the center of the entrance slit. This arrangement allows the angle of incidence to be varied between 80° and 89° without movement of the vacuum housing or the experimental arrangement.

An aperture was inserted in the vacuum system between the shock tube and the entrance slit of the spectrograph. This aperture consisted of a 5-millimeter-diameter circular hole in a copper disk about 1 millimeter thick. The disk was clamped between two flanges with the geometrical center of the circular hole on the optical axis of the system. This aperture prevented the spectragraph from "seeing" the walls of the shock tube and, consequently, the radiation emitted by the surface of the tube.

Photographic recording of spectra allows the recording of all wavelength and line intensity data in a rather large portion of the

spectrum with a single (or multiple) discharge of a laboratory experiment. This is a distinct advantage if the plasma produced by the experiment is not sufficiently reproduceable which is often the case. The determination of intensities from the developed photographic film, however, cannot be done directly. The quantity which can be measured directly from the film is the photographic density D which is related to the transmission T of the film. For visible and ultraviolet light this relationship is (Mees, 1963)

$$D = \mathrm{Log}_{10}\ (1/T) \tag{4.33}$$

This photographic density is produced by the exposure ξ which is the energy received by a square centimeter on the photographic layer during the exposure time t_e. If the light flux is denoted by $F(t)$ the exposure is

$$\xi = \int_0^{t_e} F(t)dt \tag{4.34}$$

The density D which is produced on the film will depend on other factors such as development time and temperature, the developer solution used, age of the film and wavelength of the exposing light. The quantities T and D cannot be absolutely defined as their measurement will depend on the densitometer used (light sources, transmission of various components etc.). Therefore the film is normally calibrated by exposing a section to a standard light source

with different exposures. This is normally done by the use of a stepped filter having transmissions of 100% to about 1%. The film is then developed in the normal way and the density for each exposure measured. The characteristic curve (H-D or Hurter-Driffield curve) is then constructed by plotting the density D versus $\log_{10} \xi$. A typical curve experimentally obtained in this manner is shown in Figure 12. In the wavelength region below about 100 $\mathring{A}$ the above relationships do not hold. The large photon energies in this region are sufficient to make an emulsion grain developable by the absorption of a single photon compared to the 3 or 4 required per grain in the visible region. Thus if the film density D is plotted versus the exposure ξ a straight line is obtained (Mees, 1963). This situation eliminates the threshold of the emulsion which is commonly encountered with the lower energy photons. A typical characteristic curve obtained experimentally for this short wavelength radiation is shown in Figure 13. Obtaining the necessary characteristic curve for an emulsion in this region is extremely difficult due to a lack of standard sources and density filters for use in the region. Since relative line intensities were needed in order to determine the electron temperature the following procedure was carried out in order to obtain some information about the film characteristics. Two different film strips (from the same roll) were employed, the first being exposed to a single discharge and the second to two discharges. In each case the initial filling pressure, bank voltage and all other controllable parameters were the same. Furthermore

monitoring of the continuum intensity (proportional to the electron density) and the temperature insure that these parameters were the same within a few percent on each discharge. The films were then developed in the same solution for the same length of time and then dried. These two films were then scanned on a microdensitometer at the same sensitivity. Spectral lines throughout the region of interest were compared and in each case their peak intensities differed by about a factor of two indicating that the film response was approximately linear in the region if zero threshold is assumed.

One disadvantage of the instrument is that the small diameter of the Rowland circle (100 cm) prevents the standard thickness of SWR glass plates from being used, as it proved impossible to bend them to the required curvature without breakage. This particular difficulty could be overcome to a certain extent by the use of Ilford Q-2 plates. However, the emulsion on the Q-2 plates saturated at a rather low level so that in order to record weak lines it was necessary to grossly overexpose the more intense lines. The data were finally recorded on 35-mm Eastman Kodak SWR film. This film was not completely satisfactory, as it has a tendency to stretch somewhat during development. The film also initially presented a problem in keeping it on the Rowland circle, as it tended to curve after having been clamped in place and placed under vacuum. This problem was resolved by mounting the film strip between two flat, thin metal strips in a sandwich arrangement. The outer strip had a horizontal slot 1 cm wide to allow the radiation to strike the film. Further improvement was obtained by clamping only one end of

the film in the holder and then evacuating the system. The clamping arrangement could be controlled from outside the vacuum so that the second end of the film could be clamped after the required vacuum was obtained. Some further disadvantages were encountered with the films that also occur with the glass plates. This is the normal difficulty with the Schumann-type emulsions which consist of grains of emulsion supported from behind by a thin layer of gelatin. These emulsions are very sensitive to pressure fogging, scratching, and dust, which requires that they be handled with the utmost care. There is also some variation in the sensitivity of the emulsion from box to box.

After a film had been placed in the instrument and the instrument had been evacuated, the recording of a spectrum proceeded in the following manner. A valve between the spectrograph and the shock tube was kept closed while the shock tube was evacuated to its base pressure and then filled with gas. The capacitor banks were then charged and, with the valve still closed, the discharge was initiated. This procedure was followed and carried out a minimum of five times before the valve between discharge and spectrograph was opened and the exposure made. This procedure "cleaned up" the shock tube as the accumulate contamination on the walls of the shock tube were burned off by these preliminary discharges. Normally, a good exposure was obtained with a single discharge.

After a film had been exposed, it was removed from the instrument and developed. These films were developed by constant agitation for

4 minutes in Kodak D-19 developer diluted in the ratio of three parts water to one part developer. The film was then rinsed in deionized water for 10 seconds and then immersed in Kodak Rapid Fix for 4 minutes. The fixing was followed by a 12-minute wash in running water and then dried at room temperature (23° C). The temperature of the developer, rinse, and fixer was kept at room temperature and the same development procedure was followed on each film. After the film had dried, it was examined visibly and the necessary identification information was put on the film. The film was then scanned on a microdensitometer and the film, along with the tracings, was stored until ready for data analysis.

In order to insure that the plasma conditions did not vary excessively from discharge to discharge, a monitor system consisting of a 1-meter focal length, normal incidence vacuum monochromater (McPherson Instrument Corp.) using an EMI 6256 photomultiplier tube, and a 1-meter focal length Czerny-Turner monochromater (McPherson Instrument Corp.) using an Amperex 150 AVP tube was employed. The vacuum instrument measured the total intensity of the $1s2s\ ^3S_1$ - $1s2p\ ^3P^o_1$ transition at 1637.96 Å and the $1s2s\ ^3S_1$ - $1s2p\ ^3P^o_o$ at 1639.58 Å of O VIII together. In order to obtain the high stage of ionization from which this radiation is produced, a fairly high temperature is required. By recording the intensity of the line on an oscilloscope, a time history was obtained. The appearance of this line with a reasonable intensity was sufficient to indicate that compression of the plasma had taken place and in conjunction with the

second monochromater signal, which was indicative of the density, indicated that the electron temperature had reached an acceptable value. The second monochromater measured the intensity in a 15 Å wide band at 5221 Å. At the high temperatures obtained in the plasma, the radiation at this wavelength should be due to bremsstrahlung. This was verified by spectra of the plasma recorded in this region which showed no line radiation other than that from low stages of ionization which would not exist at the higher temperature. The particular region used showed no line radiation at all, so the recorded signal was due to continuum radiation. Furthermore, during the compression stage, recombination rates which decrease with increasing temperature would be expected to lag ionization rates (Kunze, Gabriel, and Griem, 1968) so that the continuum emission should be dominated by free-free emission rather than free-bound. For a Maxwellian distribution of electron velocities the free-free emission coefficient, follows from Kramer's (1923) calculations

$$\varepsilon_\nu^{ff} = \frac{16\pi e^6 \sum n_e n_z Z^2 g^{ff}}{3c^3 \left(6\pi m_e{}^3 kT_e\right)^{1/2}} \exp\left(-\frac{h\nu}{kT_e}\right) \qquad (4.35)$$

The Gaunt factor g^{ff} is a quantum mechanical correction and to a first approximation is set equal to 1. The other symbols have their usual meaning. Thus, the intensity of the free-free emission is very nearly (at low percentage of contaminants) proportional to n_e^2 so that variation in the intensity of this signal is indicative of variations in the electron density (impurities can give a dominant

contribution if high Z ions are present). Only a 10 percent variation was accepted in these signals to insure that each spectrum was recorded under approximately the same conditions of density and temperature. Typical traces obtained with the two instruments are shown in Figures 14 and 15.

C. Data Analysis

The microdensitometer scan of the film provided a plot of film density as a function of length along the film. Wavelengths of the spectral lines were determined from these microdensitometer tracings. Traces of carbon, nitrogen, and oxygen are always present as a contaminant in the plasma and the hydrogen-like and helium-like spectra of these elements lie in the region of interest so that a convenient wavelength calibration was available on all the spectra used. The various lines used for this purpose are listed in table IV.4. The wavelengths and transitions of these lines were taken from the tables of Kelly (1968). After the known lines had been identified, the wavelengths of the unknown lines and, in particular the satellite lines could be determined. The probable error of the satellite wavelengths was established by comparing the position of the known lines used as wavelength standards to the position calculated from equation (4.20). The angle of reflectance β may be written in terms of the linear distance ℓ from the center of the grating to the corresponding wavelength. From Figure 9,

$$\ell = \frac{R}{2} (\pi - 2\beta) \qquad (4.36)$$

Table IV.4

Ion	Transition	Wavelength, Å
CV	$1s^2\ ^1S_0 - 1s2p\ ^3P^o_1$	40.731
CV	$1s^2\ ^1S_0 - 1s2p\ ^1P^o_1$	40.270
CV	$1s^2\ ^1S_0 - 1s3p\ ^1P^o_1$	34.973
CVI	$1s\ ^2S_{1/2} - 2p\ ^2P^o_{3/2}$	33.736
NVI	$1s^2\ ^1S_0 - 1s2p\ ^3P^o_1$	29.084
NVI	$1s^2\ ^1S_0 - 1s2p\ ^1P^o_1$	28.787
NVII	$1s\ ^2S_{1/2} - 2p\ ^2P^o_{3/2}$	24.781
OVII	$1s^2\ ^1S_0 - 1s2p\ ^3P^o_1$	21.804
OVII	$1s^2\ ^1S_0 - 1s2p\ ^1P^o_1$	21.602
OVIII	$1s\ ^2S_{1/2} - 2p\ ^2P^o_{3/2}$	18.969
OVIII	$1s\ ^2S_{1/2} - 3p\ ^2P^o_{3/2}$	16.006

Solving equation (4.36) for β,

$$\beta = \frac{\pi}{2} - \frac{\ell}{R} \tag{4.37}$$

and using the trigonometric identity for the sin of the difference of two angles gives

$$\sin \beta = \cos \frac{\ell}{R} \tag{4.38}$$

The difference in the wavelength calculated and the published wavelength of the line never exceeded ± 0.05 Å over the range of interest so that the calculated wavelengths of the satellites should be within this accuracy.

An attempt to record the intensity, as a function of time, of the satellite and the resonance lines was made. To this end the film holder assembly was removed from the grazing incidence spectrograph and replaced by two photoelectric detectors. These detectors consisted of a thin plastic scintillator (Naton 136) coated with a thin aluminum film on both sides. The edge of the scintillator served as the exit slit, while the aluminum coating prevented light loss out of the sides. The back edge of the scintillator was optically coupled to a glass fiber light guide by a drop of high-viscosity silicone oil. The other end of the light guide was placed in front of the photocathode of an Amperex 150 APV photomultiplier which was isolated from the vacuum chamber by a quartz (SiO_2) window.

While it was possible to obtain time resolved signals of the radiation in this manner (in particular the resonance lines), it was not possible to observe the satellite lines. This was due to the low intensity of the lines and also due to the large amount of scattered light at these wavelengths. The scattered light is due to the central image which contains all wavelengths of light. The use of filters was not possible as this reduced the intensity of the satellite as well as the scattered light. Therefore, the effort was abandoned and no time resolved data were obtained.

CHAPTER V

RESULTS AND CONCLUSIONS

A. Results with Boron and Carbon

Long wavelength satellites to the hydrogen-like resonance line of carbon VI were first reported in the spectrum of a theta-pinch plasma by Roth and Elton (1968). These lines were observed in the spectrum produced by several discharges using deuterium as a fill gas. The facility used in this investigation is very similar to that used by these authors and was expected to produce a reasonably similar plasma (i.e., same electron temperature and density if operated under the same conditions of filling pressure and main bank energy). Thus, the reasonable starting point for this investigation was to obtain a spectrum under the same experimental conditions as those used by Roth and Elton (1968). Carbon along with other impurities such as oxygen and silicon are always present in the discharge. The carbon is due to vacuum pump oil (a hydrocarbon compound) which manages to "backstream" past the liquid nitrogen cold trap between the vacuum pump and the quartz (SiO_2) tube containing the gas. Over a period of several hours of pumping, the oil is deposited on the walls of the quartz tube and is injected into the plasma along with the silicon and oxygen during the preheating phase. The spectrum obtained therefore contained carbon lines with very good intensity. After the film on which the spectrum was recorded had dried, it was scanned

on a Joyce-Loebl microdensitometer at a 50 to 1 scanning ratio so that the distance between a given pair of lines was 50 times as great on the recording as on the film. The microdensitometer employs a single lamp to measure alternatively the transmission of the film and the transmission of a calibrated density wedge so that the photometric density D is therefore recorded. While a spectrum was being scanned on the microdensitometer, the spectral region of interest was visually monitored through a magnifying glass to insure that all weak lines were recorded and noted. The microdensitometer recording of the film obtained with deuterium is shown in Figure 16. The tracing shows 11 lines (Roth and Elton reported nine, one of which was observed only in second order) to the long wavelength side of the carbon VI resonance line at 33.734 $\mathring{A}$ and lying between it and the $1s^2\ {}^1S_0 - 1s3p\ {}^1P_1^o$ transition of carbon V at 34.973 $\mathring{A}$. The measured wavelengths of these lines are included on Figure 16 along with the composition and initial pressure of the fill gas, as well as the electron temperature estimated by the method discussed in Chapter IV. The agreement between the observed wavelengths and the calculated wavelengths of the satellites is in remarkably good agreement. However, three of the observed lines correspond to satellite transition where the upper (doubly excited) state cannot be formed by inverse autoionization, as the process is forbidden by parity. A comparison between these measured and calculated values is given in table V.1.

Table V.1

Calculated Satellite Wavelength, Å		Observed Wavelength, Å
33.849	$(1s3p\,^1P^o - 2p3p\,^1D)$	33.85
33.939*	$(1s3p\,^3P^o - 2p3p\,^3P)$	33.96
34.029 34.032	$(1s3s_1\,^3S - 2p3s_1\,^3P^o)$ $(1s3s\,^1S - 2p3s\,^1P^o)$	
34.086	$(1s3p\,^3P^o - 2p3p\,^3S)$	34.10
34.125	$(1s2p\,^1P^o - 2p^2\,^1S)$	
34.153	$(1s3p\,^3P^o - 2p3p\,^3D)$	34.17
34.247*	$(1s3p\,^1P^o - 2p3p\,^1P)$	34.24
34.427	$(1s2s\,^1S - 2s2p\,^1P^o)$	34.35
34.586	$(1s2p\,^1P^o - 2p^2\,^1D)$	34.52
34.685	$(1s2s\,^3S - 2s2p\,^3P^o)$	34.68
34.804*	$(1s2p\,^3P^o - 2p^2\,^3P)$	34.79

*Upper level of this transition cannot undergo autoionization (forbidden by parity).

The intensities of these observed lines, however, were too low to allow photoelectric recording which was required in order to investigate the time history of the line intensities. This part of the investigation was required in order to determine the stage of ionization responsible for the formation of the doubly excited states since the doubly excited state could be formed by inverse autoionization involving free electrons and hydrogen-like ions or by collisional excitation of both electrons of the helium-like ion. This latter process is less likely since much more energy is involved than in the formation from a free electron and a hydrogen-like ion. The concentration of the hydrogen-like and the helium-like ions would be a maximum at different temperatures and, for the transient plasma in the theta-pinch, at different times. This is borne out by Figure 2 which shows the temperature dependence of the carbon ions. Thus if the doubly excited state were formed by inverse autoionization the intensity of the satellite would reach a maximum when the number of hydrogenic ions is a maximum. This maximum number of hydrogenic ions would be indicated by a maximum intensity of the hydrogenic resonance line as indicated by equation (3.63). Thus if,as expected,inverse autoionization were the mechanism by which the doubly excited states were formed the satellite intensity should reach a maximum simultaneously with the hydrogenic resonance line. If, on the other hand, the doubly excited states were formed by collisional excitation in helium-like ions (which is less likely)

the satellite intensity would reach a maximum when the concentration of helium-like ions is a maximum. This maximum would be indicated by a maximum in the intensity of the helium-like resonance line. Thus if collisional excitation were responsible for the formation of the doubly excited states the satellite intensity should reach a maximum simultaneously with the helium-like resonance line. Furthermore, collisional excitation should lead to the formation of doubly excited states which cannot autoionize and therefore cannot be formed by inverse autoionization so that if collisional processes were important satellites corresponding to transitions from these states should be observed. In fact, three wavelengths (33.939 Å, 34.247 Å, and 34.804 Å) which were calculated for such transitions were observed; however, this did not mean that all lines were formed by collisional processes. The percentage of carbon in the deuterium fill gas was increased to 2.5 percent by the addition of acetylene (C_2H_2). The microdensitometer recording of the satellite lines obtained on this film is shown in Figure 17. The interesting result obtained is that there is no apparent increase in the intensity of the satellites over the previous spectrum obtained with only deuterium, even though there was a noticeable increase in the other carbon lines (about a factor of two for the CV line at 34.973 Å). A third spectrum taken with the carbon concentration increased to 5 percent produced the same peculiar result of increasing the intensity of the normal carbon lines but with not apparent effect on the satellite intensities. Higher concentrations of carbon were not attempted as

impurity concentrations above this level were found to result in a lower temperature plasma.

While the above result was surprising it did not prove conclusively that the lines were not due to carbon. The rate coefficient for dielectronic recombination was examined to determine if the above result could be explained in terms of its temperature dependence. An approximate general formula for the total rate coefficient K_d has been derived by Burgess (1965b)

$$K_d = - \frac{1}{T_e^{3/2}} \sum_p f(q,p) \exp\left(- \frac{E(q,p)}{kT_e}\right) \phi \ \text{cm}^3\text{sec}^{-1} \qquad (5.1)$$

where $f(q,p)$ is the oscillator strength and $E(q,p)$ the energy of the transition $q \rightarrow p$ with q the initial state of the recombining ion. The function ϕ is separable into two slowly varying functions of Z, the charge of the recombining ion and of $X = (Z + 1)^2 \varepsilon_{q,p}$ respectively, where $\varepsilon_{q,p}(Z + 1)^2$ is defined as the energy in Rydbergs of the transition $p \rightarrow q$. The summation is carried out over all excited states p of the recombining ion, of which the first is usually the most important (Goldberg, 1966). Using this approximate formula, Goldberg (1966) derives the temperature at which K_d has its maximum value. Goldberg obtains the relation

$$T_{max} = 0.96\nu \ ^oK \qquad (5.2)$$

where ν is the frequency of the resonance line of the recombining ion in wavenumbers. Thus the simple rule for estimating the temperature at which dielectronic recombination is most effective(it can be much greater than radiative recombination) is to take the temperature equal to the wavenumber of the resonance line of the recombining ion. Using this estimate one would expect dielectronic recombination to be most important for carbon VI at a temperature of 2.96×10^6 ^oK (255.2 eV) which is slightly higher than the electron temperature obtained in the theta-pinch plasma if dielectronic recombination is ignored. Therefore, boron was chosen as the next element to be investigated since the resonance line of boron V at 48.587 $\mathring{A}$ predicts a temperature of 2.06×10^6 ^oK (177.6 eV) at which dielectronic recombination should be a maximum. This temperature is at the lower end of the electron temperature range produced in the theta-pinch. Boron was introduced into the experiment in the form of diborane (B_2H_6) gas. This gas was only available as a mixture of diborane and hydrogen with a maximum concentration of diborane of 10% (this concentration is set by the Interstate Commerce Commission). Thus the maximum concentration of boron was limited to 2.5%. The microdensitometer recording of the spectral region on the long wavelength side of the boron V resonance line obtained from this set of conditions is shown in Figure 18. The region containing the calculated satellite wavelengths (48.743 $\mathring{A}$ to 50.118 $\mathring{A}$) contains only three lines, only two of which correspond in wavelength to the calculated

values of the satellites and the third could be a silicon line. Furthermore, both of these transitions have the same upper configuration of 2p3p. This result was more surprising than the carbon results since 2p3p has five terms, two of which are forbidden by parity from inverse autoionization ($^3P, ^1P$). Of the remaining three it seemed a bit unusual that only the ^1D and ^3D terms would be observed with no indication at all of the ^3S term. Furthermore, the transition corresponding to the configuration 2s2p and $2p^2$ certainly would have been expected rather than those observed. The intensities of the two lines were also greater than expected as the intensity ratio of the observed line to resonance line was of the order of 10^{-2} which is larger than the calculated maximum ratio of 10^{-4} for the boron satellites. This indicated that the lines were not satellites but had some other origin. The first film recorded in the investigation was then reexamined and the microdensitometer recording of the region on the long wavelength side of the boron V resonance line is shown in Figure 19. The suspicion that the two lines were not due to boron was confirmed as the two lines are still in evidence in Figure 19 even though there was no boron in the system and, in fact, the spectrum had been recorded before boron had been introduced into the system so there was no possibility of boron being present as a contaminant. Examination of the wavelength tables of Kelly (1968) showed that the wavelengths of the two lines correspond to transitions in argon IX. The origin of argon in the system was not immediately apparent; however, argon had been used in the

system in the past so it was not inconceivable that some argon was still present in the system although any residual amount should have been small and not of sufficient concentration to produce observable lines. The possibility of the lines being due to argon was investigated by introducing argon into the fill gas at a concentration of 100 ppm (0.01%) and a spectrum obtained. The microdensitometer recording of the two lines recorded on this spectrum are shown in Figure 20. Obviously, the two lines are due to the argon as the line intensity of each exceeds that of the boron V resonance line. Further examination of the spectra revealed that the intensities of the lines to the long wavelength side of the carbon VI resonance line had increased considerably. The microdensitometer recording of these lines is shown in Figure 21. A further increase in the argon concentration by a factor of ten (10^3 PPM or 0.1%) resulted in the spectrum from which the microdensitometer recordings shown in Figure 22 (boron V resonance line region) and figure 23 (carbon VI resonance line region) were made. These two recordings demonstrate quite conclusively that the hydrogen-like resonance lines of boron and carbon overlap with the argon ion spectra. The wavelength of seven of the lines on the long wavelength side of the carbon resonance line as well as the two lines on the long wavelength side of the boron resonance line are listed in the wavelength tables of Kelly (1968). Of the four remaining lines adjacent to the carbon resonance line three have recently been observed and classified (Fawcett, Gabriel and Paget, 1971). The observed wavelengths, tabulated wavelength

of the argon ions as well as their transition and the wavelength and transition of the satellite lines, calculated by the Hartree-Fock program, are listed in table V.2. The last remaining line at 34.17 Å could not be identified. While there appears to be a slight increase in its intensity when argon is introduced into the plasma, the increase is not of the same order of magnitude as that of the other argon lines and is more of the order of a discharge to discharge variation. The faintness of the image recorded on the film makes a positive identification impossible, although the evidence suggests that this very weak line may not be due to the argon. The overlap of the argon ion spectra with the regions of interest precluded any further investigation until the origin of the argon could be determined. Two possibilities for the introduction of argon into the system were leakage of air into the vacuum system and contamination of the fill gas being used in the system in spite of the fact that research grade gas was always used. Air contains 0.934% argon by volume (Dubin, Sissenwine, and Wexler, 1962) which corresponds to a particle density of 2.51×10^{17} cm^{-3} at STP. If the residual background gas in the vacuum vessel is assumed to contain the same percentage of argon (i.e. 0.934%) then the background pressure of 1×10^{-6} torr would contain an argon number density of 3.3×10^{8} cm^{-3} which at maximum compression would increase to 3.3×10^{10} cm^{-3} (i.e., a compression ratio of 100). A larger contributor to the argon density, however, was the amount contained in the research grade deuterium. A complete analysis of the gas obtained from the

Table V.2

Observed Wavelength, Å	Argon Wavelength, Å	Transition	Calculated Satellite Wavelength, Å
33.85	33.84 Ar XI	$2s^2 2p^4\ {}^3P_1 - 2s^2 2p^3({}^2P)3d\ {}^3D^o_2$	33.849 CV
33.96	33.96 Ar XI	$2s^2 2p^4\ {}^3P_0 - 2s^2 2p^3({}^2P)3d\ {}^3D^o_1$	33.939
			34.029
			34.032
34.10	34.10 Ar XI	$2s^2 2p^4\ {}^3P_2 - 2s^2 2p^3({}^2D)3d\ {}^3S^o_1$	34.086
			34.125
34.17			34.153
34.24	34.24 Ar XI	$2s^2 2p^4\ {}^3P_2 - 2s^2 2p^3({}^2D)3d\ {}^3S^o_2$	34.247
34.35	34.35 Ar XI	$2s^2 2p^4\ {}^3P_2 - 2s^2 2p^3({}^2D)3d\ {}^3D^o_3$	34.427
34.52	34.52 Ar XI	$2s^2 2p^4\ {}^3P_1 - 2s^2 2p^3({}^2D)3d\ {}^3D^o_2$	34.586
34.68	34.68 Ar XII	$2s^2 2p^3\ {}^4S^o_{3/2} - 2s^2 2p^2({}^3P)3s\ {}^4P_{5/2}$	34.685
34.79	34.79 Ar XII	$2s^2 2p^3\ {}^4S^o_{3/2} - 2s^2 2p^2({}^3P)3s\ {}^4P_{3/2}$	34.804
48.73	48.73 Ar IX	$2s^2 2p^6\ {}^1S_0 - 2s^2 2p^5({}^2P^0)3s\ \frac{1}{2}\ [\frac{1}{2}]^o_1$	48.743 BIV
			48.872
			49.002
			49.006
			49.084
			49.140
49.18	49.18 Ar IX	$2s^2 2p^6\ {}^1S_0 - 2s^2 2p^5({}^2P^0)3s\ \frac{3}{2}\ [\frac{3}{2}]\ {}^o_1$	49.180
			49.316
			49.575
			49.784
			49.946
			50.118

supplier (The Matheson Company) showed an argon concentration of 15 PPM. This concentration amounts to a particle density of 3.3×10^{12} cm^{-3}, that is, two orders of magnitude greater than the background gas. The intensity of a typical argon ion line in the wavelength region of interest was estimated with the assumption that only two ionization stages of argon existed (AXI and AXII) and using only the concentration of argon in the deuterium fill gas (since the contribution of argon in the residual background gas in the vacuum vessel would contribute only one percent of the argon and could be ignored without affecting the accuracy of the estimate). The ratio of A XII ions to A XI ions was determined from equation (4.18) ignoring dielectronic recombination. At an electron temperature of 200 eV the ratio is

$$\frac{n\ (A\ XII)}{n\ (A\ XI)} = 16.5 \tag{5.3}$$

If the effects of dielectronic recombination were included a slightly lower ratio would result in equation (5.3). However, the work of Burgess and Summers (1969) suggest that the correction would be small and well within the approximations made in obtaining the value in equation (5.3). Since the sum of the argon XI and argon XII number density is assumed to equal the total density of argon, the argon XII number density is

$$n(A\ XII) \approx 3 \times 10^{12}\ cm^{-3} \tag{5.4}$$

The argon XII line radiation in the region of interest consists of transition to the ground state at a wavelength which corresponds to the transition from the doubly excited state in carbon V. Thus, the excited argon XII level lies approximately 360 eV above the ground state. The absorption oscillator strength for the argon XII transition was estimated to be 0.3 by use of the Coulomb approximation of Bates and Damgaard (1949). The rate coefficient for collisional excitation $K(1,q)$ (equation (3.18))was then evaluated using the above values of $f(1,q)$ and $E(1,q)$ and an electron temperature of 200 eV. The results

$$K(1,q) \approx 1 \times 10^{-8} \text{ cm}^3 \text{ sec}^{-1} \tag{5.5}$$

was then substituted in equation (3.43) to obtain an expression for the number density in the excited state

$$\frac{n(q)}{n(1)} = \frac{n_e}{A(q)} \times 10^{-8} \tag{5.6}$$

Taking the upper state of the argon XII transition as the first excited level (i.e., the only allowed spontaneous transition is to the ground level) and using the previously discussed values of $n(\text{A XII})$ and n_e, the number density of excited levels becomes

$$n(2) \approx \frac{10^{22}}{A(2,1)} \text{ cm}^{-3} \tag{5.7}$$

Using equation (3.65) for the intensity of the satellite line and equation (3.47) for the intensity of the argon XII line the intensity ratio of argon XII to satellite is approximately

$$\frac{I(\text{A XII})}{I(\text{sat.})} \approx \frac{10^{22}}{A_d(p,q)n(d)} \tag{5.8}$$

The number density of doubly excited states in carbon V for a 5% concentration of carbon was determined from the Saha-Boltzmann equation [equation (3.36)] since this gives a maximum, with plasma condition of $kT_e = 200$ eV and $n_e = 2.2 \times 10^{17}$ cm^{-3}. The Saha-Boltzmann equation predicts for these conditions

$$n(d) \lesssim 10^{11} \text{ cm}^{-3} \tag{5.9}$$

The calculations of oscillator strengths as discussed in Chapter II show that the transition probability for a typical carbon satellite is of the order of 10^{10} sec^{-1}. Using this value the intensity ratio of argon XII to carbon VI satellite becomes

$$\frac{I(\text{A XII})}{I(\text{sat.})} \approx 10^{1} \geq 10 \tag{5.10}$$

Thus the intensity of the argon XII line due to the contamination in the fill gas would exceed the intensity of the satellite by a factor of 10 if the number density of doubly excited states is its

equilibrium value. However, it has been pointed out that the lifetime of the doubly excited state to radiative decay is of the same order of magnitude as the time between electron collision and therefore it would be expected that the population of the doubly excited states would be below the equilibrium value. This condition was verified experimentally by the installation of a deuterium gas purifier. This purifier consisted of a palladium-silver element heated electrically. The palladium-silver alloy has the unique property of allowing only hydrogen (and its isotope deuterium) to pass through a thin wall constructed of the alloy. Thus any element heavier than deuterium is removed from the gas and only ultrahigh purity deuterium is fed into the vacuum system. The purifier used was constructed by the National Bureau of Standards (Gaithersberg, Md.) and purifies hydrogen of 95% purity to a purity level which could not be determined. A microdensitometer recording of a spectrum obtained with the purified deuterium is shown in Figure 24. The recording covers the region to the long wavelength side of the carbon VI resonance line and shows a conspicuous absence of satellite lines. A careful comparison of Figure 24 and Figure 16 shows that, at most, only three lines are faintly visible. It was not anticipated that the lines would disappear completely, as the concentration of argon due to leakage of air into the vacuum system could not be eliminated. That these three lines were not satellites was confirmed by the addition of carbon to the system (up to 5%) with no observed increase in their intensity.

The establishment of detectable intensity ratios also indicated that the lines which were observed could not be satellites. The limit of detectability was determined (for the film used) by calculating the intensity ratio of the weakest detectable line in the region of interest, to the carbon VI resonance line. It was assumed that the film had a linear response as discussed in Chapter IV and the profile of each line was assumed to be triangular. This ratio indicated that an intensity ratio of about 10^{-3} could be detected with certainty (which is about the maximum value for carbon at temperature of 200 eV.) This limit was due to saturation of the emulsion at the resonance line center and increasing the exposure in order to increase the detectability of weak lines prevented the determination of the recorded resonance line intensity and did not show any satellites. Thus it was concluded that the transitions involving doubly excited states were not observable under the experimental conditions and that even if the satellites would have appeared with a reasonable intensity the overlap of the argon ion spectra would have rendered these two cases (boron and carbon) as unsuitable for further investigation.

B. Results with Nitrogen

Since carbon and boron were shown to be unacceptable elements for the experiment, the last element, nitrogen, which was feasible to investigate in this experiment due to the accessability of the hydrogen-like resonance line and since it was possible to produce the hydrogen-like ion, was introduced into the plasma using the ultra

high purity (using the palladium leak) deuterium as a fill gas. The research grade nitrogen which was used contained about 5 PPM of argon but since the percentage of nitrogen introduced into the system would be small (a maximum of 3% N_2 or 6% N) the total amount of argon introduced into the system would only be about 0.3 PPM which would correspond to a particle density of about 7×10^9 cm^{-3} which is less than the concentration of argon in the residual gas in the vacuum vessel. Figure 25 is the microdensitometer recording of the spectrum obtained with 1% N_2 added to the fill gas. The recording covers the region to the long wavelength side of the N VII resonance line at 24.781 Å. Two lines are visible in the region and their wavelengths are in resonable agreement with the calculated values of two of the satellites. However, the intensity ratio of the observed line to resonance line was found to be approximately 7.5×10^{-2} (as determined by the method of the previous section) which is larger than the maximum value calculated for the satellites (even if the values obtained by Gabriel and Paget (1972) are used.) Spectra at high concentration of N_2 (2% and 3%) were obtained and the microdensitometer recordings of the region are shown in Figures 26 and 27. The two lines are obvious in both of these recordings and the ratio of observed line to resonance line in each case is the same as that obtained for the first case. This large intensity ratio could not be resolved in the light of dielectronic recombination and it was therefore concluded that the two lines were not due to transition from doubly excited states but were more likely to be due

to a contamination in the gas. Argon XII lines at approximately these wavelengths have recently been identified by Fawcett, Gabriel, and Paget (1971) and it was concluded that these lines most likely were due to the argon contamination in the background gas. This result was finally verified after extensive work on the vacuum system which improved the base pressure to about 10^{-8} torr. Spectra recorded under these conditions with 1% N_2 added showed that the two lines were not produced and that no satellite lines existed with sufficient intensity to be recorded. This situation existed even for a spectra recorded with as many as six discharges on a single film, even though the emulsion saturated at the center of the resonance line. Table V.3 compares the observed wavelengths with the calculated values of the satellite as well as the reported wavelengths of the argon ions.

C. Conclusions and Limits of Laboratory Experiments

Laboratory observation of transitions from doubly excited states in two electron ions does not appear to be very compatible with experimental devices such as the theta-pinch, the limiting factor being, of course, the low intensity of the spectral lines emitted in the transition from the doubly to the singly excited state. The experimental evidence indicates that even under the best conditions the detectability of the lines would not be possible in such an experiment with the photographic methods employed here. Even resorting to multiple exposures in order to increase the density on the film failed to show any evidence of satellites. This was due to

Table V.3

Observed Wavelength, Å	Argon Ion Wavelength, Å	Argon Transition	Calculated Satellite Wavelength, Å
			24.879
			24.944*
			25.001
			25.014
25.07	25.04	$2s^2 2p^3 - 2s^2 2p^2 4d^{\dagger}$	25.053
			25.082
			25.102
			25.172*
25.25	25.24	$2s^2 2p^3 - 2s^2 2p^2 4d^{\dagger}$	25.304
			25.421
			25.493
			25.581*

†Levels of these transitions have not been identified.

*Upper level of this transition cannot undergo autoionization (forbidden by parity).

the increase in the film background density due to continuum emission as well as scattered light from the central image (this is particularly bad in grazing incidence mountings when looking at the shorter wavelengths). Furthermore, the satellites are situated close to the resonance line so that increasing the exposure would increase the film density corresponding to the intensity in the wings of the line which in turn is another contribution to the film background. A minimum intensity ratio of satellite to resonance line of about 10^{-3} would be required for the satellites to be detectable with the photographic method used here. This is the maximum value calculated with the assumption of the doubly excited states being populated to their equilibrium value and even if this value were obtainable it would impose severe restrictions on such an experiment. There was, therefore, no experimental evidence to indicate that the process of dielectronic recombination is important in the theta-pinch since no lines which could be conclusively identified as true satellites were observed. This does not imply that such lines are not emitted in the plasma, but it does limit the intensity such a line would have which, at best, is of the same order of magnitude as the background noise. These conclusions also apply to previous experimental work in this field in which a high temperature discharge has been used to observe "satellites". In particular, in the experiments of Roth and Elton (1968) a theta-pinch device was used with essentially the same filling gas and electrical properties, since the design of the present experimentis very close to that of NRL, Washington. The correspondence between the lines identified here as argon and the fact that they made no special efforts to obtain pure filling gas indicate that their

identifications are in error. In addition, early work by Gabriel and Jordan (1969) who also used a theta-pinch was also incorrect for the same reasons. This has been confirmed by Gabriel (1971) (private communication).

However, recently Gabriel and Paget (1972) have reported the observation of satellites to the helium like resonance lines of nitrogen and oxygen in a theta-pinch. Their intensities ratios were of the order of their calculated values (i.e., a factor of 2 or 3 higher than the values calculated here). While oxygen satellites were not investigated in this experiment the results of Gabriel and Paget (1972) with nitrogen indicates that the failure to observe satellites in this experiment should have some reasonable explanation. The most probable explanation is based on the inverse temperature dependence of the intensity ratio. In the experiment discussed here the effect of dielectronic recombination was not taken into account in the calculation of the ionization balance required in the temperature determination. If this effect had been properly included or if a more accurate temperature measurement could have been made (by Thomson scattering) a higher temperature than the 200 eV obtained may have been found which would decrease the intensity ratio. Furthermore, higher electron densities were obtained in this experiment (by up to a factor of 10) which would give a smaller rate coefficient for dielectronic recombination. Further investigation would be required in order to determine which (if not both) of the two factors were responsible for the null result obtained.

Our conclusions that there is as yet no absolutely firm laboratory evidence for the formation of "satellites" by the process

of dielectronic recombination, does not mean that it is not an important astrophysical process. In fact, the circumstantial evidence from ionization balance is very convincing. However, the change overlap of argon with other spectra, as reported in this work, indicates that the identification of observed "satellites" in solar spectra (Fritz, et al., 1967; Rugge and Walker 1968; Jones, Freeman and Wilson 1968; Walker and Rugge, 1970) should be closely examined and the relative intensities carefully checked.

D. Suggestions for Future Work

The use of laboratory experiments to investigate the processes of dielectronic recombination still warrants further consideration. While the use of plasma devices such as theta-pinch for the investigation does not appear to be the most profitable due to lack of observation of the satellite lines for the case investigated here, other devices may be able to make a contribution in this area. The device commonly referred to as a sliding spark (Conrads and Hartwig, 1964), having a lower temperature than the theta-pinch (since R is proportional to T^{-1}) could be advantageous although the higher density could be a disadvantage. In fact, satellite lines of carbon were first observed in a spark device (Edlén and Tyrén, 1939) however, it is not clear whether dielectronic recombination or electron-excitation forms the doubly-excited states. While the diagnostics of such a device would be considerably more difficult, an investigation of the observed satellites in such a device should be carried out. Low temperature plasma devices in conjunction with a higher energy electron beam to excite the ions of interest would probably prove the most useful for this sort of investigation.

BIBLIOGRAPHY

Allen, C. W., Astrophysical Quantities, London, The Athlone Press, 1964.

Aller, L. H., The Atmospheres of the Sun and Stars, 2nd ed., New York, Ronald Press Company, 1963.

Bates, D. R., and Damgaard, A., Phil. Trans. Roy. Soc. London A, 242, 101, 1949.

Bates, D. R., and Dalgarno, A., "Electronic Recombination" in Atomic and Molecular Processes, ed. Bates, D. R., New York, Academic Press, 1962.

Beerwald, H., Bogen, P., El-Khalafawy, T., Fay, H., Hintz, E., and Kever, H., Nucl. Fusion Supp. part II, 595, 1962.

Beutler, H. G., J. Opt. Soc. Am. 35, 311, 1945.

Bodin, H. A. B., Green, T. S., Niblett, G. B. F., Peacock, N. J., Quinn, J. M. P., and Reynolds, J. A., Nucl. Fusion Supp. part II, 521, 1962.

Bohr, N., Z. Physik 9, 1, 1922.

Brown, F. W., Phys. Rev. 44, 214, 1933.

Burgess, A., and Summers, H. P., Ap. J. 157, 1007, 1969.

Burgess, A., "Dielectronic Recombination," The Formation of Spectrum Lines. Proceedings 2nd Harvard-Smithsonian Conference on Stellar Atmospheres, Cambridge, Smith. Astr. Obs. Spec. Rept. No. 174, 1965a.

Burgess, A., Ap. J. 141, 1588, 1965b.

Burton, W. M., and Wilson, R., Proc. Phys. Soc. 78, 1416, 1961.

Chandrasekhar, S., Radiative Transfer, New York, Dover Publications, Inc., 1950.

Compton, K. T., and Boyce, J. C., J. Franklin Inst. 205, 497, 1928.

Condon, E. U., and Shortley, G. H., The Theory of Atomic Spectra, Cambridge, The University Press, 1963.

Conrads, H., and Hartwig, H. Z. Angew. Phys. 17, 188, 1964.

Conrads, H., and Oertel, G., Ap. J. 153, 975, 1968.

Cooper, J., Rep. Prog. Phys. 29, 35, 1966.

Dalgarno, A., and Parkinson, E. M., Proc. Roy. Soc. A301, 253, 1967.

Delbrück, M., Proc. Roy. Soc. A129, 686, 1930.

Dirac, P. A. M., Proc. Roy. Soc. A112, 661, 1926.

Drake, G. W. F., and Dalgarno, A., Phys. Rev. A 1, 1325, 1970.

Dubin, M., Sissenwine, N., and Wexler, H., U. S. Standard Atmosphere, Washington, D. C., U. S. Govt. Printing Office, 1962.

Edlén, B., and Tyrén, F., Nature 143, 940, 1939.

Elwert, G., Z. Naturf. 7a, 432, 1952.

Evans, J. W., The Solar Corona, New York, Academic Press, 1963.

Fawcett, B. C., Gabriel, A. H., and Paget, T. M., J. Phys. B 4, 986, 1971.

Fay, H., Hintz, E., and Jordan, H., "Experiments on Shock Compression of Plasmas" in Proceedings of the Fourth International Conference on Ionization Phenomena in Gases, ed. Nilsson, R., Amsterdam, North Holland Publishing Co., 1959.

Feldman, U., and Cohen, L., Ap. J. 158, L169, 1969.

Flemberg, H., Ark. Mat. Astr. Fys. 28A, 1, 1942.

Fock, V., Z. f. Phys. 61, 126 1930a; Z. f. Phys. 62, 795, 1930b.

Fowler, R. H., Statistical Mechanics, Cambridge, Cambridge University Press, 1955.

Fritz, G., Kreplin, K. W., Meekins, J. F., Unzicker, A. E., and Friedman, H., Ap. J. 148, L133, 1967.

Froese, C., Description of a Hartree-Fock Program with Configuration Mixing, Univ. of British Columbia, 1965.

Gabriel, A. H., and Jordan, C., Monthly Not. Roy. Ast. Soc. 145, 241, 1969.

Gabriel, A. H., Private Communication, 1971.

Gabriel, A. H., and Paget, T. M., J. Phys. B 5, 673, 1972.

Garstang, R. H., Class Notes , University of Colorado, Physics 656, Atomic and Molecular Spectra, 1969.

Goldberg, L., "Astrophysical Implications of Autoionization" in Autoionization, ed. Temkin, A., Baltimore, Mono Book Corp., 1966.

Goldman, L. M., Pollock, H. C., Reynolds, J. A., and Westendorp, W. E., Phys. Rev. Letters 9, 361, 1962.

Goldman, L. M., and Kilb, R. W. C., J. Nucl. Energy C 6, 217, 1964.

Goldsmith, S., J. Phys. B 2, 1075, 1969.

Griem, H. R., Phys. Rev. 131, 1170, 1963.

Griem, H. R., Plasma Spectroscopy, New York, McGraw-Hill, 1964.

Hartree, D. R., Proc. Cambridge Phil. Soc. 24, 89, 1928.

Hartree, D. R., and Hartree, W., Proc. Roy. Soc. A150, 9, 1935.

Hearn, A. G., Proc. Sixth Conf. Ionization Phenomena in Gases, Paris, 3, ed. Hubert, P., Orsay, Faculti des Sciences, 289, 1964.

Herman, F., and Skillman, S., Atomic Structure Calculations, Englewood Cliffs, Prentice-Hall, Inc., 1963.

Hobbs , G. D., McWhirter, R. W. P., Griffen, W. G., and Jones, T. J. L., Proc. Fifth Conf. Ionization Phenomena in Gases, Munich 2, ed. Maecker, H., Amsterdam, North Holland Publishing Co., 1965, 1962.

Jackson, J. D., Classical Electrodynamics, New York, John Wiley and Sons, Inc., 1962.

Jefferies, J. T., Spectral Line Formation, Waltham, Blaisdell Publishing Co., 1968.

Jones, B. B., Freeman, F. F., and Wilson, R., Nature 219, 252, 1968.

Kelly, R. L., NRL Report 664B, 1968.

Kiang, A. T., Ma, S. T., and Wu, T. Y., Chinese J. Phys. 2, 117, 1936.

Kolb, A. C., Dobbie, C. B., and Griem, H. R.,Phys. Rev. Letters 3, 1, 1959.

Kolb, A. C., Phys. Rev. Letters 3, 5, 1959.

Kolb, A. C., Griem, H. R., Lupton, W. H., Phillips, D. T., Ramsden, S. A., McLean, E. A., Faust, W. R., and Swartz, M., Nucl. Fusion Supp. part II, 553, 1962.

Kolb, A. C., and McWhirter, R. W. P., Phys. of Fluids 7, 519, 1964.

Koopmans, T. A., Physica 1, 104, 1933.

Kramers, H. A., Phil. Mag. 46, 836, 1923.

Kunze, H. J., Gabriel, A. H., and Griem, H. R., Phys. Rev. 165, 267, 1968.

Landini, M., and Fossi, B. C. M., Solar Phys. 20, 322, 1971.

Lie, T. N., and Elton, R. C., Phys. Rev. A 3, 865, 1971.

Little, E. M., Quinn, W. E., and Ribe, F. L., Phys. of Fluids 4, 711, 1961.

Little, E. M., Quinn, W. E., Ribe, F. L., and Sawyer, G. A., Nucl. Fusion Supp. part II, 497, 1962.

Mack, J. E. Stehn, J. R., and Edlén, B., J. Opt. Soc. Am. 22, 245, 1932.

Mees, C. E. K., The Theory of the Photographic Process, New York, The Macmillan Co., 1963.

McWhirter, R. W. P., Proc. Phys. Soc. A75, 520, 1960.

McWhirter, R. W. P., "Spectral Intensities" in Plasma Diagnositc Techniques, eds. Huddlestone, R. H., and Leonard, S. L., New York, Academic Press, 1965.

Namioka, T., J. Opt. Soc. Am. 49, 446, 1959.

Namioka, T., J. Opt. Soc. Am. 51, 4, 1961.

Oertel, G. K., and Williams, M. D., Rev. Sci. Instr. 36, 672, 1965.

Oertel, G. K., and Jalufka, N. W., Bull. Am. Phys. Soc. 11, 586, 1966.

Pauli, Jr., W., Z. Phys. 31, 765, 1926.

Peacock, N. J., Speer, R. J., and Hobby, M. G., J. Phys. B 2, 798, 1969.

Perrott, R. H., and Stewart, A. L., J. Phys. B. 1, 1968.

Post, R. F., J. Nucl. Energy, C, 3, 273, 1961.

Quinn, W. E., Little, E. M., and Ribe, F. L., Bull. Am. Phys. Soc. 5, 341, 1960.

Roothaan, C. C. J., Revs. Mod. Phys. 23, 69, 1951.

Rose, D. J., and Clark, Jr., M., Plasmas and Controlled Fusion, New York, John Wiley and Sons, Inc., 1961.

Roth, N. V., and Elton, R. C., NRL Report 6638, 1968.

Rugge, H. R., and Walker, A. B. C., Space Res. 8, 439, 1968.

Runge, C. R., and Mannkopf, R., Z. Physik 45, 13, 1927.

Samson, J. A. R., Techniques of Vacuum Ultraviolet Spectroscopy, New York, John Wiley and Sons, Inc., 1967.

Sawyer, G. A., Jahoda, F. C., Ribe, F. L., and Stratton, T. F., JQSRT 2, 467, 1962.

Seaton, M. J., "The Theory and Excitation and Ionization by Electron Impact" in Atomic and Molecular Processes, ed. Bates, D. R., New York, Academic Press, 1962.

Shamey, L. J., Private Communication, 1970.

Shore, B. W., and Menzel, D. H.; Ap. J. Suppl. 12, 187, 1965.

Shore, B. W., and Menzel, D. H., Principles of Atomic Spectra, New York, John Wiley and Sons, Inc., 1968.

Slater, J. C., Phys. Rev. 35, 210, 1930.

Slater, J. C., Phys. Rev. 81, 385, 1951.

Slater, J. C., Quantum Theory of Atomic Structure, Vol. I and II, New York, McGraw-Hill Book Co., Inc., 1960.

Spitzer, Jr., L., Physics of Fully Ionized Gases, New York, Interscience Publishers, 1967.

Strömgren, B., Ap. J. 108, 242, 1948.

Uhlenbeck, G. E., and Goudsmit, S., Naturwiss. 13, 953, 1925.

Uhlenbeck, G. E., and Goudsmit, S., Nature 117, 264, 1926.

Vasilev, A. P., Dolgov-Sovelev, G. G., and Kogan, V. I., Nucl. Fusion Supp. part II, 655, 1962.

Walker, A. B. C., and Rugge, H. R., Ap. J. 164, 181, 1971.

Wilson, R., J. Quant. Spectrosc. Rad. Transfer 2, 477, 1962.

Wooley, R. v.d. R., and Stibbs, D. W. N., The Outer Layers of a Star, London, Oxford University Press, 1953.

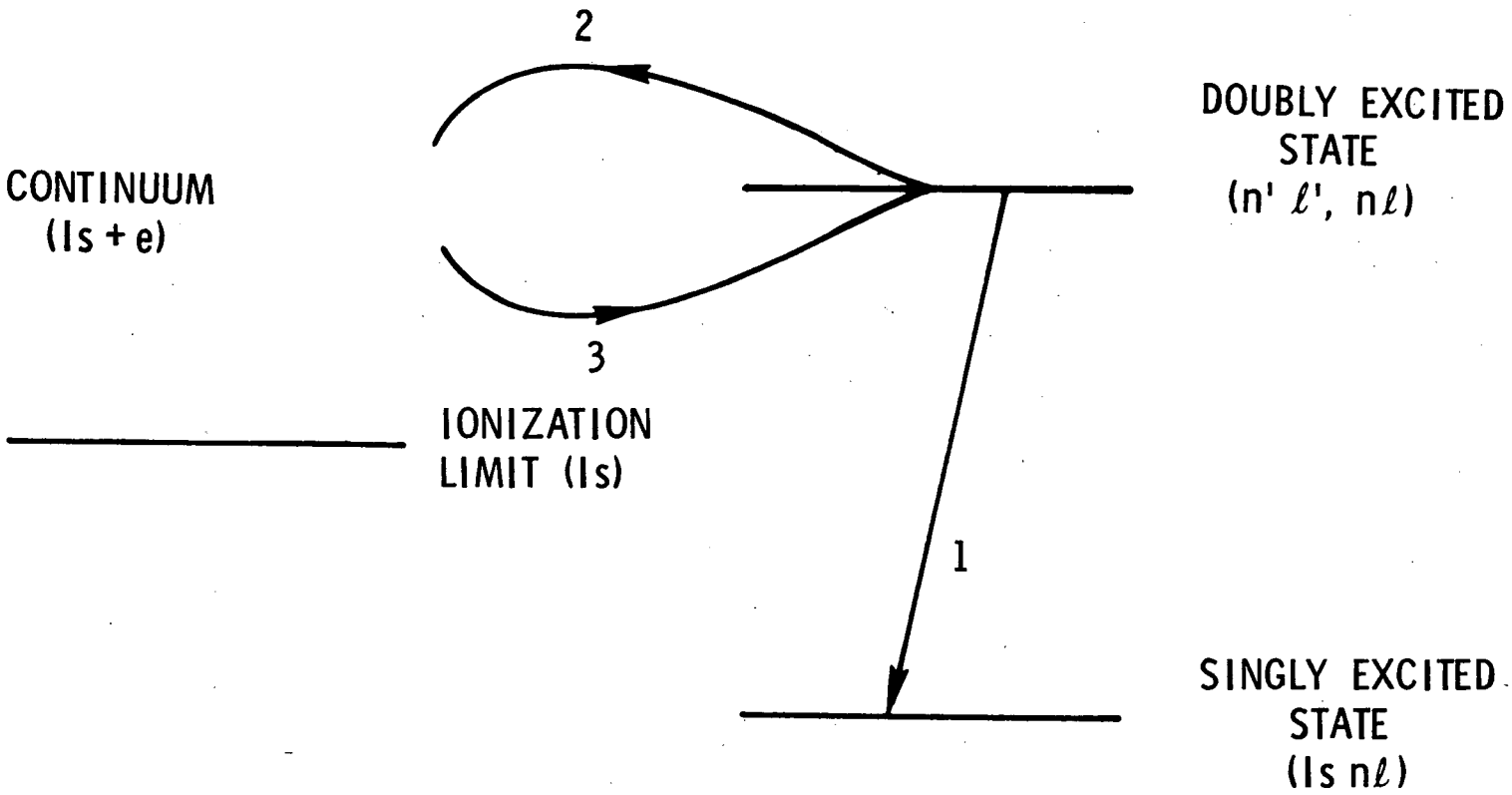

Schematic of Processes Involving Doubly Excited States

Figure 1

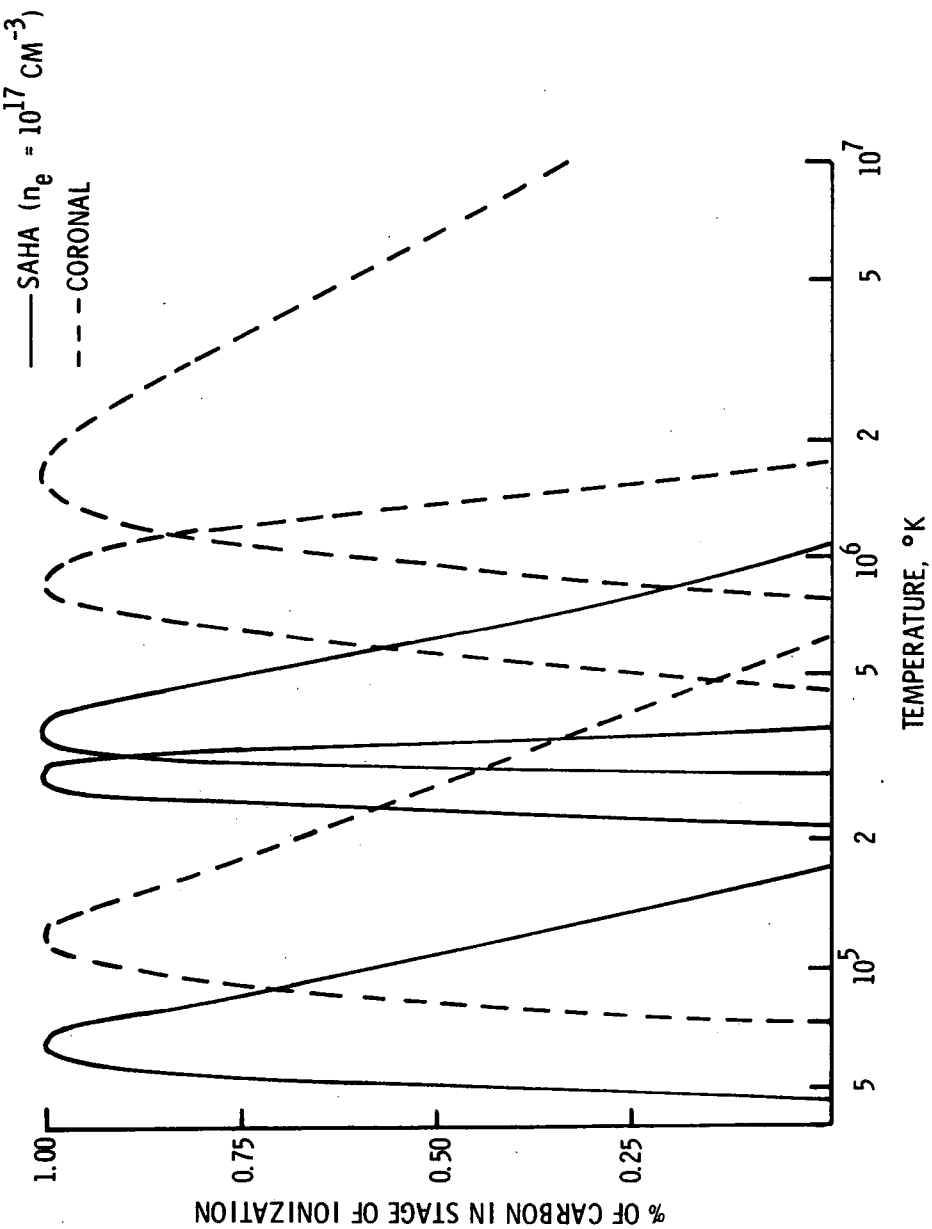

Population Density of Carbon Ions for SAHA and Coronal Equilibrium

Figure 2

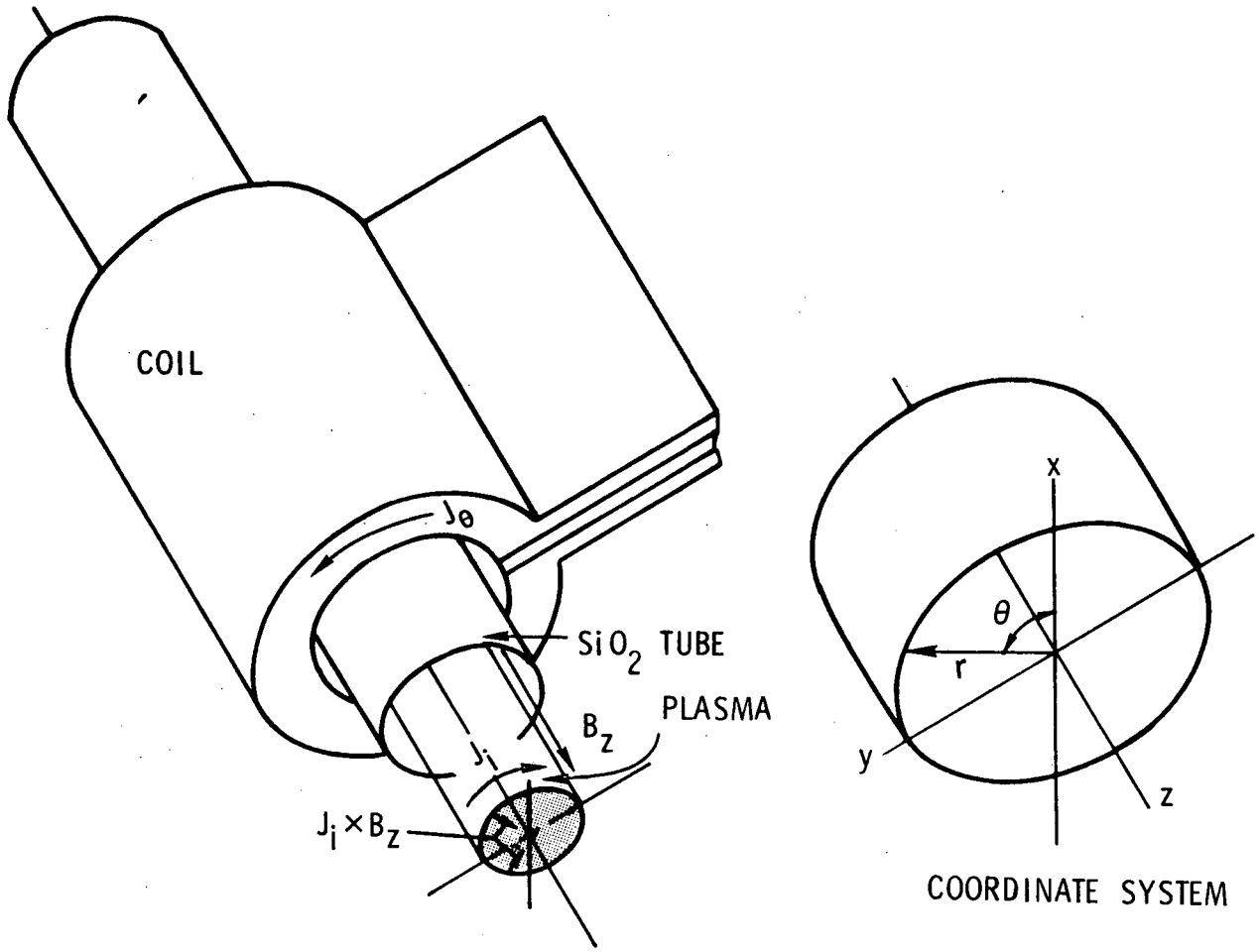

Theta-Pinch Coil and Field Geometry

Figure 3

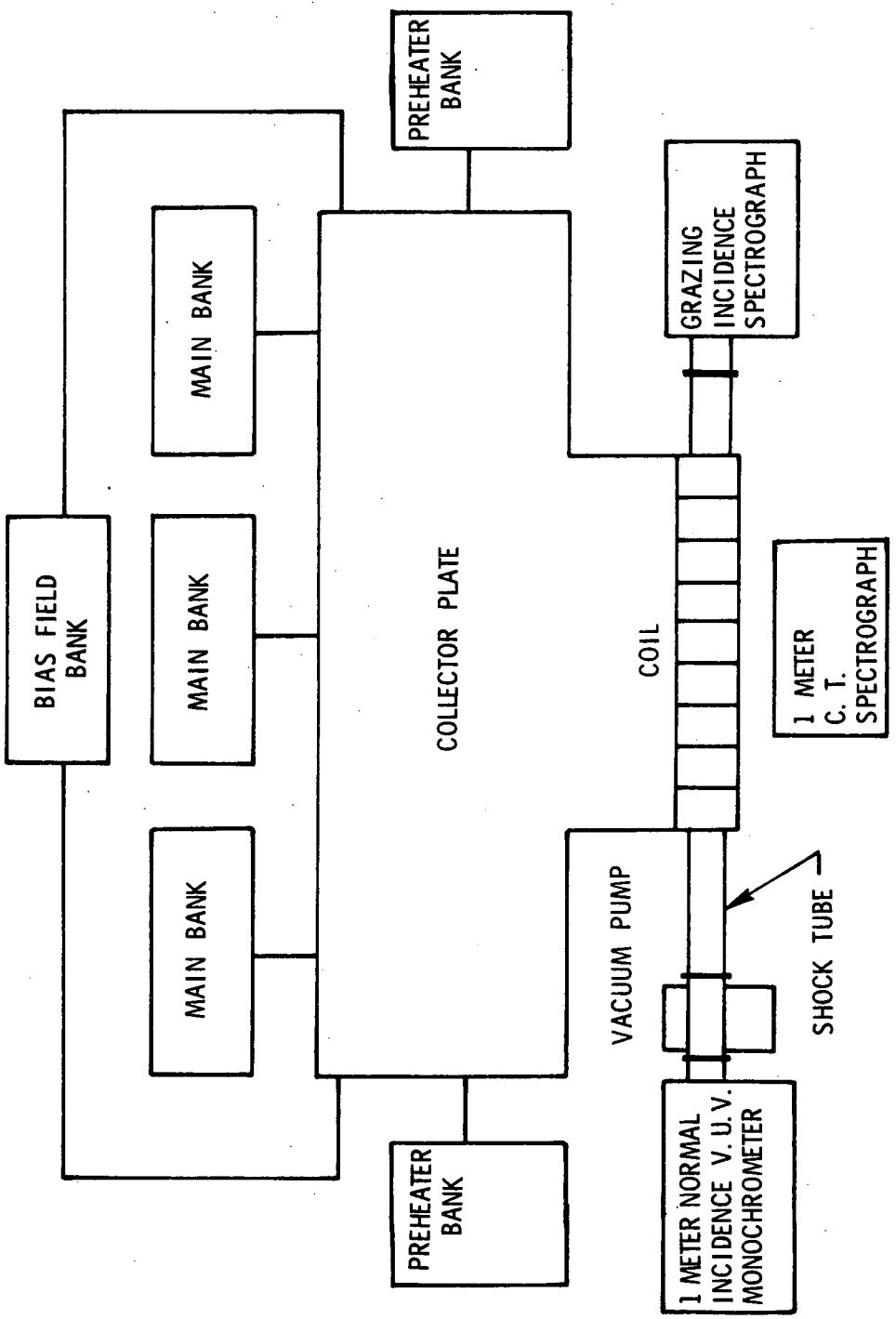

Theta-Pinch Physical Arrangement

Figure 4

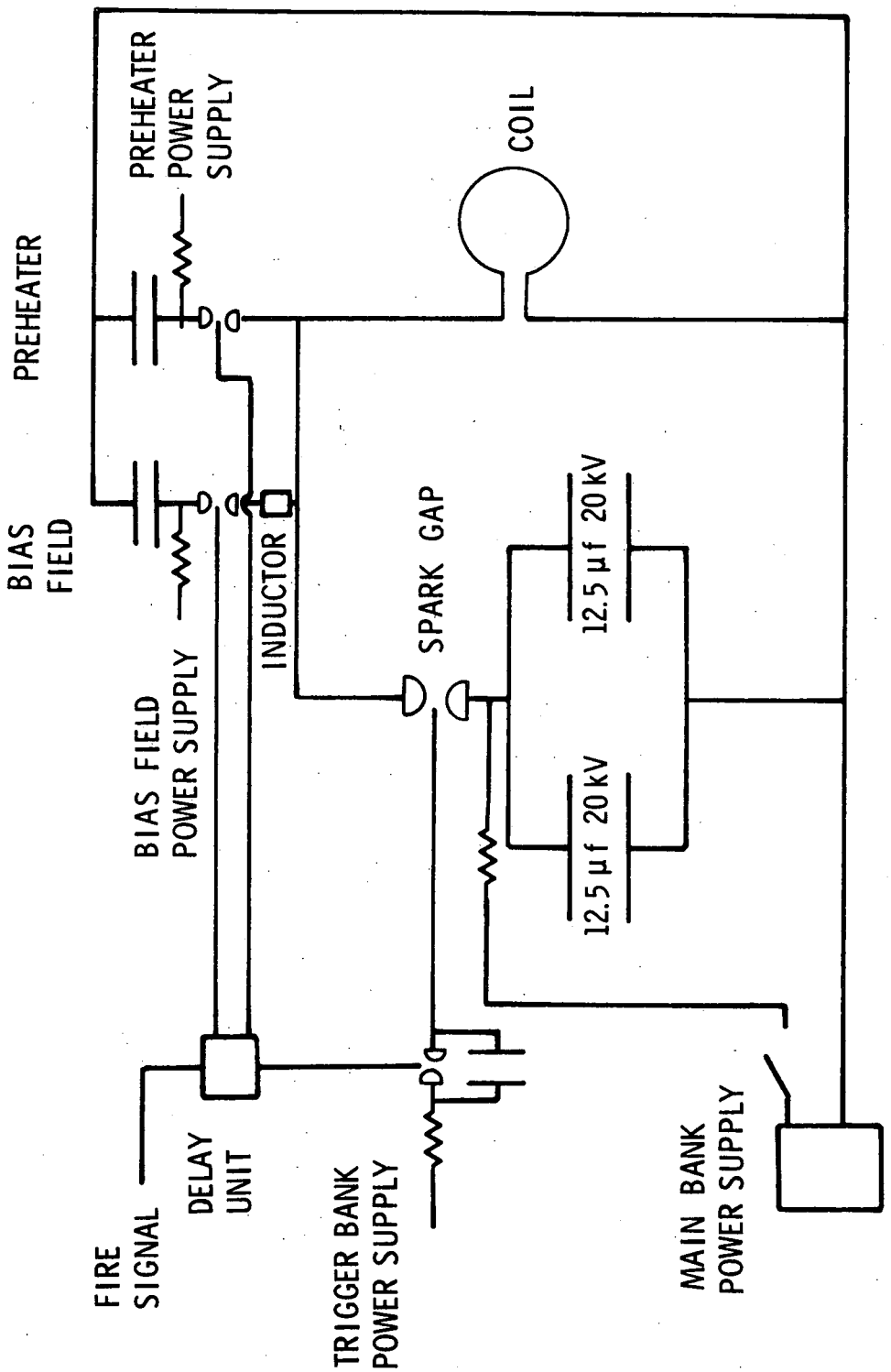

Electrical Schematic of the Theta-Pinch

Figure 5

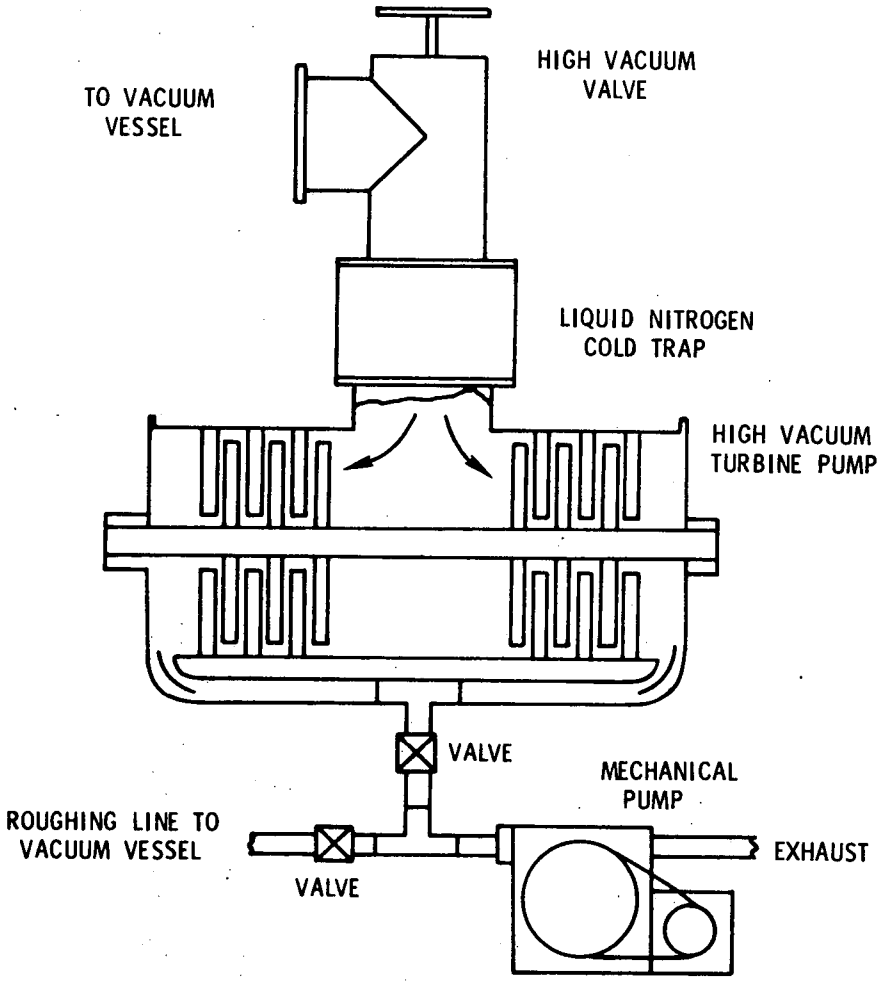

Vacuum System Schematic

Figure 6

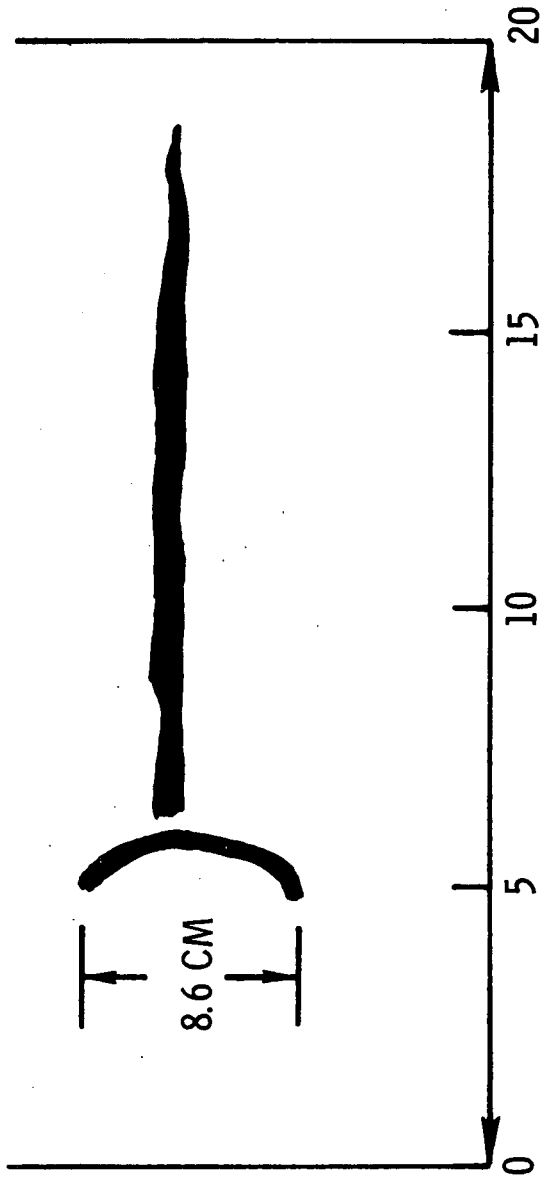

Streak Photograph of Plasma Compression

Figure 7

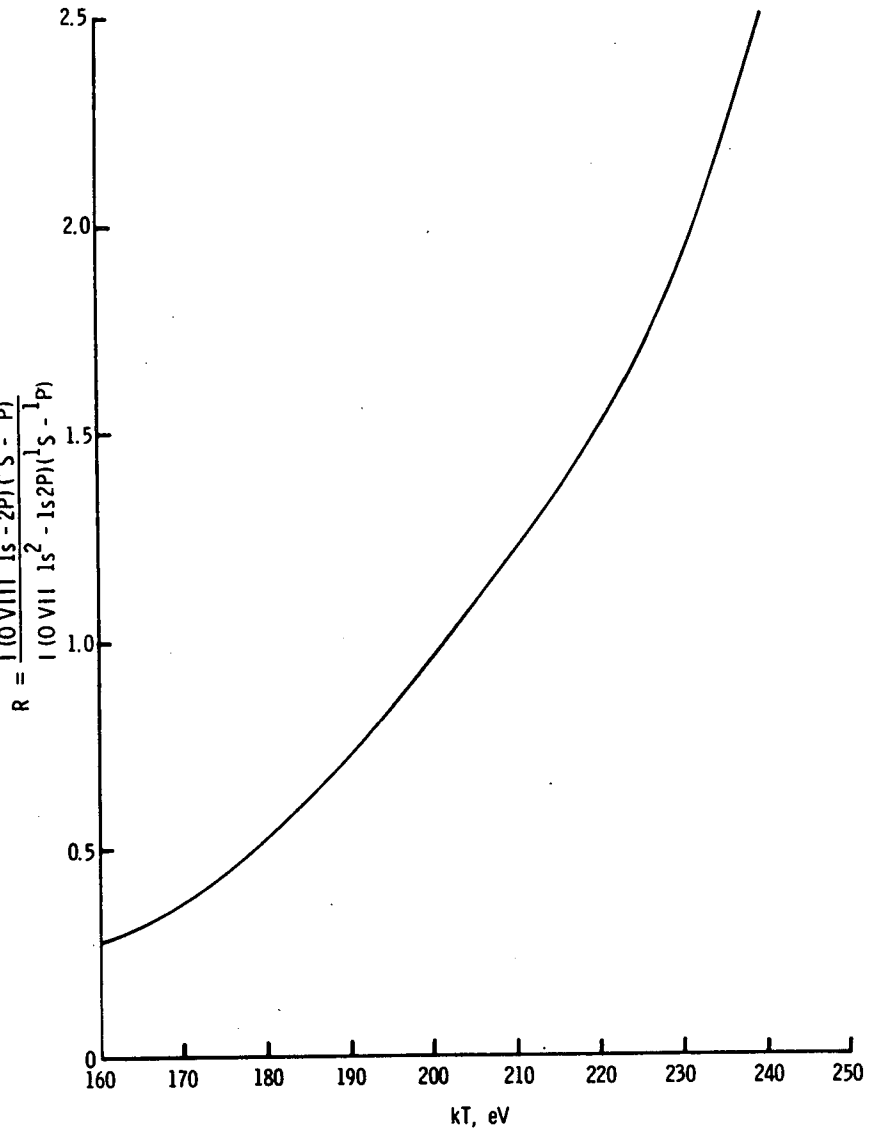

Intensity Ratio of OVIII to OVII Resonance Lines as a Function of Temperature

Figure 8

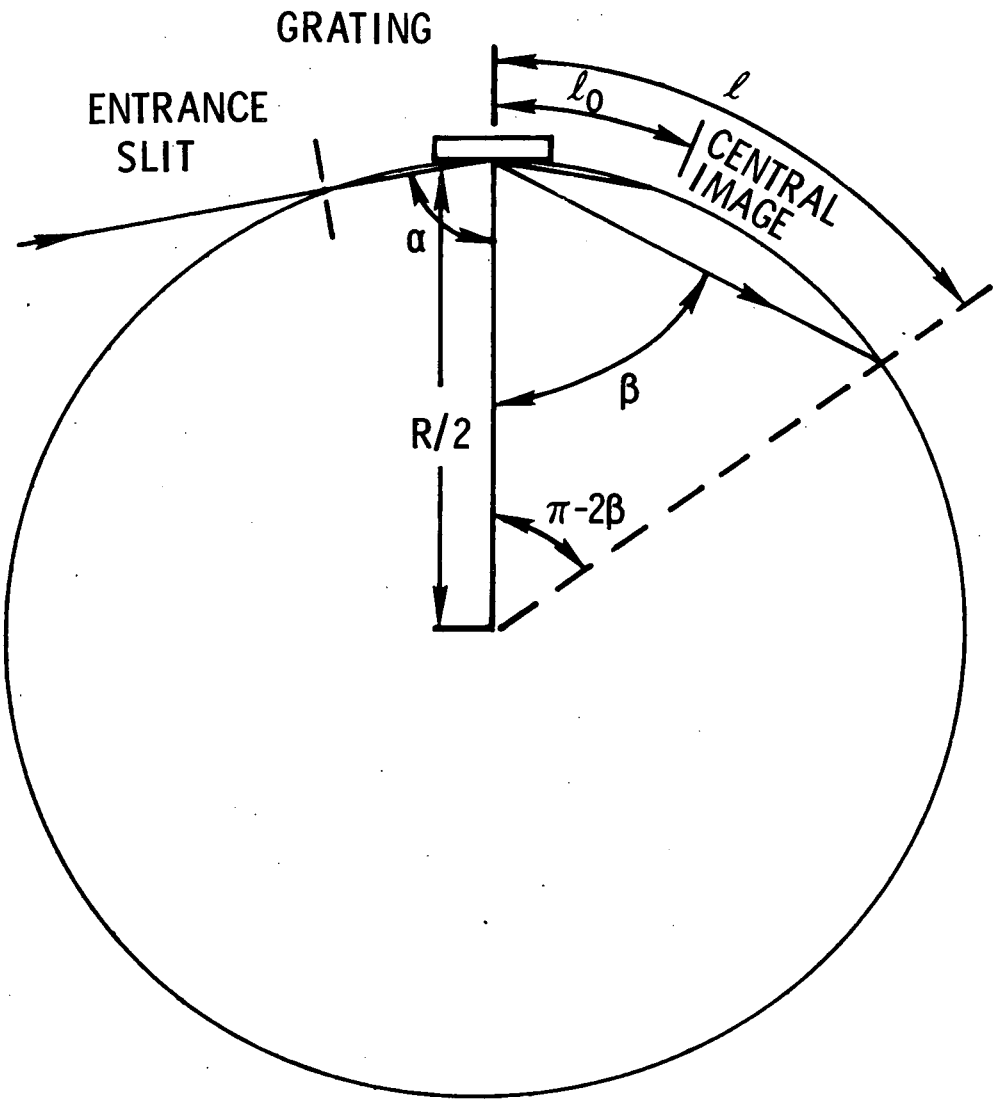

Optical Arrangement for the Grazing Incidence Mounting

Figure 9

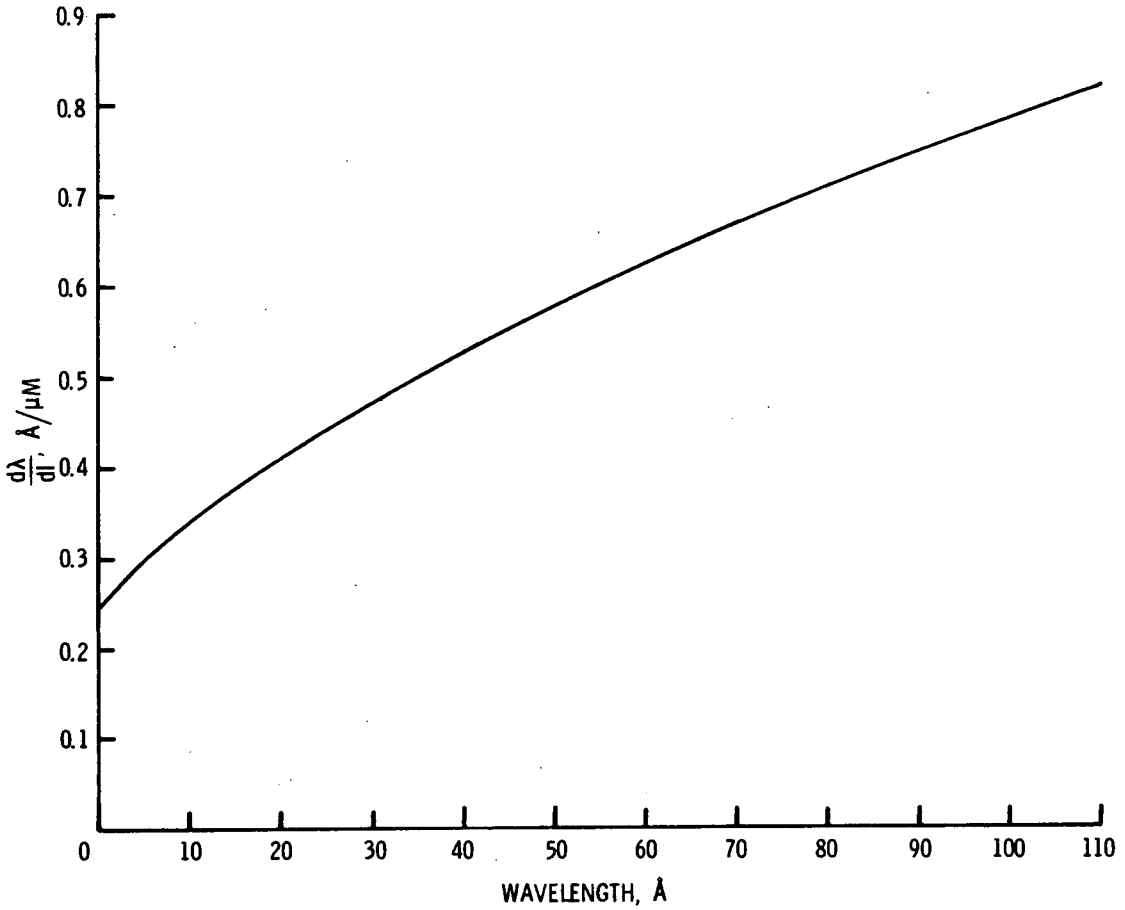

Theoretical Dispersion Curve for Grazing Incidence Spectrograph

Figure 10

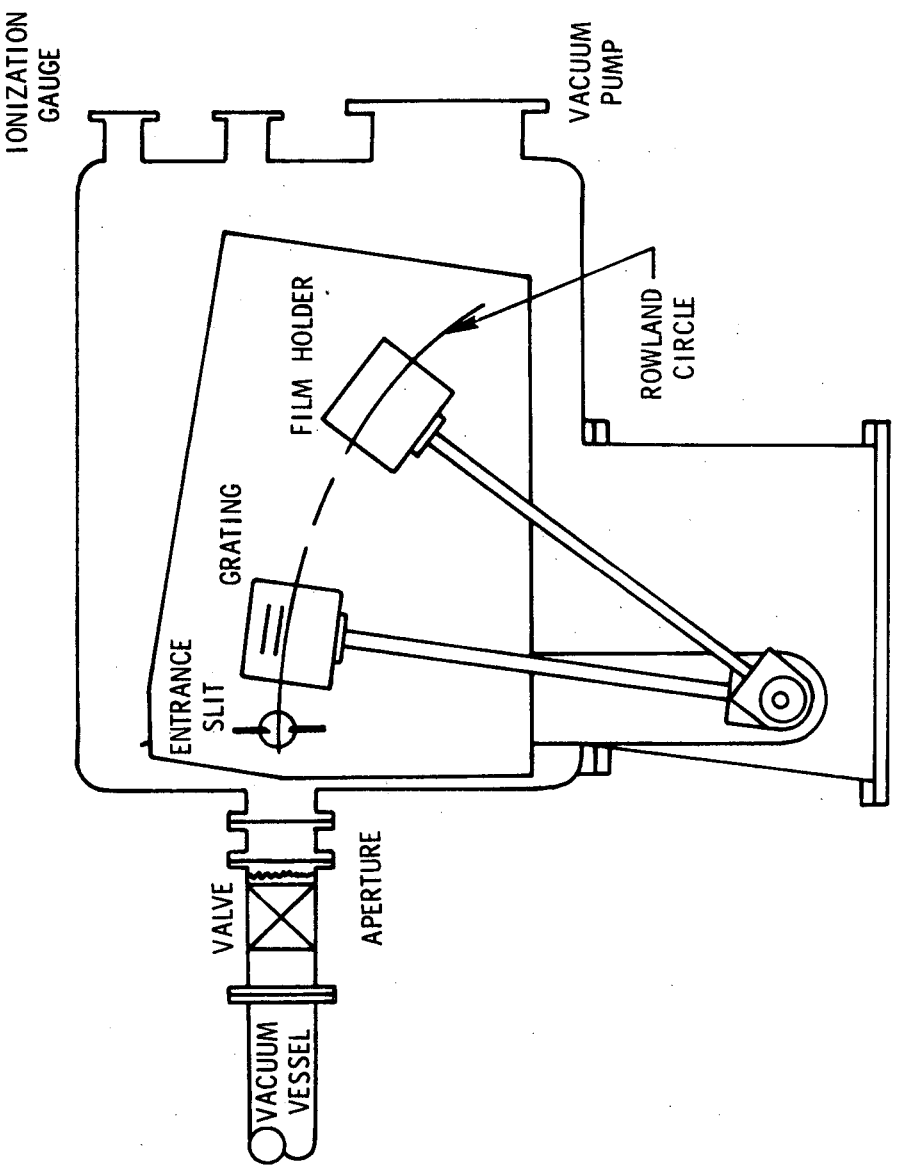

Grazing Incidence Spectrograph

Figure 11

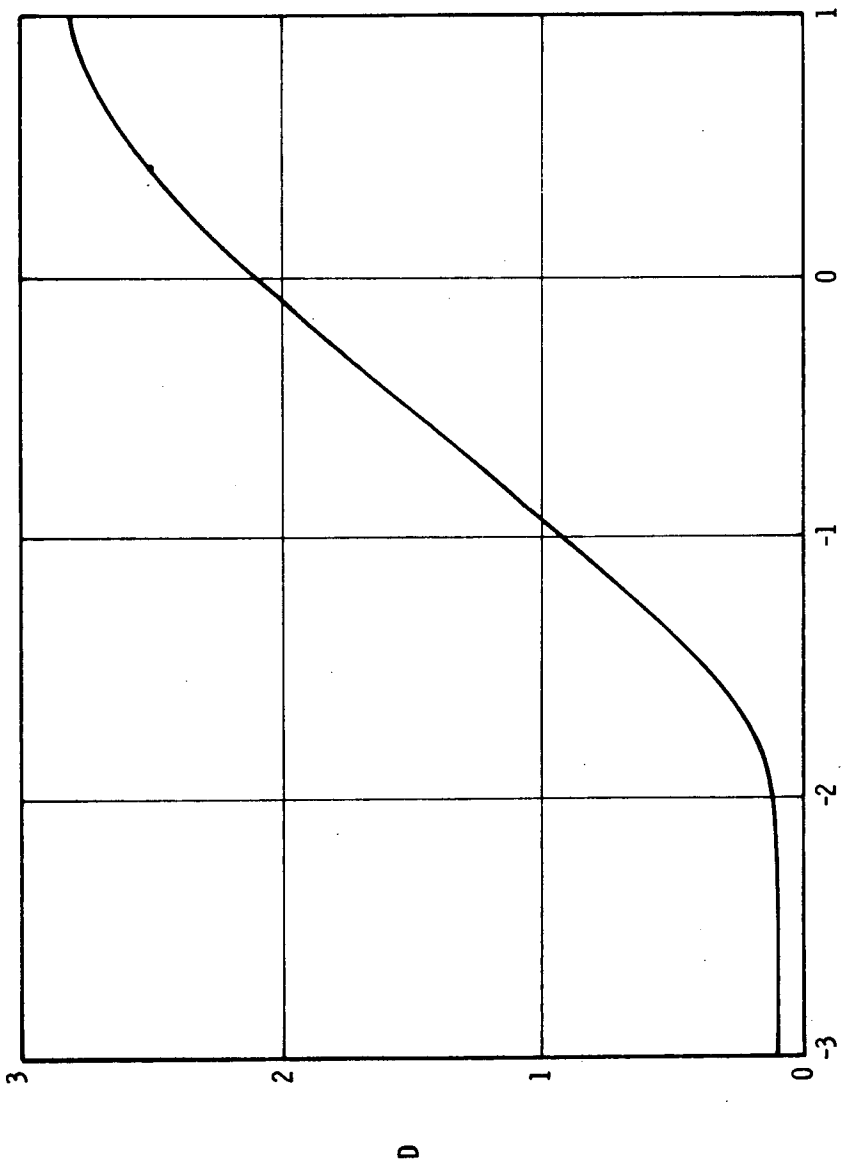

Typical H-D Curve
Figure 12

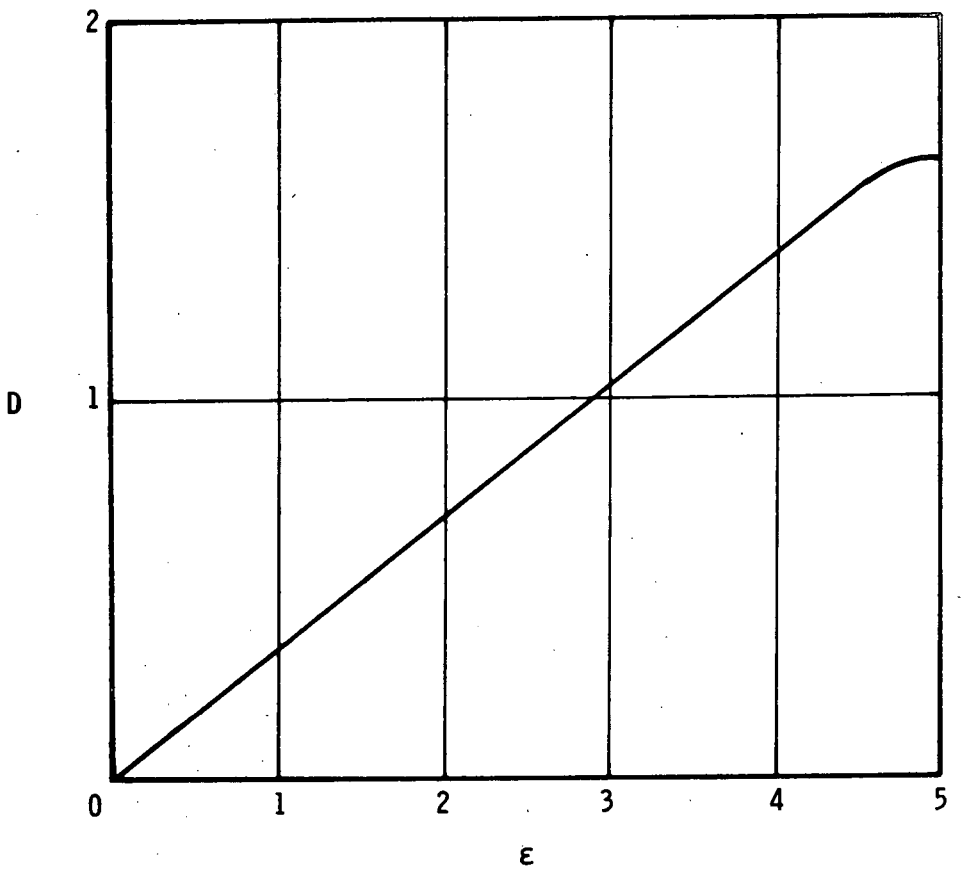

Typical Characteristic Curve, Soft X-Ray Region

Figure 13

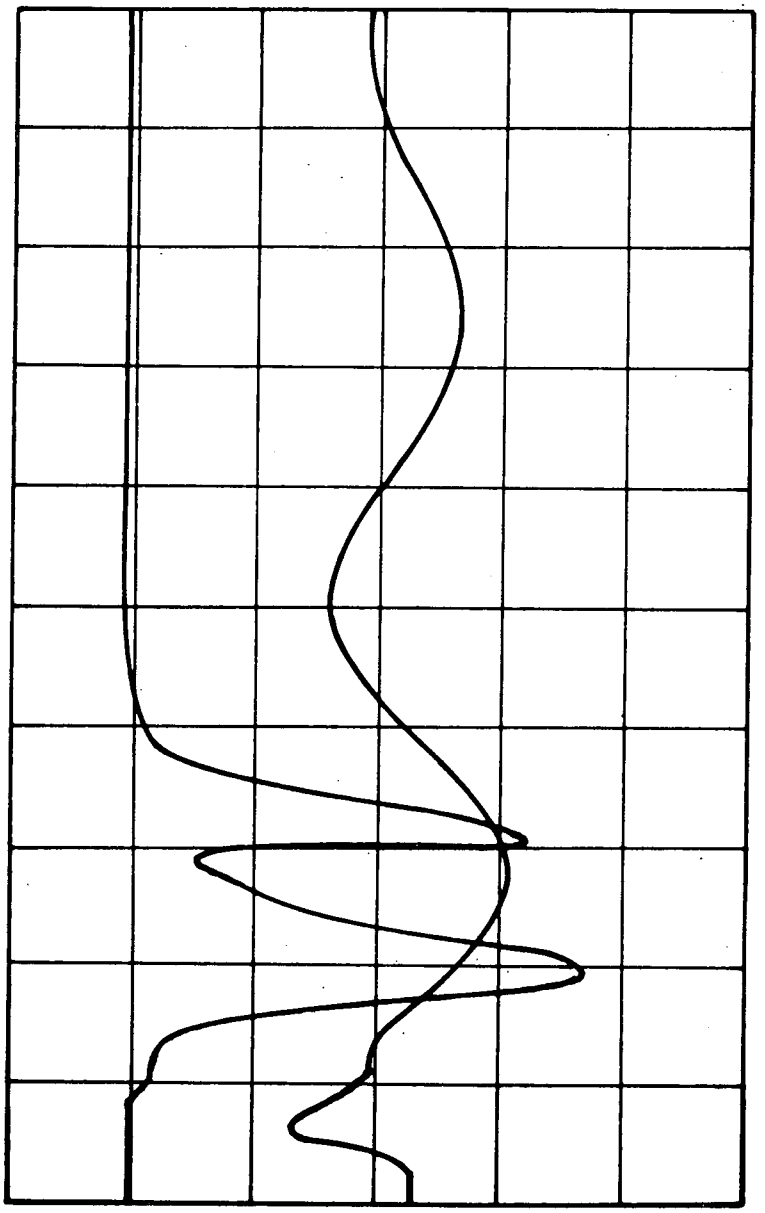

Intensity of OVII 1637.96 Å + 1639.58 Å

Figure 14

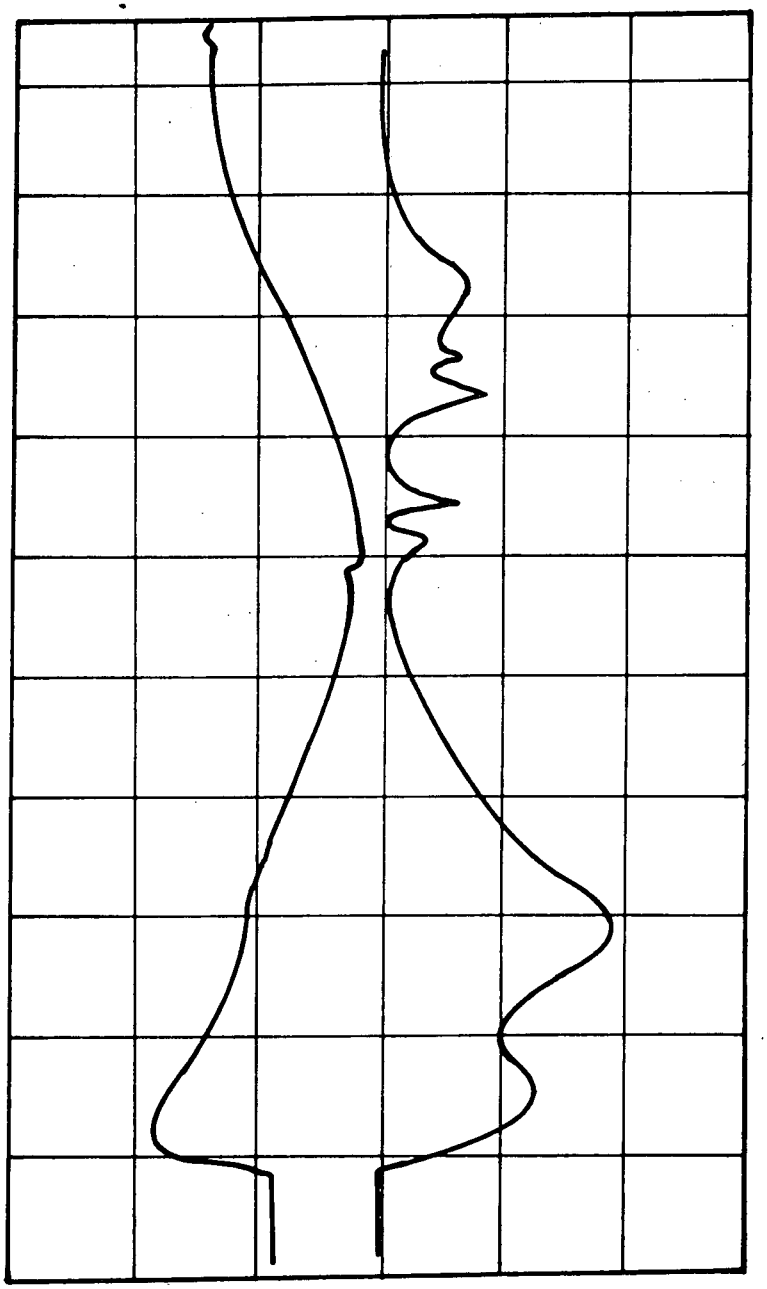

Intensity of Continuum at 5221 Å

Figure 15

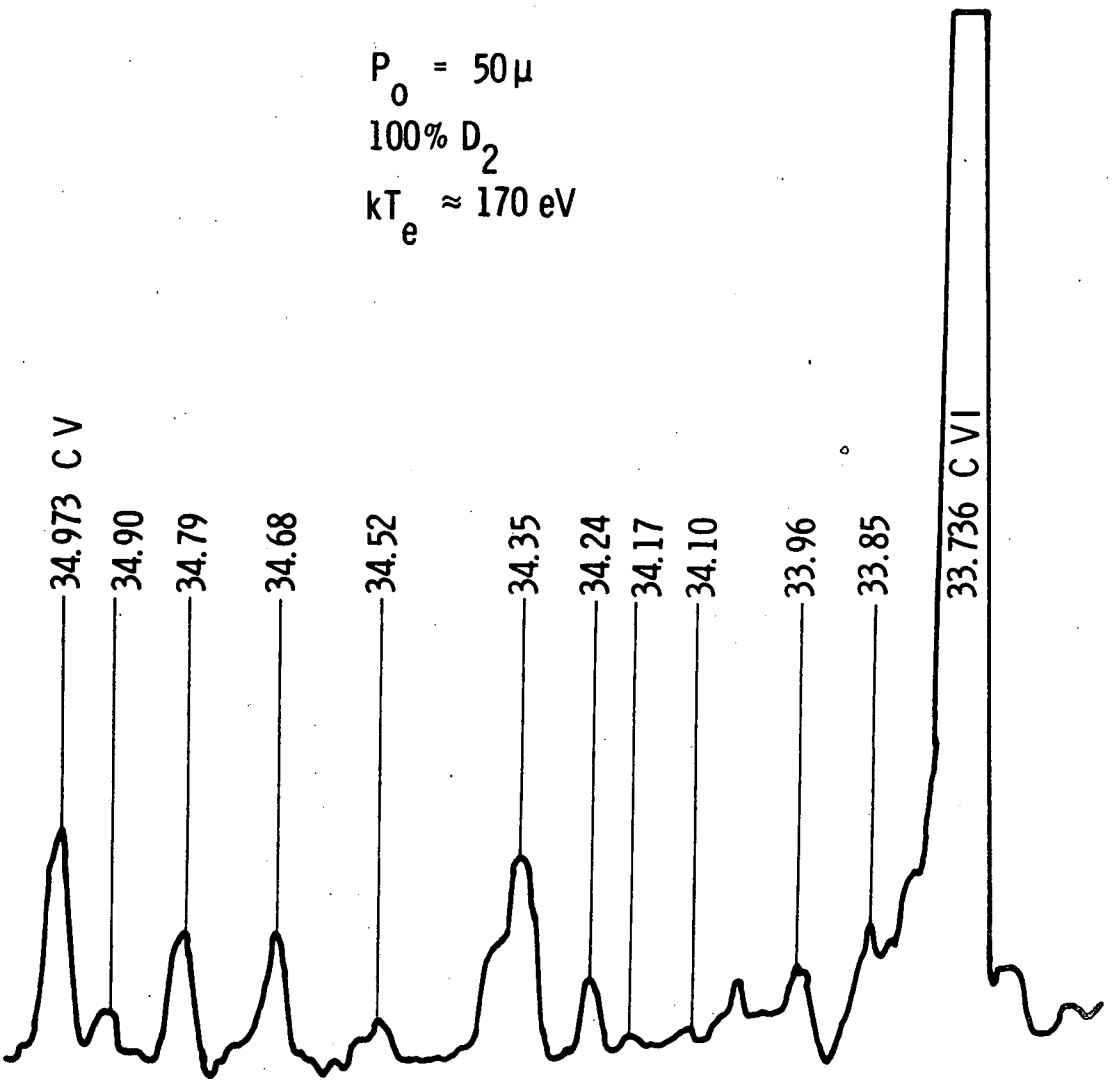

Spectrum Between 33.734 Å and 34.973 Å - No Added Impurities

Figure 16

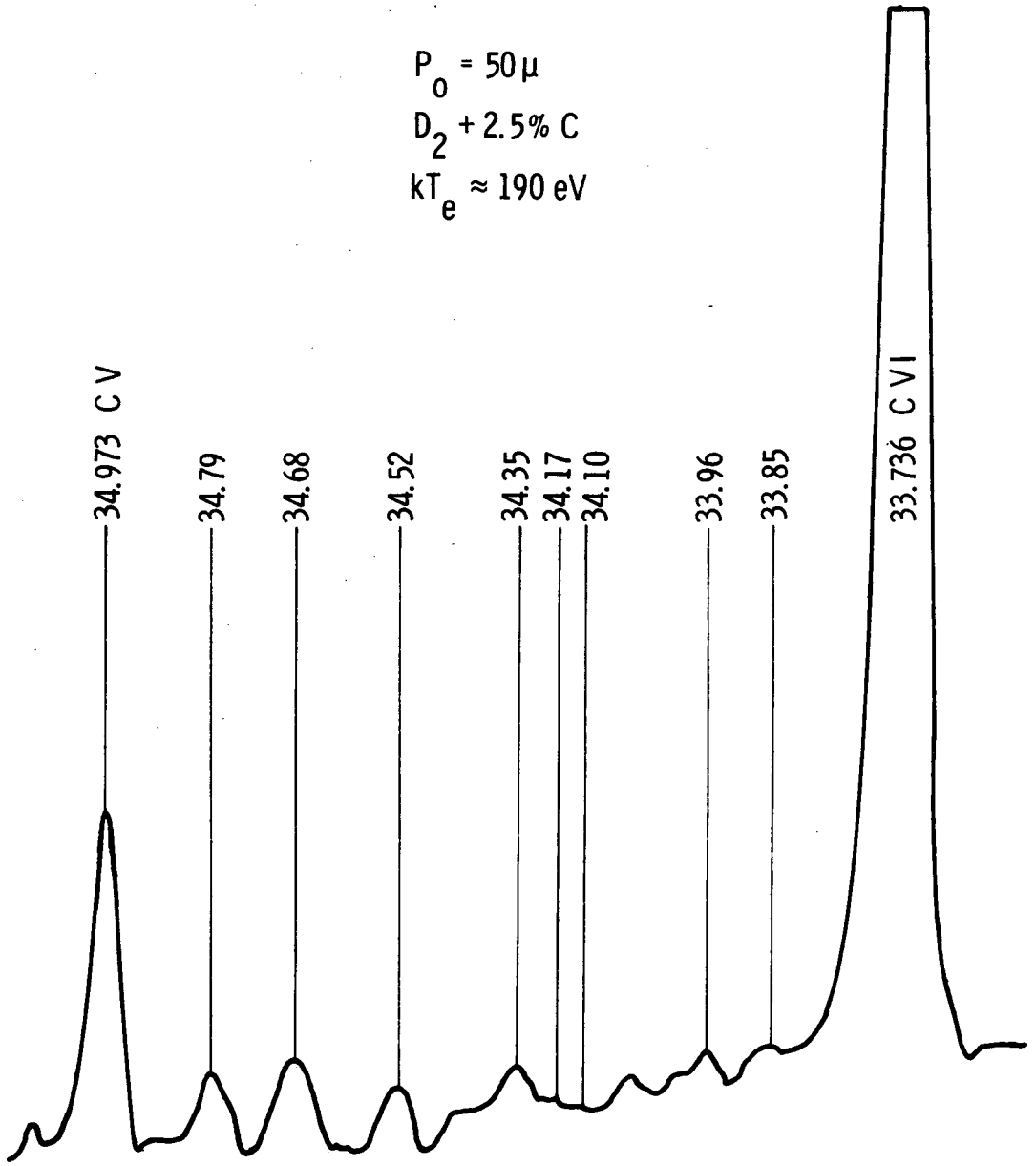

Spectrum Between 33.734 Å and 34.973 Å, 2.5% Carbon Added

Figure 17

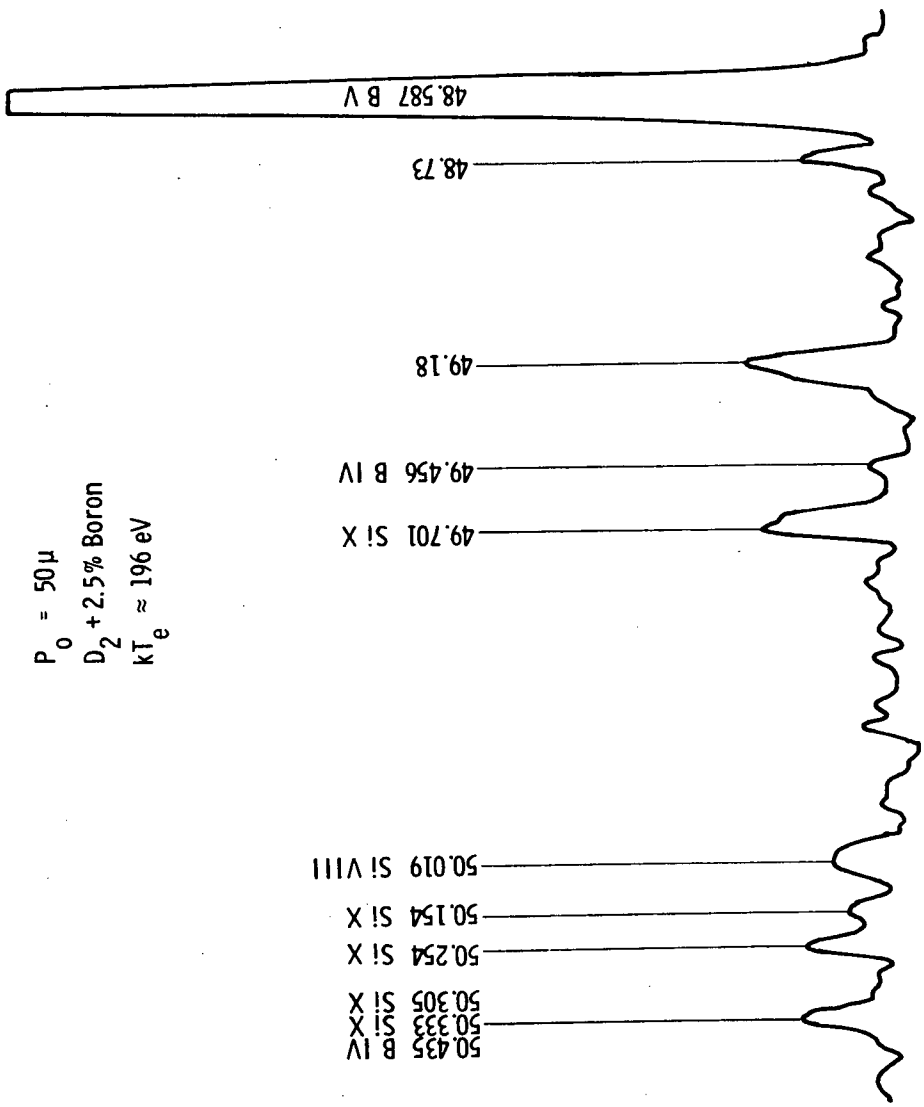

Spectrum Between 48.587 Å and 50.435 Å, 2.5% Boron Added

Figure 18

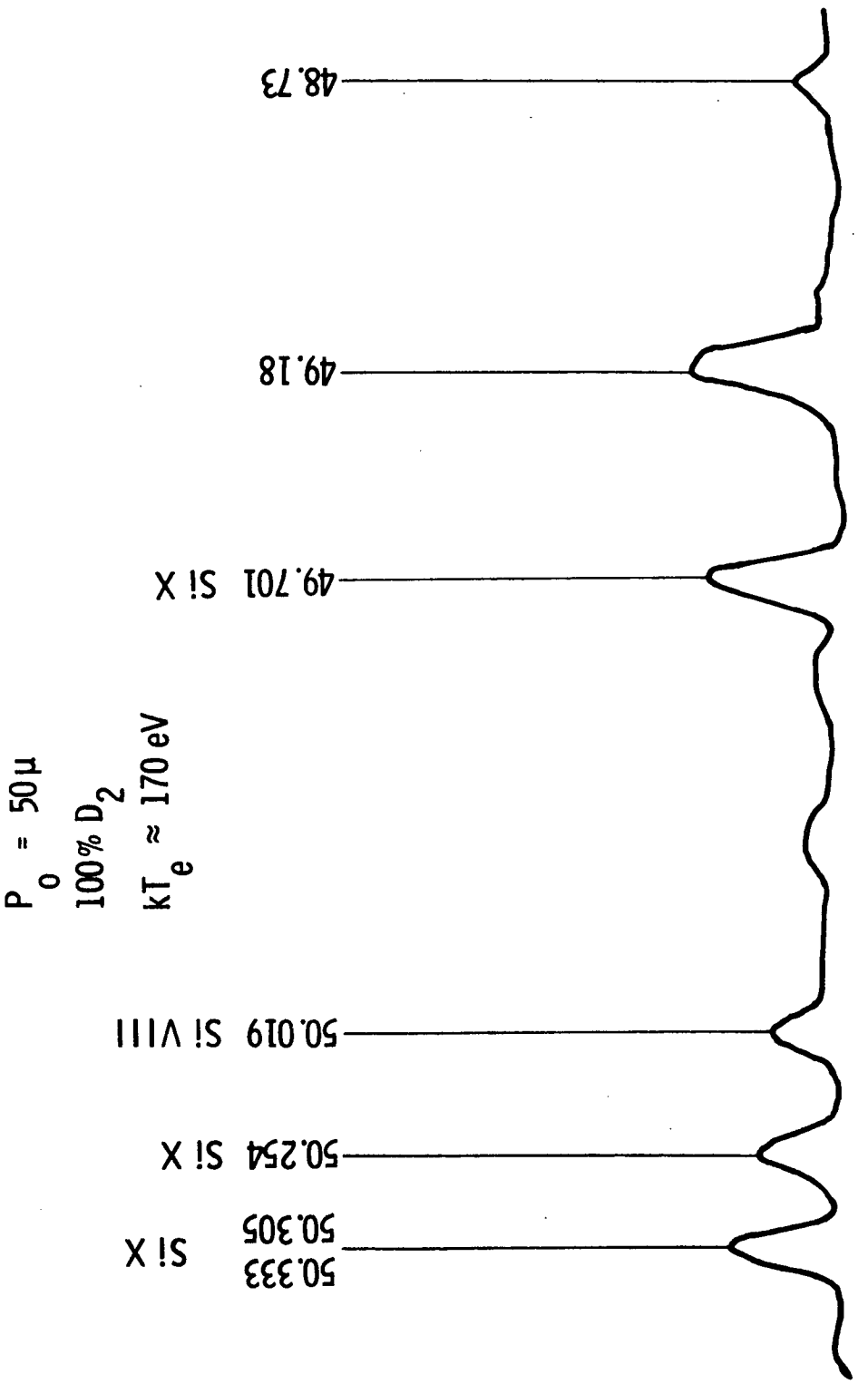

Spectrum Between 48.587 Å and 50.435 Å - No Impurities Added

Figure 19

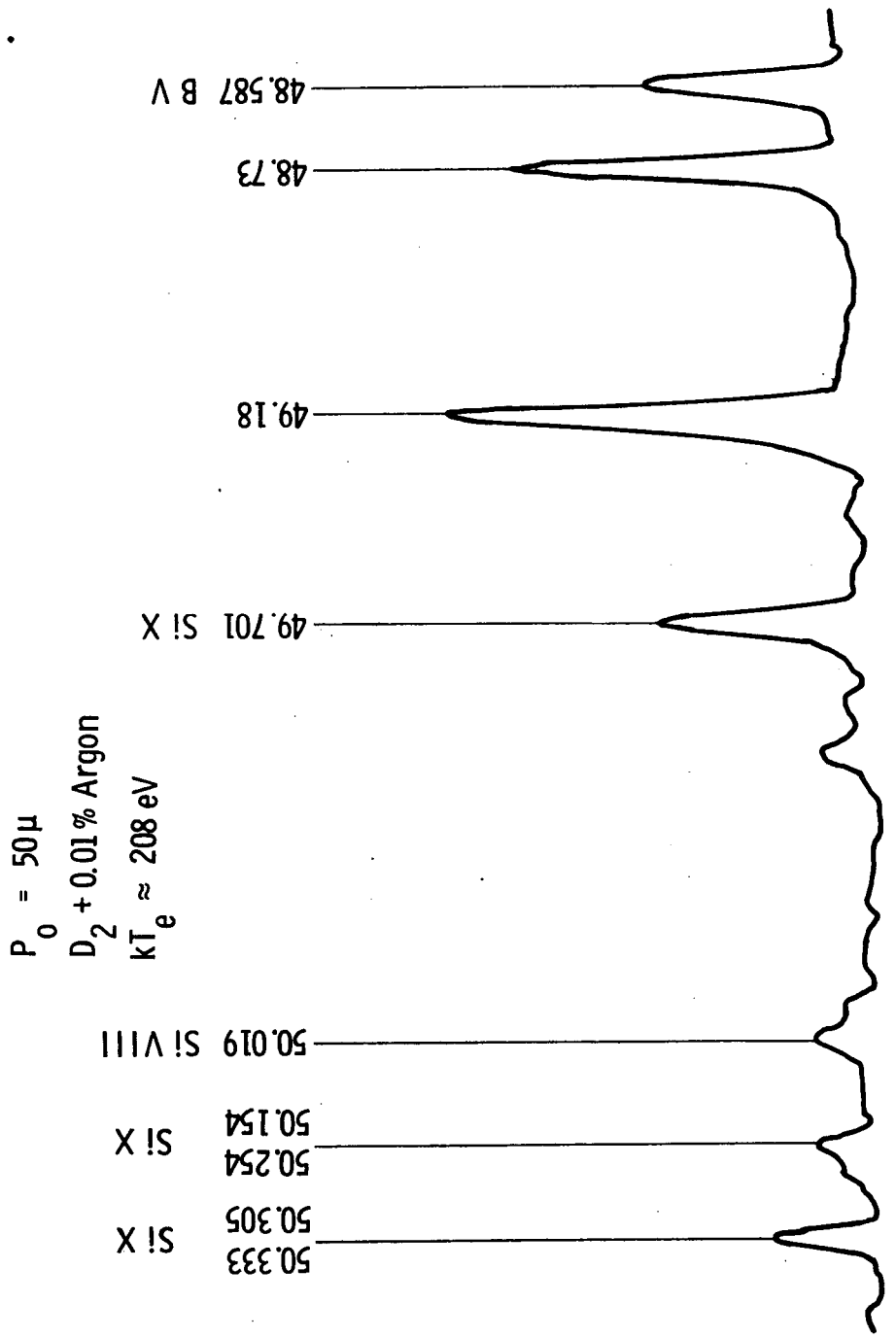

Spectrum Between 48.587 Å and 50.435 Å, 0.01% Argon Added

Figure 20

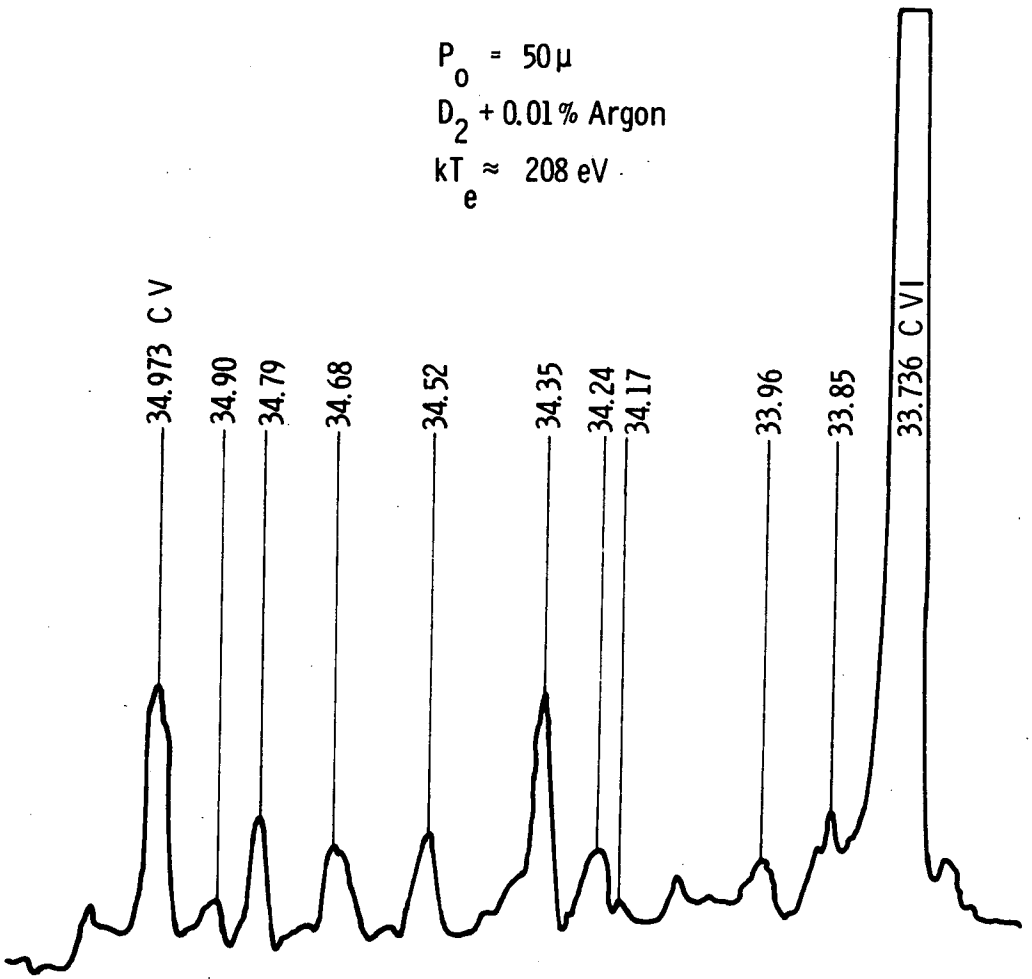

Spectrum Between 33.734 Å and 34.973 Å, 0.01% Arbon Added

Figure 21

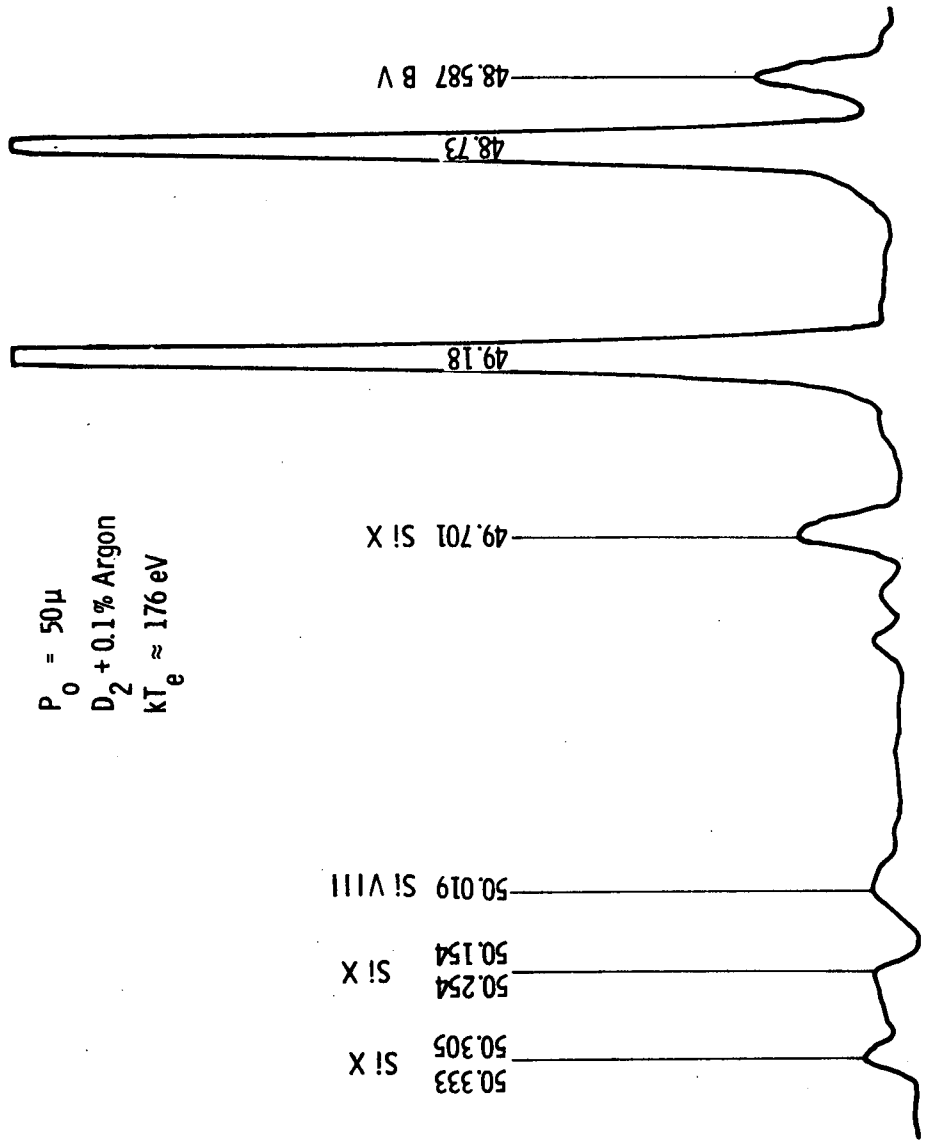

Spectrum Between 48.587 Å and 50.435 Å, 0.1% Argon Added

Figure 22

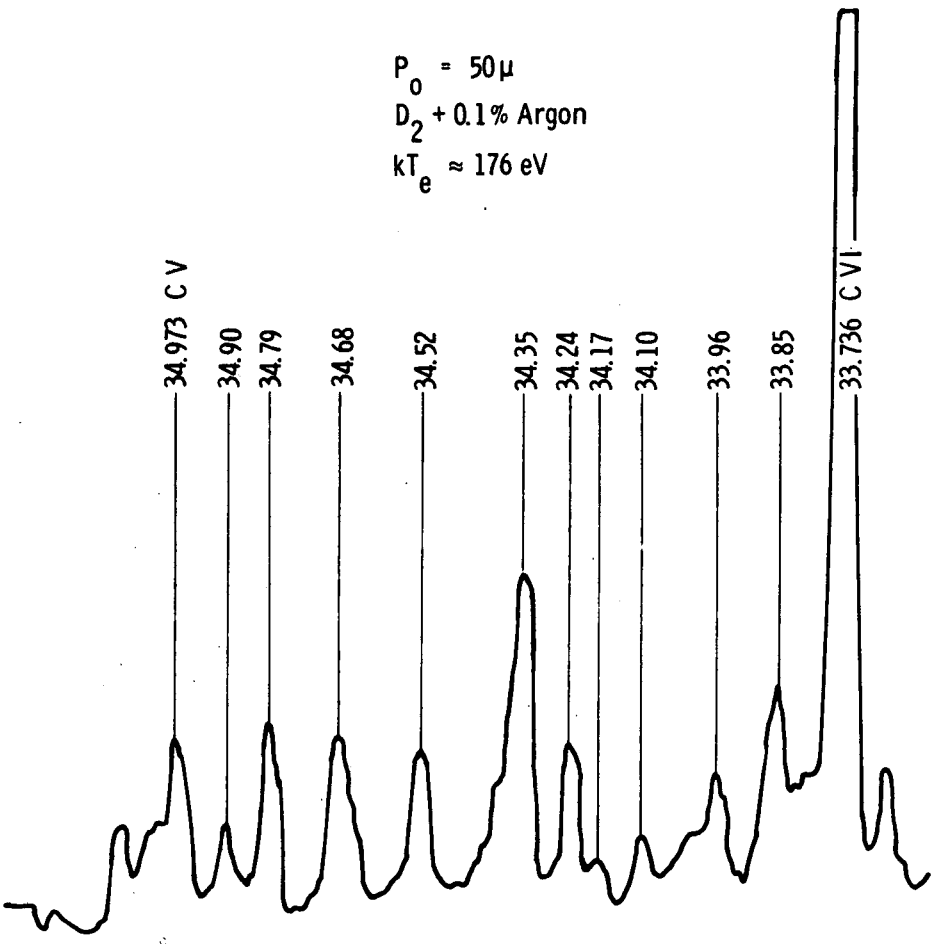

Spectrum Between 33.734 Å and 34.973 Å, 0.1% Argon Added

Figure 23

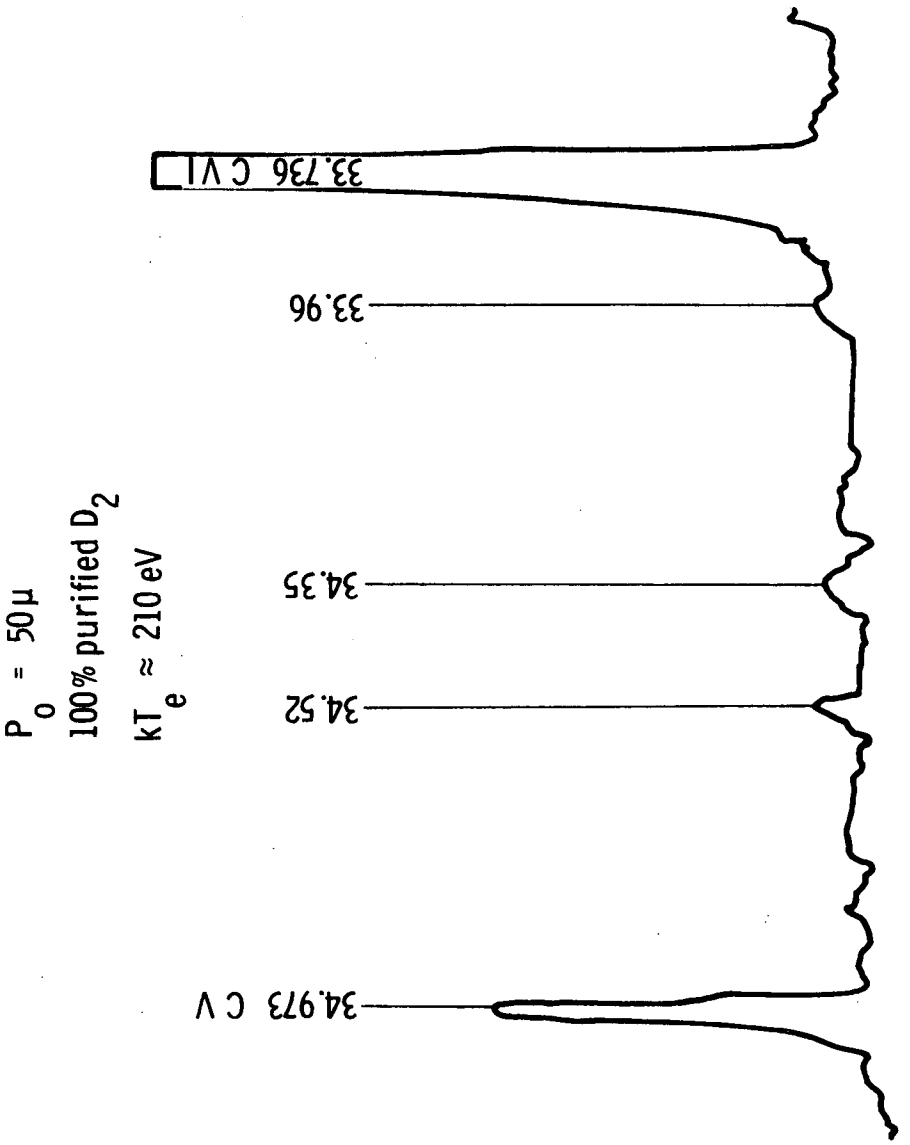

Spectrum Between 33.734 Å and 34.973 Å, No Impurities Added and With Purified Deuterium

Figure 24

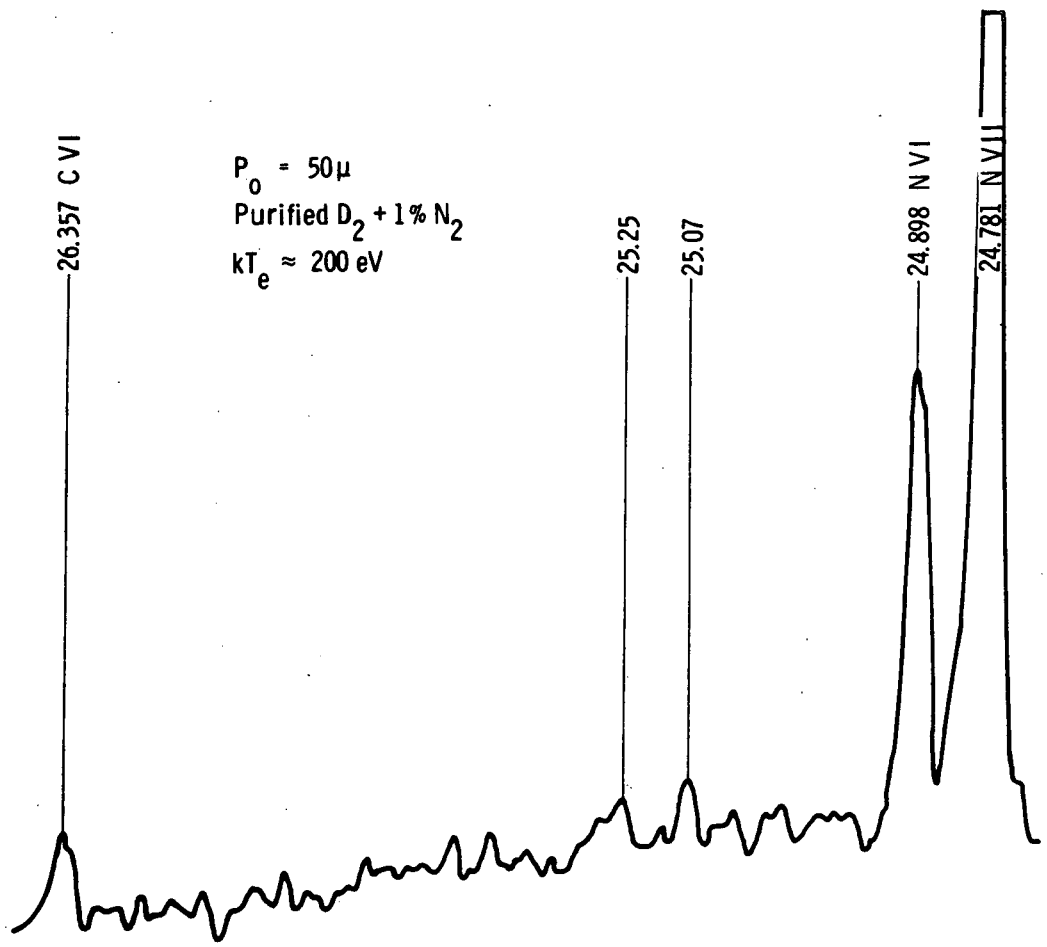

Spectrum Between 24.781 Å and 28.787 Å, 1% N_2 Added

Figure 25

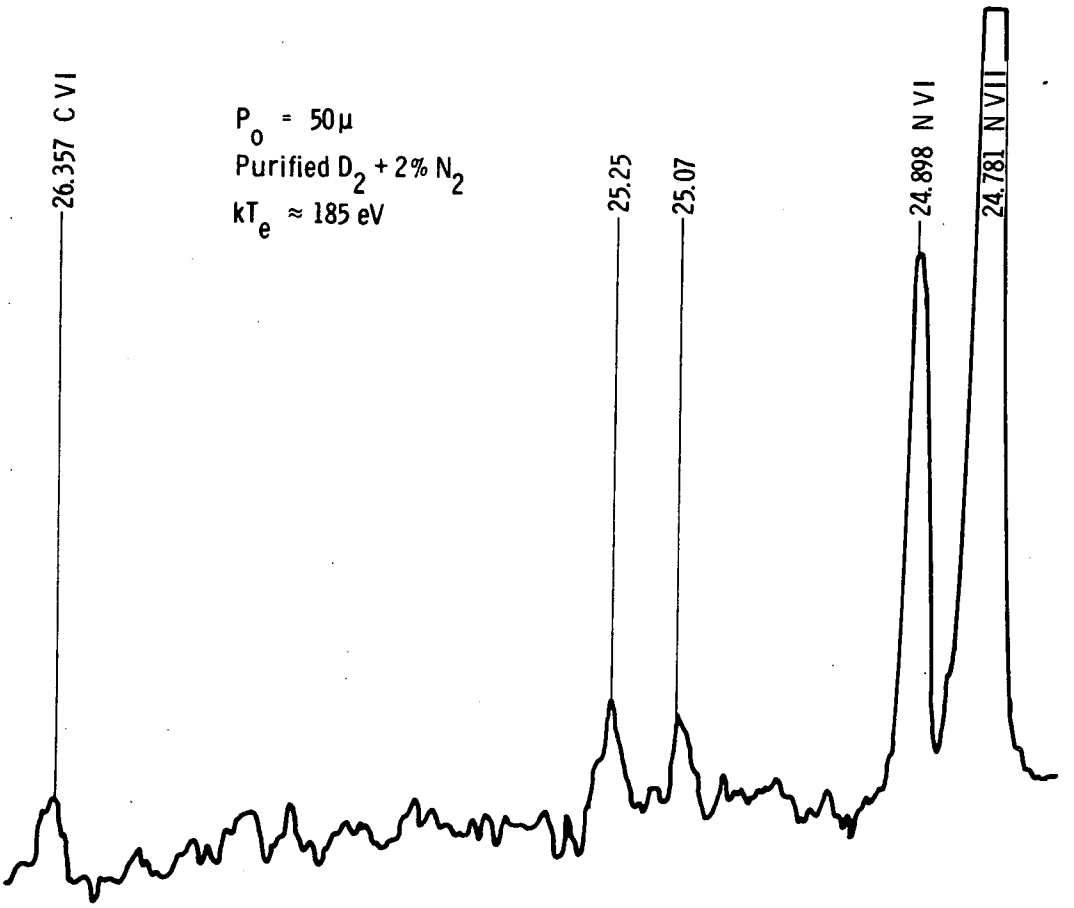

Spectrum Between 24.781 Å and 28.787 Å, 2% N_2 Added

Figure 26

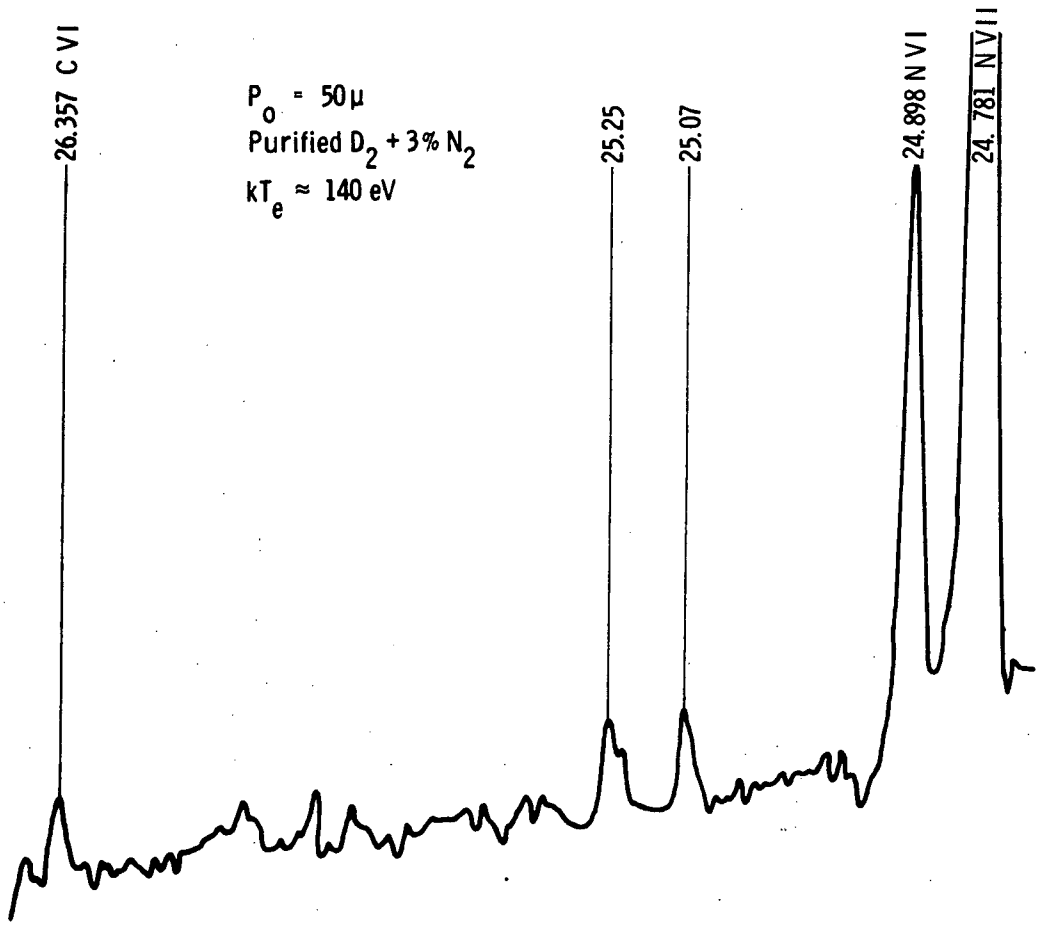

Spectrum Between 24.781 Å and 28.787 Å, 3% N_2 Added

Figure 27